Constraining uncertainty in *climate sensitivity*

An ensemble simulation approach based on glacial climate

DISSERTATION

zur Erlangung des akademischen Grades
"doctor rerum naturalium"
(Dr. rer. nat.)
in der Wissenschaftsdisziplin
"Klimaphysik“

eingereicht an der
Mathematisch-Naturwissenschaftlichen Fakultät
der Universität Potsdam

vorgelegt von
von
Thomas Schneider von Deimling

Potsdam, im Februar 2006

Doubt is not a pleasant condition, but certainty is an absurd one.

Voltaire (Francois Marie Arouet),

Letter to Frederick the Great, April 6, 1767

Abstract

Uncertainty about the sensitivity of the climate system to changes in the Earth's radiative balance constitutes a primary source of uncertainty for climate projections. Given the continuous increase in atmospheric greenhouse gas concentrations, constraining the uncertainty range in such type of sensitivity is of vital importance. A common measure for expressing this key characteristic for climate models is the *climate sensitivity*, defined as the simulated change in global-mean equilibrium temperature resulting from a doubling of atmospheric CO_2 concentration. The broad range of climate sensitivity estimates (1.5-4.5°C as given in the last Assessment Report of the Intergovernmental Panel on Climate Change, 2001), inferred from comprehensive climate models, illustrates that the strength of simulated feedback mechanisms varies strongly among different models.

The central goal of this thesis is to constrain uncertainty in climate sensitivity. For this objective we first generate a large ensemble of model simulations, covering different feedback strengths, and then request their consistency with present-day observational data and proxy-data from the Last Glacial Maximum (LGM). Our analyses are based on an ensemble of fully-coupled simulations, that were realized with a climate model of intermediate complexity (CLIMBER-2). These model versions cover a broad range of different climate sensitivities, ranging from 1.3 to 5.5°C, and have been generated by simultaneously perturbing a set of 11 model parameters. The analysis of the simulated model feedbacks reveals that the spread in climate sensitivity results from different realizations of the feedback strengths in water vapour, clouds, lapse rate and albedo. The calculated spread in the sum of all feedbacks spans almost the entire plausible range inferred from a sampling of more complex models.

We show that the requirement for consistency between simulated pre-industrial climate and a set of seven global-mean data constraints represents a comparatively weak test for model sensitivity (the data constrain climate sensitivity to 1.3-4.9°C). Analyses of the simulated latitudinal profile and of the seasonal cycle suggest that additional present-day data constraints, based on these characteristics, do not further constrain uncertainty in climate sensitivity.

The novel approach presented in this thesis consists in systematically combining a large set of LGM simulations with data information from reconstructed regional glacial cooling. Irrespective of uncertainties in model parameters and feedback strengths, the set of our model versions reveals a close link between the simulated warming due to a doubling of CO_2, and the cooling obtained for the LGM. Based on this close relationship between past and future temperature evolution, we define a method (based on linear regression) that allows us to estimate robust 5-95% quantiles for climate sensitivity. We thus constrain the range of climate sensitivity to 1.3-3.5°C using proxy-data from the LGM at low and high latitudes. Uncertainties in glacial radiative forcing enlarge this estimate to 1.2-4.3°C, whereas the assumption of large structural uncertainties may increase the upper limit by an additional degree. Using proxy-based data constraints for tropical and Antarctic cooling we show that very different absolute temperature changes in high and low latitudes all yield very similar estimates of climate sensitivity.

On the whole, this thesis highlights that LGM proxy-data information can offer an effective means of constraining the uncertainty range in climate sensitivity and

thus underlines the potential of paleo-climatic data to reduce uncertainty in future climate projections.

Zusammenfassung

Eine der entscheidenden Hauptquellen für Unsicherheiten von Klimaprojektionen ist, wie sensitiv das Klimasystem auf Änderungen der Strahlungsbilanz der Erde reagiert. Angesichts des kontinuierlichen Anstiegs der atmosphärischen Treibhausgaskonzentrationen ist die Einschränkung des Unsicherheitsbereichs dieser Sensitivität von entscheidender Bedeutung. Ein häufig verwendetes Maß zur Beschreibung dieser charakteristischen Kenngröße von Klimamodellen ist die sogenannte *Klimasensitivität*, definiert als die Gleichgewichtsänderung der simulierten globalen Mitteltemperatur, welche sich aus einer Verdoppelung des atmosphärischen CO_2-Gehalts ergibt. Die breite Spanne der geschätzten Klimasensitivität (1.5-4.5°C), welche ein Vergleich verschiedener komplexer Klimamodelle nahe legt (IPCC, 2001), verdeutlicht, wie groß die Unsicherheit in der Klimasensitivität ist. Diese Unsicherheit resultiert in erster Linie aus Unterschieden in der Simulation der entscheidenden Rückkopplungs-mechanismen in den verschiedenen Modellen.

Das zentrale Ziel dieser Dissertation ist die Einschränkung des breiten Unsicherheitsbereichs der Klimasensitivität. Zunächst wird hierzu ein großes Ensemble an Modellsimulationen erzeugt, in welchem gezielt spezifische Modellparameter variiert, und somit unterschiedliche Rückkopplungsstärken der einzelnen Modellversionen realisiert werden. Diese Simulationen werden dann auf ihre Konsistenz mit sowohl heutigen Beobachtungsdaten, als auch Proxy-Daten des Letzten Glazialen Maximums (LGM) überprüft. Unsere Analysen basieren dabei auf einem Ensemble voll gekoppelter Modellläufe, welche mit einem Klimamodell intermediärer Komplexität (CLIMBER-2) realisiert wurden. Die betrachteten Modellversionen decken eine breite Spanne verschiedener Klimasensitivitäten (1.3-5.5°C) ab und wurden durch gleichzeitiges Variieren von 11 Modellparametern erzeugt. Die Analyse der simulierten Rückkopplungs-mechanismen offenbart, dass unterschiedliche Werte der Klimasensitivität in unserem Modellensemble durch verschiedene Realisierungen der Rückkopplungsstärken von Wasserdampf, Wolken, Temperatur-Vertikalprofil und Albedo zu erklären sind. Die berechneten Gesamt-Rückkopplungsstärken unser Modellversionen decken hierbei fast den gesamten möglichen Bereich von komplexeren Modellen ab.

Wir zeigen, dass sich die Forderung nach Konsistenz zwischen simuliertem vorindustriellem Klima und Messdaten, die auf einer Wahl von sieben global gemittelten Datensätzen basieren, als vergleichsweise schwacher Test der Modellsensitivität erweist: Die Daten schränken den plausiblen Bereich der Klimasensitivität lediglich auf 1.3-4.9°C ein. Zieht man neben den genannten global gemittelten Messdaten außerdem klimatische Informationen aus Jahreszeit und geografischer Breite hinzu, lässt sich die Unsicherheit in der Klimasensitivität nicht weiter einschränken.

Der neue Ansatz dieser Dissertation besteht darin, in systematischer Weise einen großen Satz an LGM-Simulationen mit Dateninformationen über die rekonstruierte glaziale Abkühlung bestimmter Regionen zu kombinieren. Unabhängig von den Unsicherheiten in Modellparametern und Rückkopplungsstärken offenbaren unsere Modellversionen eine ausgeprägte Beziehung zwischen der simulierten Erwärmung aufgrund der CO_2-Verdoppelung und der Abkühlung im LGM. Basierend auf dieser engen Beziehung zwischen vergangener und zukünftiger Temperaturentwicklung definieren wir eine Methode

(basierend auf linearer Regression), welche es uns erlaubt, robuste 5-95%-Quantile der Klimasensitivität abzuschätzen. Indem wir Proxy-Daten des LGM von niederen und hohen Breiten heranziehen, können wir die Unsicherheitsspanne der Klimasensitivität auf 1.3-3.5°C beschränken. Unsicherheiten im glazialen Strahlungsantrieb vergrößern diese Abschätzung auf 1.2-4.3°C, wobei die Annahme von großen strukturellen Unsicherheiten die obere Grenze um ein weiteres Grad erhöhen kann. Indem wir Proxy-Daten über tropische und antarktische Abkühlung betrachten, können wir zeigen, dass sehr unterschiedliche absolute Temperatur-Änderungen in hohen und niederen Breiten zu sehr ähnlichen Abschätzungen der Klimasensitivität führen.

Vor dem Hintergrund unserer Ergebnisse zeigt diese Dissertation, dass LGM-Proxy-Daten ein effektives Mittel zur Einschränkung des Unsicherheitsbereichs der Klimasensitivität sein können und betont somit das Potenzial von Paläoklimadaten, den großen Unsicherheitsbereich von Klimaprojektionen zu reduzieren.

Contents

1 Introduction

One of the central tasks of climate science is to predict the sensitivity of the climate system to changing greenhouse gas (GHG) concentrations. The answer crucially determines how serious the consequences of global warming will be. It is uncertain as the magnitude of climate feedbacks is inadequately known.

One common indicator for the feedback strength of a given climate model is the change in simulated global-mean surface temperature once the system has reached a new equilibrium following a doubling of atmospheric CO_2 concentration, referred to as *climate sensitivity* (ΔT_{2x}). If there were no feedbacks in the climate system to act besides the negative feedback, resulting from an increase in long-wave radiation for increasing surface temperatures, the global-mean surface temperature would increase by about 1.2°C for doubling CO_2 concentrations (HANSEN et al., 1984; SCHLESINGER, 1988; IPCC WG-I, 2004). This value is rather consistent among climate models and indicates that the large uncertainty in climate sensitivity results from incomplete knowledge of the feedback strengths in water vapour, clouds, lapse rate and albedo. In this context it is commonly accepted that uncertainty in cloud feedback plays a key role, as the representation of cloud behaviour can be realized so far only in a crude manner in climate models through the need for parametrising the cloud physics. This large uncertainty is expressed by the fact that even the sign of this feedback is unknown for future climate change (IPCC, 2001).

More than a hundred years ago Arrhenius calculated the sensitivity of Earth's mean temperature to increased atmospheric CO_2 concentrations and obtained a sensitivity for CO_2 doubling of 5.5°C (ARRHENIUS, 1896). With the birth of climate models a more accurate estimate of ΔT_{2x} became possible, but the large uncertainty in climate sensitivity, which was estimated as 1.5-4.5°C (CHARNEY, 1979) in the 1970's, remained essentially unchanged during the last decades. Yet with increasing computer power ensemble studies have been realized in recent years with the aim to systematically account for so far unexplored uncertainty in climate models and to provide probabilistic estimates of ΔT_{2x}. The outcome of those studies was a pronounced shift of the upper bound of ΔT_{2x} and the concern was raised that the hitherto consensus-range of 1.5-4.5°C may strongly underestimate the risk of large future warming.

1.1 Motivation of the thesis

In the context of future climate projections the concept of climate sensitivity has proven to be a useful tool to characterize the performance of a specific model, for the following reason: To a large extent, given a prescribed forcing scenario, the broad range in estimates of future global warming can be traced back to uncertainty in the magnitude of ΔT_{2x}. Hence uncertainty in climate sensitivity is generally assumed to represent the greatest source of uncertainty in climate change projections for the 21st Century (GREGORY et al., 2002; STOTT and KETTLEBOROUGH, 2002).

In its last report, the Intergovernmental Panel on Climate Change (IPCC)

confirms the range of 1.5-4.5°C by evaluating the performance of a set of comprehensive climate models. This estimate is dissatisfying in three respects: (1) the interval is large, (2) it lacks the information about the probability whether the lower or the upper range is more likely, (3) the interval does not yet account for model parameter uncertainty. In view of a need for deciding on an adequate combination of adaptation and mitigation strategies, this situation is uncomfortable. Higher confidence in the estimate of ΔT_{2x} would in particular be desirable for the upper end of climate sensitivity as impacts of global warming are expected to scale strongly with global-mean temperature (IPCC, WGII, TAR, 2001).

The United Nations Framework Convention on Climate (UNFCCC, Article 2) calls for

"…stabilization of greenhouse gas concentrations in the atmosphere at a level that would prevent dangerous anthropogenic interference with the climate system."

In view of assessing the risks associated with specific targets for stabilizing GHG levels it is important to consider the full range of possible responses of the climate system to rising GHG concentrations. This range is ultimately linked to the spread in estimates of ΔT_{2x}, thus constraining climate sensitivity uncertainty has become a key target in climate research for better informing mitigation and adaptation policies.

The motivation of this thesis is to undertake an attempt of constraining uncertainty in climate sensitivity and to contribute to the ongoing discussion about a need for increasing the upper end of the IPCC estimate (4.5°C) in order to capture all known uncertainties. Given the failure of recent studies to constrain the upper bound of ΔT_{2x} by comparing simulated climate with observational data of present-day climate and of 20th Century warming, the question arises whether one can use information from past climate changes to constrain uncertainty in climate sensitivity. Such an approach is motivated, amongst others, by the fact that Antarctic ice cores reveal an impressive correlation between past levels of GHG concentration and reconstructed glacial temperatures (PETIT et al., 1999; STAUFFER et al., 2004). Furthermore a similar strong link can be inferred between Antarctic GHG concentrations and past changes in tropical sea surface temperatures (LEA et al., 2003), demonstrating the global relevance of changes in CO_2 concentration for past temperature evolution. Thus there exists an obvious motivation to use paleo-climatic information to evaluate, which models reveal the most likely climate sensitivity. We follow such a paleo-based approach and focus our analysis on the climate state of the Last Glacial Maximum (LGM, 21 kiloyears before present).

This climate state has attained a lot of attention in previous studies and is promising to constrain ΔT_{2x} (especially the upper end) for the following reasons:

- The changes in GHG concentrations are large.
- The climate signal is large.
- The cold climate persisted for millennia, so is in near-equilibrium.
- The forcing and response are reasonably well-known.
- Successful model simulations of glacial climate are available.
- Uncertainty in negative aerosol forcing affects the lower, not the upper limit of climate sensitivity.

Those arguments indicate a large potential embedded in paleo-climatic data for constraining the range of realistic model sensitivity. This is especially the case as shortcomings of recent studies, based on a comparison of simulated temperature evolution of 20th Century warming with observational data, can be avoided. Those approaches suffer from a weak signal to constrain the model response, and from non-equilibrium conditions, requiring to account for large uncertainty in oceanic heat uptake. In view of constraining high climate sensitivities, large uncertainty in negative aerosol forcing strongly affects the estimate of the upper ΔT_{2x} limit (as it partly shields the GHG warming – in contrast to the LGM, where negative aerosol forcing reinforces the temperature change).

We thus consider the LGM climate to be an ideal test case for constraining model sensitivity to changing GHGs and explore the key question of this thesis:

- *Can proxy-data, inferred from the LGM climate, effectively constrain the uncertainty range of climate sensitivity?*

Our way of approaching this task consists in running an huge ensemble of models versions, covering a broad range of ΔT_{2x}, for pre-industrial and LGM boundary conditions. We then analyse the simulated LGM cooling for constraining the set of realistic model versions. We describe the steps we undertook to answer the above question in the following section.

1.2 Outline of the thesis

It is standard practice to analyse the simulated temperature change, following a radiative perturbation of the system, by separating the model response into a radiative forcing and into a climate feedback component. As we apply this concept for the interpretation of our results we start with outlining its physical background in chapter 2.

Given the need for an improved quantification of uncertainty in climate sensitivity, a variety of studies have estimated the range of ΔT_{2x}. The analyses range from studies performed with simple climate models to simulations with state-of-the-Art climate models, from estimates inferred from a single model realization to ensemble-based approaches. Additionally, as there is no agreement for a “best method” of how to constrain the uncertainty range in an effective manner, several methods have been applied to estimate ΔT_{2x}. As we want to compare our results with recent ΔT_{2x} estimates for evaluating the potential of our approach, it is crucial to point out the differences in the methods applied. We therefore shortly introduce the status quo of this research area and outline the different approaches and results of those works (chapter 3). This helps us to classify the way we have chosen: The attempt to constrain the uncertainty range of ΔT_{2x} by applying LGM paleo-climatic information in an ensemble-based framework. To the best of our knowledge this is the first systematic approach into this direction, which we describe in section 3.1.

The prerequisite for the feasibility of our ensemble simulation study was to provide a set of computationally efficient climate models or model versions, which

cover a broad range of different sensitivity behaviour. In chapter 4 we motivate our choice for the model of intermediate complexity, CLIMBER-2, and shortly outline its main model characteristics in section 4.1. Additionally we describe our methodology for generating a large ensemble of model versions, that reveal a large spread in simulated ΔT_{2x}, by perturbing a set of specified model parameters (section 4.2 and 4.3).

In chapter 5 we present the different sets of performed ensemble experiments and discuss our modelling results. An often raised criticism regarding approaches, which infer ΔT_{2x} from information about past climate changes, is that the past is no direct analogue to future warming and that the feedback strength, being characteristic for the glacial climate, may well differ from the feedback strength, inferred from a doubling of CO_2 experiment ($2xCO_2$). We circumvent this problem by first performing an ensemble of $2xCO_2$ simulations for the whole set of model versions to calculate the value of climate sensitivity for each ensemble member (section 5.1), and then run the same model set for LGM boundary conditions (section 5.2) for checking the realism of simulated LGM climate and thus of model sensitivity (section 5.3).

Before we apply LGM proxy-data for constraining the range of ΔT_{2x} we want to ensure that we apply our method to a set of model versions that cannot be further constrained by present-day climate data. Therefore we first reject all ensemble members, which fail to meet a set of chosen consistency criteria for present-day climate characteristics (section 5.1). We then could proceed by defining a set of LGM data constraints, checking which set of models is compatible with reconstructed glacial cooling, and infer the range of likely ΔT_{2x} from those models. Yet we want to provide a broad basis to evaluate the realism of our glacial simulations and thus analyse the simulated LGM climate response in chapter 5.2. In doing so, we calculate the simulated individual glacial forcing strengths and analyse their impact on the LGM cooling response. This allows us to calculate the feedback parameter (the ratio of global-mean cooling to radiative forcing) not only for the glacial climate, but also separately for each individual forcing agent. We thus can evaluate to what extent the glacial feedback parameter is comparable to the value inferred from the $2xCO_2$ experiment, and can study the dependency of the feedback behaviour on the type of forcing. We then use this information for the interpretation of ΔT_{2x} estimates that are purely based on paleo-data.

The central part of our study consists in applying LGM proxy-data to narrow down the range of realistic model sensitivity. As the global coverage of proxy-data is rather poor, we perform the model-data comparison for well-defined regions. Concerning the choice for specific regions we considered the following criteria to be important: Availability of well-calibrated proxy-data, presence of a strong GHG induced cooling signal, large-scale representativeness of the temperature anomaly. In addition we considered the magnitude of model spread in regional temperature response for effectively discriminating between different model versions. In section 5.3.1 we motivate our choice for specific regions by performing additional ensemble simulations to evaluate the impact of GHG affected regional cooling and model spread. In section 5.3.3 we outline our methodology of how to infer statistical robust estimates of ΔT_{2x}, when we apply LGM proxy constraints. We evaluate the significance of our results in section 5.3.4 by analysing whether our ΔT_{2x} range is robust to assuming uncertainty in the model structure and in the glacial radiative forcing. Additionally we constrain ΔT_{2x} with proxy-information from different regions to investigate the impact of the

choice for a specific paleo constraint on our results.

Finally, in section 5.4. we explore the significance of our results in view of model independency. For this purpose we analyse the strengths of the key model feedbacks and compare those with a sampling of more complex models. This analysis allows us to interpret which physical processes mainly contribute to the inferred spread in climate sensitivity, and prepares the ground for future activities in the same line of constraining ΔT_{2x}. A proposal for an improvement for such a study is made in chapter 6, where we summarise our main findings.

2 Theoretical background

In this chapter we explain the underlying physics of the *greenhouse effect* and discuss how the earth system reacts to a perturbation of the energy balance between incoming and outgoing radiative fluxes (section 2.1). Assuming that this perturbation is small compared to a global-mean surface temperature of about 288°K (as is the case for anthropogenic warming) we describe a linear approximation for the temperature response (section 2.2).

Throughout this thesis we use the concept of *radiative forcing* and climate *feedbacks*, which allows a physical interpretation of the simulated temperature response. We therefore outline its theoretical background in section 2.3.

2.1 Theory of the greenhouse effect

We start with the planetary energy budget[1], which we express by the net flux *N* at the top of the atmosphere:

$$N = R\downarrow - R\uparrow \tag{2.1}$$

The flux $R\downarrow$ into the system describes the amount of energy received from the sun:

$$R\downarrow = \frac{1-\alpha}{4} S_0 \tag{2.2}$$

α describes the *planetary albedo* of the system (~ 0.3 for the earth-atmosphere system), defined by the ratio of reflected to received sun light. S_0 is the solar constant, given by the average amount of energy that reaches the top of the atmosphere, on a plane perpendicular to the sun's rays, at an average distance from the sun. Its actual value (~1366 W/m^2) depends on Earth's orbital parameters and on the activity of the sun. The factor of four accounts for the fact, that the earth surface is approximately a sphere. Thus the net solar energy flux into the earth-atmosphere system ($R\downarrow$) is about 240 W/m^2.

The temperature of the earth surface and of the atmosphere tends to adjust in a way that the absorbed solar energy is balanced by the thermal (long-wave) emission of the system to space. In equilibrium the flux $R\uparrow$ out of the system cancels the incoming solar radiation and is given by the thermal radiation of the earth system, which falls almost entirely into the infrared spectrum (λ between 4 to 50µm). According to the *Stefan-Boltzmann Law* the maximum amount of

[1] Energy fluxes entering (leaving) the system have a positive (negative) sign.

radiation that can be emitted by a body is given by:

$$R\uparrow_{\max} = \sigma T^4 \qquad (2.3),$$

with the *Stefan-Boltzmann constant* σ=5.66*10^{-8}Wm^{-2}K^{-4} and temperature T of the body. Objects that emit this maximum amount of radiation are referred to as *blackbodies*.

The incoming solar energy (240 W/m^2) is balanced by thermal emission if the earth system would radiate as a black body with an *effective temperature* of ~255°K. This implies, if the earth had no atmosphere (and the planetary albedo were unchanged), that the surface temperature would be around 33°K colder than what is measured in the presence of an atmosphere (about 288°K for global-mean surface temperature).

In the following we discuss a two-component system consisting of the earth surface and an atmosphere, in which the latter is a weak absorber in the visible and a strong absorber in the infrared. The *emissivity* ε describes the ratio of actual emission to blackbody emission and allows expressing the actual emission as:

$$R\uparrow = \varepsilon\sigma T^4 \qquad (2.4).$$

The earth surface and clouds (thicker than cirrus clouds) emit almost as blackbodies (ε*~1*), whereas the atmosphere emits with ε*~0.4-0.8*. Importantly the absorption of infrared radiation by the atmosphere is not caused by the main atmospheric constituents (N_2 and O_2), but by trace gases (H_2O, CO_2, O_3, and CH_4), which account for less than 1% of the atmospheric mass. According to Kirchhoff's Law, which states that absorptivity is equal to emissivity, the atmosphere with temperature T_A absorbs a fraction $\varepsilon_A \sigma T_S^4$ of the thermal energy radiated from the Earth surface to space (with ε_A*<1*), the rest ($(1-\varepsilon_A)\sigma T_S^4$) being transmitted. At the same time the atmosphere re-emits the absorbed energy by its own temperature ($\varepsilon_A \sigma T_A^4$). The radiation leaving the earth system than might be expressed by the fraction of transmitted thermal emission of the Earth surface and of re-emitted radiation by the atmosphere:

$$R\uparrow = (1-\varepsilon_A)\sigma T_S^4 + \varepsilon_A \sigma T_A^4 \qquad (2.5),$$

which can be re-formulated as

$$R\uparrow = \sigma T_S^4 - \underbrace{\varepsilon_A \sigma (T_S^4 - T_A^4)}_{greenhouse\,effect} \qquad (2.6).$$

Since the earth surface temperature exceeds that of the atmosphere (i.e. $T_S > T_a$) it can be seen from equation (2.6) that the thermal emission $R\uparrow$ is reduced by the presence of an atmosphere. The second term in equation (2.6) represents the so-called *greenhouse effect*. Its magnitude is increasing with either increasing

temperature difference ($T_S - T_a$) or increasing atmospheric emissivity ε_A.

For $R\uparrow$~ 240 W/m^2 and a surface temperature T_S ~288°K, the contribution of the greenhouse effect to the radiative balance is about 150 W/m^2. This energy flux represents that portion of the total long-wave radiation, which is trapped by the atmosphere, and constitutes the *natural* greenhouse effect. Through anthropogenic emission of greenhouse gases and other radiatively active components into the earth atmosphere the energy balance between $R\downarrow$ and $R\uparrow$ is perturbed in a way that the natural greenhouse effect is increased, i.e. that the trapping of infrared radiation by the atmosphere is more effective (*anthropogenic* greenhouse effect). In physical terms the increase of greenhouse gas concentrations results in a larger emissivity ε of the atmosphere, which means that the atmospheric level of mean emission is increased. Thus the mean thermal radiation of the atmosphere occurs at a colder temperature, which results in a reduction of thermal energy radiated to space.

We should note that the strongly simplified description of the system by its separation into a surface and an atmospheric component can not account for the fact, that there is not a single atmospheric temperature T_a, but that in nature the temperature strongly decreases with height. We thus should regard T_a as the effective temperature of the atmosphere and equation (2.6), which captures the fundamental mechanism of the greenhouse effect, as a strong simplification of the real system.

2.2 Perturbation of the energy balance

In the following we investigate how the earth system reacts to a perturbance of the radiative balance (e.g. caused by the emission of greenhouse gases). We start with assuming, that the net flux N at the top of the atmosphere is a function of quantities, which are either external (E) or internal $(I(T_S), T_S)$ to the system (SCHLESINGER, 1988). As we will focus our analysis on changes in the surface temperature T_S of the system, we explicitly describe T_S as an internal variable. All internal variables other than T_S are described by $I(T_S)$:

$$N = N(E, I(T_S), T_S) \qquad (2.7).$$

E is a vector, which represents a set of quantities, whose changes affect the climate state but which themselves are independent of the climate (which means they show no functional dependency on temperature). Typically E may represent such climate impacts as a change in the solar constant S_0, the release of radiatively active particles from volcanic eruptions and the anthropogenic release of greenhouse gases into the earth atmosphere. $I(T_S)$ describes a vector of internal processes, whose changes affect the climate and who themselves are modified by a changing climate, which means they constitute a feedback loop. Typical constituents are represented by the climatically induced changes in clouds, water vapour, vertical temperature profile and surface albedo.

We now consider a perturbation $\Delta N=\Delta R\uparrow+\Delta R\downarrow$ of the system, which is small compared to the magnitude of N, and thus express the change in the energy flux by:

$$\Delta N = \underbrace{\sum_i \frac{\partial N}{\partial E_i}\Delta E_i}_{RF} + \underbrace{(\frac{\partial N}{\partial T_S} + \sum_j \frac{\partial N}{\partial I_j}\frac{dI_j}{dT_S})}_{-\lambda^{-1}} \Delta T_S \qquad (2.8).$$

The first term in this equation describes the impact of a change in the external quantities E and will be referred to in the following as the so-called *radiative forcing RF*. The second summand represents the change in N owing to a change in surface temperature T_S and describes the feedback characteristic of the system (*feedback parameter* λ)[2]. Requiring a balanced energy budget ($\Delta N=0$) we can express the equilibrium temperature change of the system as

$$\Delta T_S = \lambda RF \qquad (2.9).$$

We further decompose λ into a component λ_0, the *direct temperature feedback*, and into a component F, the *indirect feedbacks*:

$$\lambda^{-1} = \lambda_0^{-1} - F \qquad (2.10)$$

λ_0 describes the surface temperature change $\Delta T_{0,S}$ owing exclusively to direct changes in temperature T_S. Thus it characterizes the response of a system, in which the energy balance can only be restored by a change in the temperature according to the Stefan Boltzmann Law and no other feedbacks besides λ_0 are allowed to come into play (i.e. all variables besides T_S are held constant). This feedback represents the largest negative feedback of the system and is given by:

$$\lambda_0 = -(\frac{\partial N}{\partial T_S})^{-1} \qquad (2.11),$$

The component F represents the sum of all feedbacks besides λ_0 (indirect feedbacks), characterizing those variables other than temperature T, whose changes affect the thermal emission to space:

$$F = \sum_j F_j = \sum_j \frac{\partial N}{\partial I_j}\frac{\partial I_j}{\partial T_S} \qquad (2.12).$$

Using equation (2.10) and (2.9) we express the change in surface temperature

[2] Some authors define a feedback parameter λ' the inverse way: $\lambda' = RF / \Delta T_S$.

as:

$$\Delta T_S = \frac{RF}{\lambda_0^{-1} - F} = \frac{\lambda_0}{1 - \lambda_0 F} RF \tag{2.13}$$

If there were no feedbacks besides the direct temperature feedback λ_0 the resulting temperature change would be given by

$$\Delta T_{0,S} = \lambda_0 RF \tag{2.14}.$$

We define the *gain G* of the system as the ratio of the temperature response including all (i.e. direct and indirect) feedbacks (ΔT) to the temperature response with only the direct temperature feedback acting (ΔT_0):

$$G = \frac{\Delta T_S}{\Delta T_{0,S}} = \frac{1}{1 - \lambda_0 F} \tag{2.15},$$

or when combining indirect and direct feedback contributions by defining the *feedback factor* $f = \lambda_0 F$ or individual feedback factors $f_j = \lambda_0 F_j$:

$$G = \frac{1}{1 - f} = \frac{1}{1 - \sum_j f_j} \tag{2.16}.$$

When describing the system response by the sum of all individual indirect feedbacks (F_j), we assume that the strength of each feedback is independent of all the other feedbacks and that the strength of the feedback is independent of the climate state. We thus assume linearity in the system. The validity of these assumptions will be discussed in section 2.3.4. Yet even if the feedback factors behave linearly the gain does not, as can be seen from Fig. 2.1, which illustrates the dependence of the gain *G* from the magnitude of the feedback factor *f*.

For a feedback factor of $f = 0$, the system response is given by the direct temperature response $\Delta T_{0,S}$ without indirect feedbacks controlling the temperature change. For $f < 0$ the system gain *G* falls in the range between 0 and 1, thus *f* represents a negative feedback. A feedback factor between 0 and 1 yields an amplification of the temperature response ΔT_0, thus representing a positive feedback. As *f* increases, the system gain increases sharply and approaches infinity as *f* approaches 1. We neglect values of $f > 1$ in our consideration, which yield physically meaningless results (e.g. an increase in the incoming energy ($RF > 0$) would result in a cooling of the system ($\Delta T < 0$)).

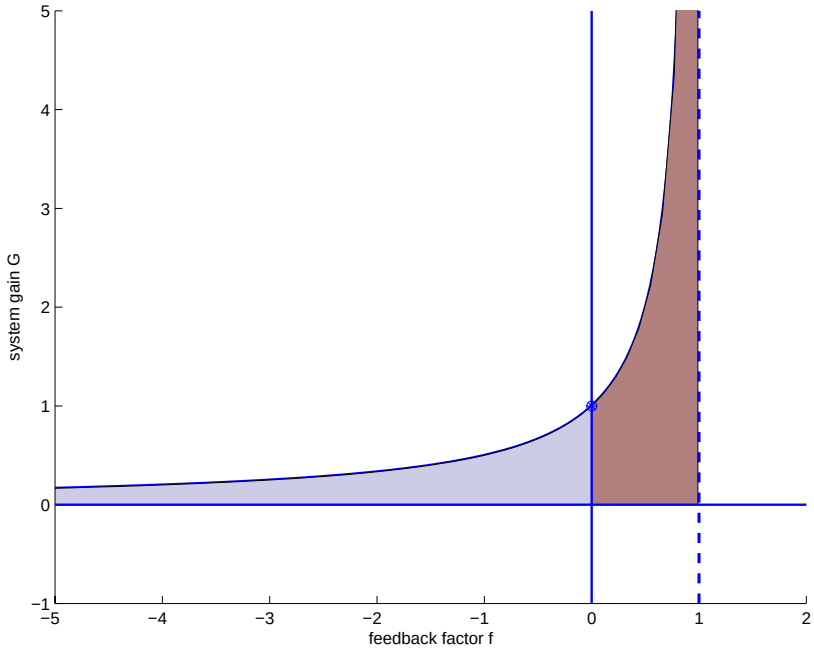

Fig. 2.1: Non-linear relationship between system gain *G* and feedback factor *f*. The bluish (reddish) shaded area under the curve illustrates a damping (amplification) of the system response, resulting from a negative (positive) feedback factor. The circle represents the system response without indirect feedbacks. The system behaviour for $f > 1$ yields physically implausible results and is not shown.

The non-linear relation between *f* and the system gain *G* illustrates the importance of an accurate guess in the magnitude of the feedback factor for estimating the system's temperature response following a radiative perturbation. The larger the assumed initial value of *f*, the larger is the absolute effect on ΔT, which results from an additional increase in *f* (HANSEN et al., 1984; SCHLESINGER, 1988). This means that the impact of a given feedback on ΔT is strongly dependent on the presence of other feedbacks: If once a strong positive feedback exists, the addition of a rather moderate positive feedback may produce a large additional temperature change. If we assume e.g. a feedback factor f_1 of 0.5 for water vapour, then the equilibrium temperature change will be twice the magnitude of $\Delta T_{0,S}$ (equation (2.15) and (2.16)). If now a further feedback factor f_2 of only half the magnitude of f_1 will be added (f_2=0.25), then the equilibrium change in temperature will be four times the value of $\Delta T_{0,S}$.

2.3 Radiative forcing and climate feedbacks

Having analysed how the earth system reacts to a small perturbation of the radiation budget, we now further explore the basic concepts of *radiative forcing* and of *climate feedbacks*.

As we have seen from equation (2.8) we can express the change in the radiative

balance of the earth system by a term, which results from changes in the external quantities (radiative forcing *RF*), and by a term, which accounts for the internal system's feedback behaviour (feedback parameter λ). The fundamental basis for many climate change studies is the assumption of a universal relationship between the global-mean forcing *RF* and the global-mean equilibrium surface temperature response ΔT_S (equation (2.9), independent of the magnitude and nature of the applied forcing and independent of the climate state. This implies an universality of the feedback parameter λ. If the feedback parameter was known, the equilibrium temperature response could simply be scaled corresponding to the magnitude of the applied forcing (HARVEY, 2000; IPCC, 2001) and there would be no need to calculate λ for each type of forcing and background climate separately.

In the following we explore in how far the above assumptions hold in view of the dependency of λ on the nature (agent, magnitude, pattern) of the forcing and on the climate state.

2.3.1 Invariance of the feedback parameter λ

The issue of invariance of the feedback parameter λ has been subject to many model studies (e.g. HANSEN et al., 1997; JOSHI et al., 2003; HANSEN et al., 2005b). It is not self-evident that λ should be the same for different types of forcings. The degree to which λ might differ depends on the degree to which a different feedback behaviour might be evoked (HARVEY, 2000).

The dependence of λ on the *nature* of the forcing has been analysed by comparing the surface temperature response, resulting from changes in well-mixed greenhouse gas concentrations, to those inferred from changes in the solar constant (IPCC, 2001). At a first glance the system's behaviour in view of the partitioning between tropospheric and surface radiative fluxes may appear much different. In case of the greenhouse gas forcing, the mean heating occurs in the troposphere, whereas for solar forcing the surface is heated most. Yet the tight coupling between those two system components reveals that the difference in the initial partitioning between troposphere and surface warming is not crucial for the equilibrium surface temperature response (HARVEY, 2000). Further studies (HANSEN et al., 1997; JOSHI et al., 2003) have underlined that the temperature response is rather independent (with deviation up to about 20%) of the type of forcing what concerns solar variation, well mixed greenhouse gases and scattering aerosols. Yet distinct differences in the system response had been inferred from simulations, where the forcing was realized by changes in ozone concentration and absorbing aerosols. The main reason for discrepancy is seen in the vertical distribution of these forcings, which may provoke pronounced changes in the lapse rate and cloud behaviour (HANSEN et al., 1997). A positive forcing in a given atmospheric layer (e.g. through absorption of tropospheric aerosols) warms that layer and thus tends to decrease cloud cover. Since the net effect of clouds depends on their height, the cloud feedback depends on the vertical partitioning of the forcing. Thus the sensitivity of the climate response to the altitude and latitude of the forcing should be accounted for, when considering not homogeneously distributed forcings.

Regarding the invariance of λ on the *climate state* several studies with

comprehensive climate models have shown that λ may exhibit a dependence on the background climate, but results exhibit a large degree of model dependency (e.g. BOER and YU (2003) find a slight decrease in λ as the climate warms, whereas SENIOR and MITCHELL (2000) find an increase, and WATTERSON (2000) almost no dependency).

To summarize, the concept of radiative forcing and climate feedbacks has proven to be a useful tool (given the limitations discussed above) for analysing the simulated climate response – regarding global-mean temperature change, and (to a minor extent) for regional temperature change (IPCC, 2001).

2.3.2 Time scale separation between forcing and feedbacks

The separation between a climate *forcing* and a climate *feedback* is motivated by the fact that different components of the earth system react on different time scales given a perturbation in the energy balance. The radiative forcing constitutes an instantaneous perturbation of the energy budget: It may be realised through the modification of the fluxes $R\downarrow$ (resulting e.g. from variations in S_0) or $R\uparrow$ (resulting e.g. by an increase in atmospheric CO_2 content) but with surface and atmospheric temperature and climate state held fixed at their unperturbed values (*instantaneous forcing*). The climate feedbacks represent a time evolving process and only successively come into play as the climate changes. The radiative forcing is meant to describe that amount of energy flux, that actually forces or drives the equilibrium climate response. Yet it has been shown, that the instantaneous forcing is not an ideal approximation for the equilibrium surface temperature change. The definition of an *adjusted* forcing, which accounts for the fast response time of the stratosphere, proved to be a much better predictor for the resulting change in equilibrium surface temperature (HANSEN et al., 1997; IPCC, 2001; JOSHI et al., 2003). As the stratosphere and the troposphere are only weakly coupled, the former reacts quickly to a radiative perturbation (within months) and independently of the surface-troposphere system, while the latter reacts on a timescale of decades, caused by the strong coupling of the troposphere to the surface (the thermal inertia of the oceans strongly delay the atmospheric response). To account for the difference in the time scale of tropospheric and stratospheric temperature response, the adjusted forcing is calculated *after* the stratosphere has been allowed to reach its radiative equilibrium. Yet this calculation requires defining where the tropopause is located, which may introduce a certain degree of model dependency (SHINE et al., 2003). Since the release of the third assessment report (TAR) of the IPCC further concepts of describing the radiative forcing have been developed for providing improved predictors of equilibrium temperature change (HANSEN et al., 2005b; JOSHI et al., 2003).

2.3.3 Climate feedbacks

The magnitude of the equilibrium temperature response to the applied radiative

forcing is controlled by the climate feedbacks[3]. Their magnitude is strongly model-dependent and is the main reason, why predictions of future temperature change differ for the same radiative forcing scenario. In the following we discuss the main feedback mechanisms, which amplify or dampen an initial radiative perturbation of the earth-atmosphere system.

2.3.3.1 Water vapour feedback

The largest positive feedback in the system results from the ability of water vapour to trap thermal (long-wave) radiation by increasing the infrared opacity of the atmosphere. This means that the mean level of long-wave emission is shifted to higher altitudes, where the temperature is lower. This results in a more effective trapping of long-wave radiation (see equation (2.6)). In the presence of water vapour an initial change in surface temperature is assumed to be approximately doubled (CESS et al., 1990; HELD and SODEN, 2000; IPCC, 2001).

Changes in the *amount* and in the *vertical distribution* of water vapour determine the strength of this feedback. In a warmer climate the atmosphere can hold more water vapour. A theoretical constraint on the water vapour feedback is given by the *Clausius Clapeyron equation,* which predicts an approximately exponential increase in the maximum amount of water vapour with temperature (while *relative humidity*, the ratio of the actual vapour pressure of the air to the saturation vapour pressure, is conserved). As the absorptivity of water vapour is proportional to the logarithm of its concentration, the fractional change in water vapour mass, not the absolute change governs its strength as a feedback mechanism (SODEN et al., 2005). Thus changes in the vertical profile play an important role for the magnitude of the overall feedback. Especially changes of water vapour content in high altitude layers, where the concentration of water vapour is low, may constitute a rather large increase in the strength of the water vapour feedback. Although it should be noted that such an increase tends to be (partially) cancelled by the negative feedback produced by concurrent changes in the vertical temperature profile (HANSEN et al., 1984; COLMAN, 2001; see next section).

2.3.3.2 Lapse rate feedback

If the decrease in surface temperature with height (*lapse rate*) is not fixed but allowed to evolve freely, then a feedback comes into play, which either amplifies (the vertical profile increases) or dampens (the profile decreases) the equilibrium response. If the lapse rate decreases with rising surface temperature, then the upper troposphere warms more than the lower atmospheric layers and by more compared to a fixed lapse rate. This results in a larger increase of outgoing long-wave radiation than without changes in the vertical temperature profile. This in turn means that the surface temperature has to increase less to balance the energy budget. Thus a decrease in the lapse rate constitutes a negative feedback. This kind of behaviour is seen in the temperature response of low latitudes. In high latitudes the lapse rate feedback reverses its sign and amplifies the initial temperature change. This characteristic latitudinal behaviour of this

[3] In the following we use the term “feedback” for referring to the indirect feedbacks described in section 2, unless we explicitly refer to direct or indirect feedback components.

feedback is expressed in the typically “U-shaped” temperature response seen in doubling of CO_2 experiments (maximum warming at the poles, minimum warming at the equator)[4].

As noted in the previous section, modelling studies inferred an anti-correlation between global lapse rate and water vapour feedback (HANSEN et al., 1984; COLMAN, 2003a). A physical explanation is given by the fact that a major contribution to both feedbacks comes from the tropical upper troposphere, where a maximum of warming (strong negative lapse rate feedback) produces a sharp increase in the amount of water vapour (positive water vapour feedback) (HARVEY, 2000).

2.3.3.3 Cloud feedback

The most uncertain of the feedback components is that due to changes in clouds. Even the sign of this feedback is uncertain, as clouds can amplify or dampen an initial perturbation of the energy budget. Clouds cool the climate by reflecting the incoming solar radiation, as they increase the planetary albedo. This effect is the more important the larger the incident radiation and the smaller the albedo of the underlying surface. On the other hand clouds warm the climate as they absorb infrared radiation from the earth surface and re-emit this energy at a colder temperature, thus reduce the energy emission to space (greenhouse effect). The higher the clouds are located the larger is the resulting warming. The net effect of clouds on the climate thus is a warming for high clouds and a cooling for low clouds.

Additional to changes in the altitude and amount of clouds, changes in the thickness and cloud radiative properties (optical depth) crucially contribute to the magnitude and sign of the resulting cloud feedback. Although compensating effects between long-wave and short-wave cloud feedbacks (i.e. models tend to produce offsetting long-wave and short-wave responses (COLMAN et al., 2001) help to stabilize the climate response (YAO and DEL GENIO, 1999), the spread in the remaining net feedback is still very large. The broad variety of processes which contribute to cloud formation and cloud-radiation interaction complicate a representation of this feedback in climate models and lead to a need to describe (most of) these processes by means of parametrisations (IPCC, 2001). As specific descriptions of the cloud behaviour may differ greatly between climate models, uncertainty in the cloud feedback has proved to yield the largest contribution to the uncertainty in total feedback strength (CESS et al., 1990; COLMAN, 2003a) and often is regarded as *the* key uncertainty in climate modelling studies.

2.3.3.4 Surface albedo feedback

As the climate warms, the area covered by sea ice or snow covered regions is reduced and replaced by surfaces types with smaller albedo, which in turn further

[4] Sea ice and snow albedo feedbacks additionally contribute to the poleward amplification of the warming.

enhances the warming. This amplification is referred to as *surface albedo feedback*. Although this feedback may exert a strong amplification of an initial warming (or cooling) the net feedback may be strongly dependent on concurrent changes in cloud cover (RANDALL et al., 1994; HARVEY, 2000).

Besides changes in the area of ice and snow, vegetation changes also can strongly contribute to this feedback by replacing one biome by another and thus significantly alter the surface reflectivity.

2.3.4 Feedback interactions and non-linear feedback contributions

When we have described the temperature response (2.13) as a result of the sum of all feedbacks (2.12), we have assumed the individual feedbacks to be independent from each other and from the climate state.

In view of the feedbacks' independence, in the previous section we have pointed at the anti-correlation between water vapour and lapse rate feedback. Although the non-linear contributions (cross terms) by those feedbacks may be large, they do not invalidate the linear approximation (2.8) as they constitute physically competing effects (with a tendency to cancel out each other through their pronounced anti-correlation; COLMAN et al., 1997).

Regarding the dependence of the feedback strength on the climate state COLMAN et al., (2001) showed that for increasing global temperatures a slight increase in water vapour feedback strength arises next to a (more pronounced) decrease in the albedo feedback strength. The non-linearities, although important for individual feedback components, generally are assumed to represent second order effects on a global scale (and for small perturbations of the energy budget), as they largely constitute offsetting feedback contributions (HANSEN et al., 1984; SCHLESINGER, 1988; COLMAN and MCAVANEY, 1997; COLMAN et al., 2001). Thus locally highly non-linear processes (e.g. due to a change in cloud behaviour) are not assumed to provoke dominating global non-linearities.

2.3.5 Transient climate change

So far we have neglected transient aspects in our considerations. As we will focus our analysis described in this thesis exclusively on changes in equilibrium characteristics of the earth system we only shortly discuss the transient system behaviour.

As soon as the Earth warms, a large heat flux from the atmosphere into the ocean arises, which offsets to a large amount the increase in atmospheric temperature. Thus equation (2.9) has to be extended to describe this additional heat flux $\dot{H}(t)$ by:

$$\Delta T_S = \lambda(RF - \dot{H}(t))$$

The last term describes the time-dependent rate of ocean heat uptake, which disappears in case the system has reached its equilibrium state. Measurements of ocean temperatures during the last 50 years allow estimating this quantity in case of anthropogenic climate change (LEVITUS, 2001; LEVITUS et al., 2005). This additional heat flux into the ocean causes a pronounced transient imbalance in the energy budget (HANSEN et al., 2005a): The earth system is absorbing more energy from the sun than is emitted to space.

Studies, which aim to determine λ from a transient experiment, thus have to explicitly account for the rate of ocean heat uptake, which constitutes an additional large source of uncertainty for those approaches.

3 Uncertainty in climate sensitivity

The uncertainty range of 1.4-4.5°C (IPCC, 2001) for climate sensitivity has remained essentially unchanged during the last decades. Yet within the recent years increasing computational power has allowed accounting more systematically for so far unexplored parameter uncertainty. A number of ΔT_{2x} estimates have been made, based on different approaches, and the concern was raised that the commonly accepted consensus-range of 1.4-4.5°C might strongly underestimate the risk of a much larger warming. In this chapter we shortly outline the main approaches to constrain uncertainty in ΔT_{2x}, describe the way we pursue, and shortly discuss recently made estimates of climate sensitivity.

3.1 Approaches for constraining uncertainty in climate sensitivity

Several approaches have been pursued in the past to estimate the magnitude of climate sensitivity. The first ("bottom-up") approach is based on a quantitative understanding of the physical mechanisms: The direct changes in radiation balance and associated positive and negative feedbacks, such as water vapour, cloud, albedo and lapse rate feedbacks, which can be calculated by models. The underlying processes can only be validated to some extent by observations of modern climate, as observational data always include the information of all the feedbacks, which are present in the climate system. A separation into the individual feedback components is only feasible to a certain degree, e.g. by distinguishing between cloud free and cloud covered regions to separate the impact of cloud feedback (CESS et al., 1990; WATTERSON et al., 1999). Thus uncertainty in the strength of the main feedback mechanisms is still considerable, and hence it has not been possible on this basis to reduce the range of uncertainty of ΔT_{2x} in the recent decades.

The second ("top-down") approach is to analyse how climate has changed in the past when greenhouse gas (GHG) concentrations have changed. Several studies have followed the latter approach in considering data for the Last Glacial Maximum (LGM, ~21 kilo years before present) (HOFFERT and COVEY, 1992; HANSEN et al., 1993; COVEY et al., 1996). One of the difficulties here is that there is no direct past analogue for a future large increase in GHG concentrations, with all other factors influencing climate being the same as today. Generally, several climate forcings have changed simultaneously, making it difficult to isolate the effect of GHGs, although this can be tried by using multivariate analysis on long time series (LORIUS et al., 1990). Also, the mean climate state was different in the past (e.g., much colder during Glacials), hence the strength of feedbacks such as albedo or cloud feedback probably differed as well.

In this thesis, we apply a "third way" of deriving ΔT_{2x}, based on systematically combining our understanding of the physics with data from past climate evolution, including uncertainty in both factors. The basic idea is to generate an ensemble of many climate model versions with different parameters and hence different strengths of relevant feedbacks, in order to span the current uncertainty in

physical understanding, and then use observational or proxy-data to constrain which subset of these models (and hence what range of ΔT_{2x}) is compatible with pre-industrial climate and past climate evolution. In chapter 5.3 we apply this method for the climate of the Last Glacial Maximum. This period represents probably one of the largest deviations from present climate in recent geologic history and thus offers an important test to reject those model versions, which fail to reproduce the distinctively different glacial temperature regime.

In the past several studies have focused on the glacial climate to estimate the sensitivity of the climate system. While some authors have discussed ΔT_{2x} in the context of a single LGM simulation (HEWITT and MITCHELL, 1997; BROCCOLI, 2000), our approach represents the first estimate of ΔT_{2x} (to the best of our knowledge) that is based on an ensemble of fully-coupled simulations for the LGM climate[5].

3.2 Recent estimates of climate sensitivity

The approach of combining ensemble simulations with observational data has previously been applied to the 20th Century climate change, i.e. the period of anthropogenic increase in CO_2 concentration (FOREST et al., 2002; KNUTTI et al., 2002). The conclusion from these ensemble simulations is that the anthropogenic warming signal is too weak to effectively constrain ΔT_{2x}, due to uncertainty in the radiative forcing over the industrial period (see Fig. 3.2), in the observational data and in the rate of ocean heat-uptake. Similar studies in this line, also focusing on the historical warming (about 0.7-0.8°C for global-mean surface temperature between the pre-industrial climate and today (IPCC, 2001), fail as well in effectively constraining the ΔT_{2x} range, particularly the upper bound (ANDRONOVA and SCHLESINGER, 2001; GREGORY et al., 2002); i.e., within current physics uncertainty it is possible to construct models with a very high ΔT_{2x} (~7°C), and such models are not ruled out by the relatively small 20th Century warming. An overview of probabilistic ΔT_{2x} estimates, inferred from those recent studies, is given in Fig. 3.1. This compilation is not complete, as most recent data of forthcoming studies are not yet available, but it impressively illustrates the main conclusion of those studies: A pronounced increase in the upper limit of ΔT_{2x} compared to the IPCC range.

For those studies, which follow the approach to constrain climate sensitivity by focusing on the temperature increase between the pre-industrial and modern climate, the uncertainty in the observational data, in the rate of heat uptake by the ocean and especially the large uncertainty in aerosol forcing constitute the main reasons for the inability to reject high sensitivity model versions. The latter uncertainty reflects the fact that large values of the direct and indirect forcing (Fig. 3.2) can not be rejected by observations (ANDERSON et al., 2003) such that a possibly large aerosol shading in combination with a high climate sensitivity yields a comparatively moderate simulated temperature increase over the last

[5] Recently a similar LGM ensemble study has been published with a low resolution atmospheric GCM coupled to a slab ocean (ANNAN et al., 2005). In section 5.3.4 we will discuss the differences in the inferred ΔT_{2x} range between this study and our simulations.

century, consistent with observational data (ANDREAE et al., 2005).

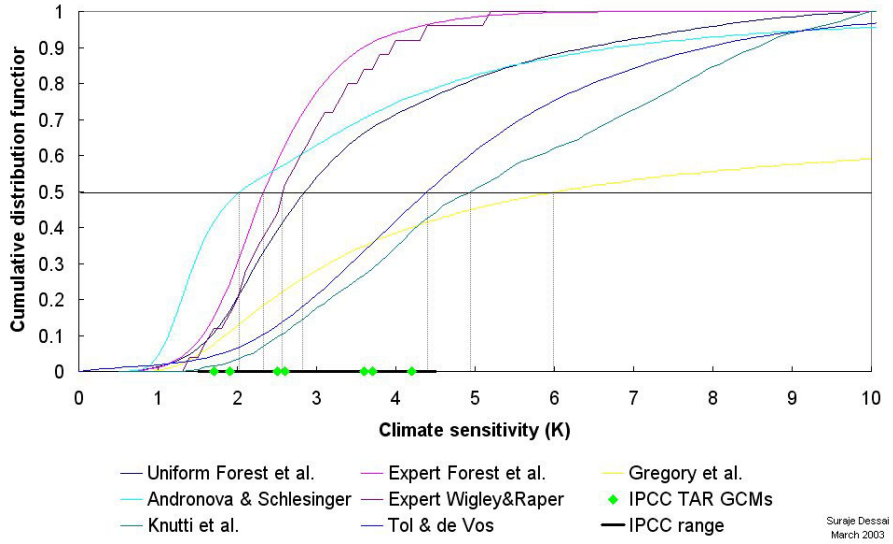

Fig. 3.1: Cumulative distribution of climate sensitivity from recent studies (courtesy of S.Dessai (DESSAI and HULME, 2004)). Green diamonds indicate the inferred magnitude of comprehensive climate models (IPCC 2001), while the black line represents the IPCC "consensus" range. The thin horizontal black line intersects each study at its most likely value.

SCHWARTZ (2004) suggests that uncertainty in aerosol radiative forcing must be reduced at least three-fold to reach a meaningful bound on climate sensitivity. Although observational methods have been improved over the last decades, especially in view of the availability of satellite data, uncertainty in anthropogenic aerosol radiative forcing will remain the likely major contributor to the inability of comparisons between simulated and observed anthropogenic temperature change to effectively constrain the uncertainty range in climate sensitivity in the near future.

Fig. 3.2 illustrates the large uncertainties regarding the main forcings for the industrial period (1750-2000), and especially demonstrates the strong weight of the indirect aerosol forcing: Its estimated range is large and underlines the possibility of low net radiative forcing over the industrial period.

Due to their high computational demand fully-coupled General Circulation Models (GCMs) have not been used so far for exploring uncertainty in climate sensitivity in an ensemble-based framework. Yet the use of public computer resources has recently enabled to perform a first grand ensemble (an ensemble of ensembles) of a state-of-the-Art atmospheric model (ALLEN, 1999; STAINFORTH et al., 2005), coupled to a mixed layer ocean. The authors generated a set of different model versions by perturbing six model parameters to explore the range of likely ΔT_{2x} and then constrained this ensemble by annual mean data of modern day climate. The outcome was that climate sensitivities as high as eleven degrees could not be rejected. Although this range seems dramatic and demonstrates impressively that a change in a small number of uncertain model parameters can crucially modify the sensitivity of a given climate model, the study demonstrates at the

same time that this test of model quality is not very informative. When considering additional data information, such as the annual cycle, those extreme models reveal to be inconsistent with climatology (KNUTTI et al., 2006). It is the *change* in simulated temperature, which has to be focused on for evaluating the performance of climate models regarding changes in the energy balance of the system. As a final comment it should be noted that an inferred large upper limit for climate sensitivity from studies, following the top-down approach, is no positive evidence for large values of ΔT_{2x} but a lack of ruling those out.

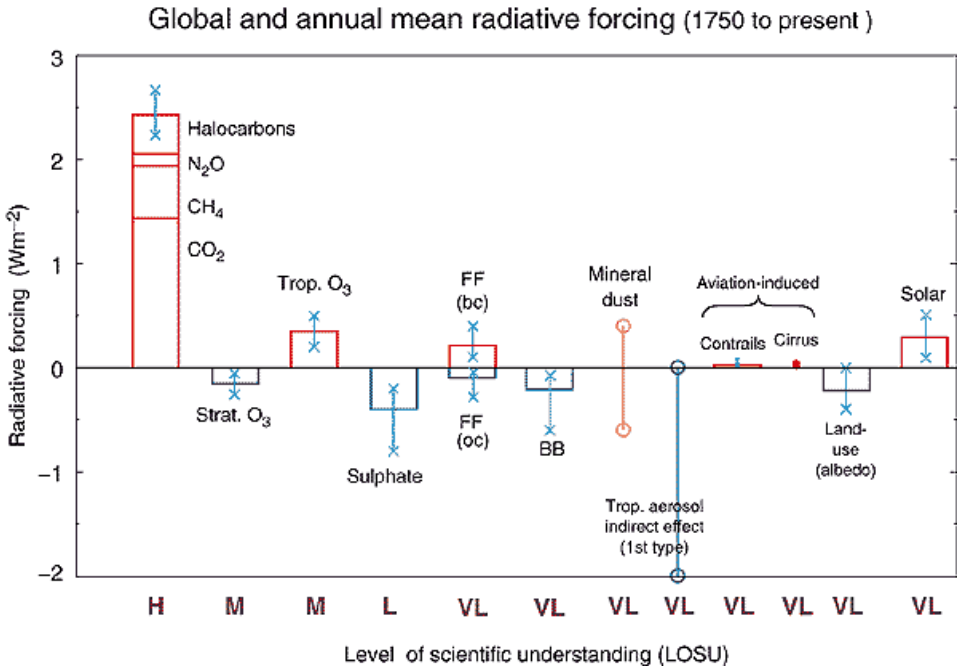

Fig. 3.2: Global, annual mean radiative forcings for the industrial period (1750 to 2000); figure from IPCC (2001). The height of the rectangular bar indicates that a central or best estimate value while its absence denotes no best estimate is possible. The vertical line about the rectangular bar with “x” delimiters indicates an estimate of the uncertainty range, a vertical line without a rectangular bar and with “o” delimiters denotes a forcing for which no central estimate can be given owing to large uncertainties. A “level of scientific understanding” index is accorded to each forcing, with H, M, L and VL denoting high, medium, low and very low levels, respectively.

4 Experimental design

In the framework of our study we aim to perform a large ensemble of fully-coupled equilibrium climate simulations, for boundary conditions of present-day climate, of doubled atmospheric CO_2 content, and of the Last Glacial Maximum (LGM). For the analysis of our simulation results, e.g. the calculation of the model inherent feedback strengths, an additional large amount of model runs is required. Given the long time scale for reaching equilibrium conditions for fully-coupled climate models (in the order of some thousand of years) the computational burden for such simulation experiments in an ensemble framework is huge. Thus one important requirement for our study regards computational efficiency of the climate model used.

One further requirement concerns the degree of model complexity and spatial resolution: We aim to compare simulated large-scale regional temperature change at the LGM with reconstructed temperature data. Thus the model should resolve large-scale temperature anomalies and should incorporate the main physical processes, which determine the pronounced difference in the temperature regime between the present-day and glacial climate.

Comprehensive climate models (GCMs) are the best tools in view of the latter aspect, yet due to their large computational demand they cannot be applied for an excessive ensemble study in a fully-coupled simulation design[6]. Simplified climate models (e.g. energy balance models) fulfil the requirement of computational efficiency but fail in terms of a sufficient degree of model complexity. To fill the gap between comprehensive and simplified climate models, Earth system Models of Intermediate Complexity (EMICs) have been developed (CLAUSSEN et al., 2002). We will focus our analysis on this model type and will use the CLIMBER-2 model for our climate simulations. Its computational efficiency (1000 model years equal about 1 CPU hour) and degree of model complexity make it an ideal tool for the type of extensive ensemble studies presented in this thesis.

The model will be shortly described in the next section, with a focus on the atmospheric module, given that we concentrate our analysis on key atmospheric feedback characteristics. The remaining sections of this chapter inform about the choice of model parameters, which enter our analysis, and about the scheme for sampling our eleven dimensional parameter space. Finally an overview of all applied boundary conditions for the different type of experiments, performed in this thesis, is given.

[6] In this context the *Climateprediction Project* should be mentioned, which uses public computer resources for the realization of ensemble based climate simulations (www.climateprediction.net). Although first results demonstrate the feasibility of realizing GCM ensembles, the computational burden is still too demanding for an excessive simulation design (e.g. including a large set of sensitivity experiments as presented in this thesis).

4.1 Description of the applied climate model

We use the climate model of intermediate complexity CLIMBER-2, consisting of a statistical-dynamical 2.5-dimensional atmosphere model (with parametrisations of the synoptic-scale activity), coupled without flux adjustments to a multi-basin, zonally averaged ocean model (PETOUKHOV et al., 2000). The model has a coarse spatial resolution, but captures the main characteristics of Earth's geography (Fig. 4.1).

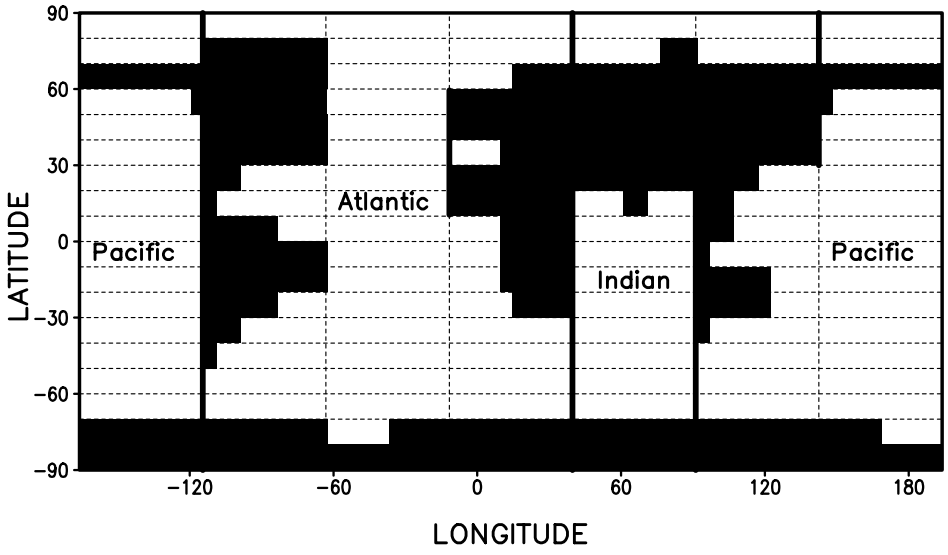

Fig. 4.1: Continental mask of CLIMBER-2. Solid lines separate the three ocean basins (Pacific, Atlantic, Indic), dashed lines illustrate the atmospheric grid boxes.

The latitudinal resolution of the atmospheric model amounts to 10°, whereas the longitudinal model dimension is separated into seven sectors of equal width (51.4°). A universal vertical structure for temperature and humidity is assumed, which allows us reducing the atmospheric description to two dimensions by describing vertically averaged prognostic equations for temperature and water vapour. The vertical profile, which is supported by many empirical studies (OORT and EM, 1971; WALLACE and HOBBS, 1977), thus allows reconstructing the 3-dimensional structure of temperature and humidity for the computation of horizontal transport and radiative fluxes. All variables other than temperature T and humidity q are diagnostically expressed in terms of T and q.

The atmospheric module ranks among the class of *statistical-dynamical* models (SALTZMAN, 1978), which describe the long-term evolution of the atmosphere by large-scale long-term fields of the main atmospheric variables, and represent the synoptic scale by means of averaged statistical characteristics. This approach is phenomenologically based on (i) the existence of a pronounced stable minimum

in the power spectra of the main atmospheric variables (timescale from 10 days to a couple of months) (VINNICHENKO, 1970; MITCHELL, 1976), and (ii) on the existence of a characteristic horizontal spatial correlation radius for the synoptic component (order of 1000-3000 km) (HASSELMANN, 1976; LEMKE, 1977) .

The oceanic module is represented by a multi-basin, zonally averaged model (STOCKER et al., 1992) with a latitudinal resolution of 2.5° and 20 non-equidistant vertical levels, and an oceanic diffusion scheme after BRYAN and LEWIS (1979).

A crucial aspect for our analysis is that the CLIMBER-2 model does not rely on flux adjustments to avoid climate drift from present-day climate. As we want to realize ensemble simulations of the LGM climate, which strongly differs from present-day conditions, the use of flux adjustments would impose a strong limitation on the applicability of the model for such type of simulation experiment. For a detailed model description the reader is referred to PETOUKHOV et al. (2000) concerning the atmospheric module and to STOCKER et al. (1992) concerning the representation of the ocean module.

The simulated atmospheric and oceanic characteristics of the pre-industrial climate agree well with observational data (PETOUKHOV et al., 2000). Several sensitivity studies, e.g. of the model's response to a CO_2 concentration increase, qualitatively agree with results of GCMs (GANOPOLSKI et al., 2001). Driven by natural and anthropogenic forcings, the model reproduces the temperature variations over the last millenium (BAUER et al., 2003). Simulated glacial climate shows many characteristics seen in proxy-data, both for the mean state (GANOPOLSKI et al., 1998) and for abrupt climate changes (GANOPOLSKI and RAHMSTORF, 2001).

An important requirement for our study is that the model simulates the key feedbacks that determine the magnitude of climate sensitivity (ΔT_{2x}), namely the cloud-, water vapour-, albedo- and lapse rate feedback. This is the case, with simulation of two cloud types, atmospheric lapse rate and tropopause height, a thermodynamic sea-ice and a land snow-cover module.

4.2 Parameter choice

The aim of our study is to generate a set of CLIMBER-2 versions, which covers a broad range of climate sensitivities. In contrast to more simplified models, ΔT_{2x} is not a tuning parameter in our model, but arises from the model dynamics. We thus selected those tuning parameters of CLIMBER-2 that are most influential on the strength of the model intrinsic individual feedbacks (see Appendix B). For this choice we have not touched parameters, which are known empirically or from theory, but those model parameters, which are subject to uncertainty. In the view of model tuning we stress that – in contrast to simple models – the number of degrees of freedom for CLIMBER-2 is some orders of magnitude higher than the number of tunable parameters.

As we focus our analysis on the model sensitivity to changes in CO_2 content (ΔT_{2x}), i.e. on a model characteristic that is strongly determined by atmospheric processes (MEEHL et al., 2004), we mainly concentrate on the atmospheric module for the choice of our parameters. We begun our analysis with a set of

sensitivity experiments, in which we investigated the effect of 13 atmospheric parameters (describing cloud and water vapour characteristics, lapse rate behaviour, tropopause height, direct radiative forcing of CO_2) on the simulated present-day climate and on the temperature response to doubled CO_2 concentrations. From those simulations we decided to focus on a subset of 9 parameters which strongly affect the sensitivity behaviour of CLIMBER-2. Additionally we account for uncertainty in the simulated oceanic heat uptake by including two further parameters into our analysis (horizontal and vertical ocean diffusivity), which describe mixing properties in the ocean.

For each run of our ensemble simulations all 11 model parameters have been simultaneously perturbed over carefully chosen ranges, which are given in Appendix B. The sampling of the individual parameter values is described in the following section.

4.3 Sampling strategy

The high dimensionality of our parameter space requires an appropriate sampling scheme in order to infer a robust estimate of the statistical moments or quantiles of interest. As (FOREST et al., 2002; KNUTTI et al., 2002) have done for their parameters choice, we explore the parameter space according to a systematic Monte Carlo scheme. First, for any of the 11 perturbed parameters we specified the interval for which the related parametrisation is meaningful according to the authors of the model (see Appendix B). For our study, these authors represent the "experts" specifying "prior knowledge" according to the requirements of the Bayesian School. As no pronounced prior knowledge on correlations among the parameters was formulated, we follow the standard procedure and assume the prior distribution as uncorrelated among the parameters. Furthermore, as a continuous cut-off at the boundaries appears most natural we assume symmetrically beta-distributed (shape parameter of 1.75) uncorrelated parameters, hence, we conservatively assume a rather broad maximum of any marginal prior distribution. Finally, as we vary some parameters over orders of magnitude, we link the distributions to the logarithms of the parameters rather than the parameters themselves.

We sampled this 11 dimensional, uncorrelated prior by a *Latin-Hypercube* scheme (HELTON and IMAN, 1982) that represents an efficient variant of the Monte Carlo method. The purpose of this sampling scheme is to achieve a better coverage of the sample space than realized by a pure random sampling. For this method the specified range of each of our model parameters x_i, (i=1,2,…,11) is divided into N intervals of equal probability, and one parameter value is selected for each interval at random. The result are N non-overlapping realisations for each of the 11 model parameters. The N values for parameter x_1 then are paired at random (without replacement) with the n values of x_2. These n pairs are again randomly combined with x_3, and so forth. The process is continued until we have created a set of N 11-dimensional input parameter vectors for our analysis.

This sampling strategy resulted in a quite narrow range of ΔT_{2x} (2.0-3.8°C) for an ensemble of 5,000 model runs (in the following termed "uncorrelated ensemble" (*UE*)). While so far we have followed the standard procedure to initiate a rigorous Bayesian analysis, we also would like to ensure that the intervals we derive for

ΔT_{2x} are a result of climate dynamics constraints rather than of the prior probability density chosen (see for a discussion on the choice of prior (FRAME et al., 2005)). Hence, in the spirit of robust Bayesian statistics, we employ a second prior distribution that shall lead to much more conservative estimates of ΔT_{2x}. For that purpose we modified the sampling scheme with the aim of higher weighting those parameter combinations that yield low and high ΔT_{2x}, thus increasing the sampling probability for the tails of the resulting distribution of ΔT_{2x}. We achieved a large range of ΔT_{2x} by positively (negatively) correlating (factor ±0.9) all atmospheric parameters whose variations change ΔT_{2x} in the same (opposite) direction, e.g. we *systematically* (not randomly) combine positive and negative contributions to ΔT_{2x} of each parameter x_i, and thus of the corresponding feedbacks. For the generation of this highly correlated parameter ensemble we have used the program *SIMLAB* (*www.jrc.cec.eu.int/uasa/primer-sa.asp*), which applies the *restricted pairing technique* for the generation of correlated parameter samples, as proposed by IMAN and CONOVER (1982). In addition to the modification of the sampling, we replaced the beta distribution by a uniform distribution, again stressing extreme values for ΔT_{2x}. We call the ensemble generated from this second prior the "correlated ensemble" (*CE*).

As a final step for the setup of our ensemble simulations we have implemented the CLIMBER-2 model into a multi-run environment (SIMENV, FLECHSIG et al., 2005), which allows to effectively distribute the simulation of individual ensemble members among different nodes of the used high performance computer (IBM Power-4 processor).

4.4 Boundary conditions

In the framework of this thesis we have run several CLIMBER-2 ensembles for boundary conditions of the pre-industrial climate, for $2xCO_2$ conditions and for the Last Glacial Maximum (LGM). Those runs have been performed for the uncorrelated as well as for the correlated parameter ensembles discussed in the previous section. Additionally we have realised a lot of further ensemble runs, e.g. to test the sensitivity of our inferred ΔT_{2x} range against uncertainty in the radiative forcing, or for inferring the magnitude of LGM cooling of specific forcing agents. The table listed below gives an overview of all performed ensemble simulations for this study, specifying the individual experiments that we present in the following chapters.

Experiment	Year	Forcing	Parameter setting
SIM_2CO_2	1-3,500 3,501-3,570 3,571-6,500	-Pre-industrial boundary conditions -1% CO_2 increase (280 to 560 p.p.m.) -constant CO_2 (560 p.p.m)	Ensemble-1
SIM_LGM	1-3,500	LGM ice-sheets (ICE-4G), CO_2 (180 p.p.m.), dust, solar insolation, vegetation	Ensemble-1
SIM_LGM_PMIP2	1-3,500	LGM ice-sheets (ICE-5G), CO_2 (167 p.p.m.), dust, solar insolation, vegetation	Ensemble-1
SIM_LGM0.5	1-3,500	Same as SIM_LGM, but only 50% dust forcing	Ensemble-1
SIM_CO_2_LGM	1-3,500	Pre-industrial conditions, but CO_2=180 p.p.m.	Ensemble-2
SIM_abCO_2_LGM	1-3,500	Same as SIM_LGM, but CO_2=280 p.p.m.	Ensemble-2
SIM_CO_2_PMIP	1-3,500	Same as SIM_CO_2_LGM, but no dust and vegetation forcing	Ensemble-2
SIM_uncor	1-6,500	Same as SIM_2CO_2	Ensemble-3
SIM_uncor_LGM	1-3,500	Same as SIM_LGM	Ensemble-3
Factor Analysis			
SIM_CO_2	1-3,500	Pre-industrial conditions, but CO_2=167 p.p.m.	Ensemble-1
SIM_ICE	1-3,500	Same as SIM_CO_2, but LGM ice sheets (ICE-5G)	Ensemble-1
SIM_VEG	1-3,500	Same as SIM_ICE, but LGM vegetation cover	Ensemble-1
SIM_DUST	1-3,500	Same as SIM_VEG, but LGM dust content	Ensemble-1
Uncertainty Analysis			
SIM_lowRF	1-3,500	CO_2=180 p.p.m., LGM ice sheets (ICE4-G, albedo 10% reduced), dust (50%), vegetation	Ensemble-1
SIM_highRF	1-3,500	CO_2=170 p.p.m., LGM ice sheets (ICE4-G), dust (100%), vegetation	Ensemble-1

Table 1: Ensemble-1: 1,000 parameter combinations, uniform-distributed, atmospheric parameters correlated; Ensemble-2: same as Ensemble-1, but only for present-day consistent model members (123 parameter combinations); Ensemble-3: 5,000 parameter combinations, beta-distributed, uncorrelated.

5 Model results

In this chapter we present the main results of our performed ensemble simulations, which are based on the simultaneous perturbation of eleven model parameters. We first analyse the doubling of CO_2 simulations to determine the value of climate sensitivity (ΔT_{2x}) for each model version and apply observational data of present-day climate to constrain the uncertainty range in ΔT_{2x} (chapter 5.1). We then focus on the simulated characteristics of the LGM climate and investigate the prescribed glacial radiative forcings, the simulated glacial temperature response and the assumption of invariance in the feedback parameter λ (chapter 5.2). The central part of this thesis is our approach to effectively narrow down the uncertainty in ΔT_{2x} by constraining our model ensemble with reconstructed regional LGM cooling (chapter 5.3). We conclude our study by a detailed analysis of the range of simulated feedback strengths (chapter 5.4) to provide an insight to what extent our results are model independent.

5.1 Simulated climate sensitivity

In the following we will present the ranges of ΔT_{2x}, which we infer from performing a doubling of CO_2 experiment ($2xCO_2$) for model versions from the correlated and uncorrelated ensemble (*CE* and *UE*). We will discuss in how far the ranges can be constrained by observational data from *present-day* climate[7].

In contrast to highly simplified climate models (e.g. energy balance models) we can not simply tune the climate sensitivity of our model by modifying the value of a single parameter. For generating a set of model versions with differing ΔT_{2x} we have focused on a set of eleven model parameters that strongly affect the main model inherent feedback cycles. A detailed description of the parameter choice and of the scheme to sample this high-dimensional parameter space is given in chapter 4. In terms of the variation of climate feedbacks, our ensemble compares well with a sampling of more complex models and is analysed in detail in chapter 5.4.

We have used the following scenario for calculating the value of ΔT_{2x} for all ensemble members: The first 3500 years of the simulation were run as a spin-up to reach equilibrium for pre-industrial boundary conditions (a CO_2 concentration of 280 p.p.m.), followed by a period of a 1% CO_2 increase until the concentration has doubled (70 years), and then CO_2 was kept constant at 560 p.p.m. until the system has reached a new equilibrium in year 6500. In both ensembles (*CE* and *UE*) we varied the same eleven parameters simultaneously to span a range of different feedback behaviour. Together with the glacial ensembles discussed in

[7] By present-day climate we understand modern Earth geography, modern solar insolation, and pre-industrial CO_2 concentration of 280 p.p.m. (see Table 1).

the next chapter and some additional tests, a total of about 90 million years of model simulations was performed, requiring 130 cpu-months on an IBM Power-4 processor (1.1GHz).

The value of ΔT_{2x} is calculated as the difference in global-mean surface temperature between both equilibrium climate states (defined by the time average over the last hundred years). Having performed this large set of ensemble runs we generated a large set of CLIMBER-2 model versions of different climate sensitivity. The results of the $2xCO_2$ simulations are shown in Fig. 5.1.

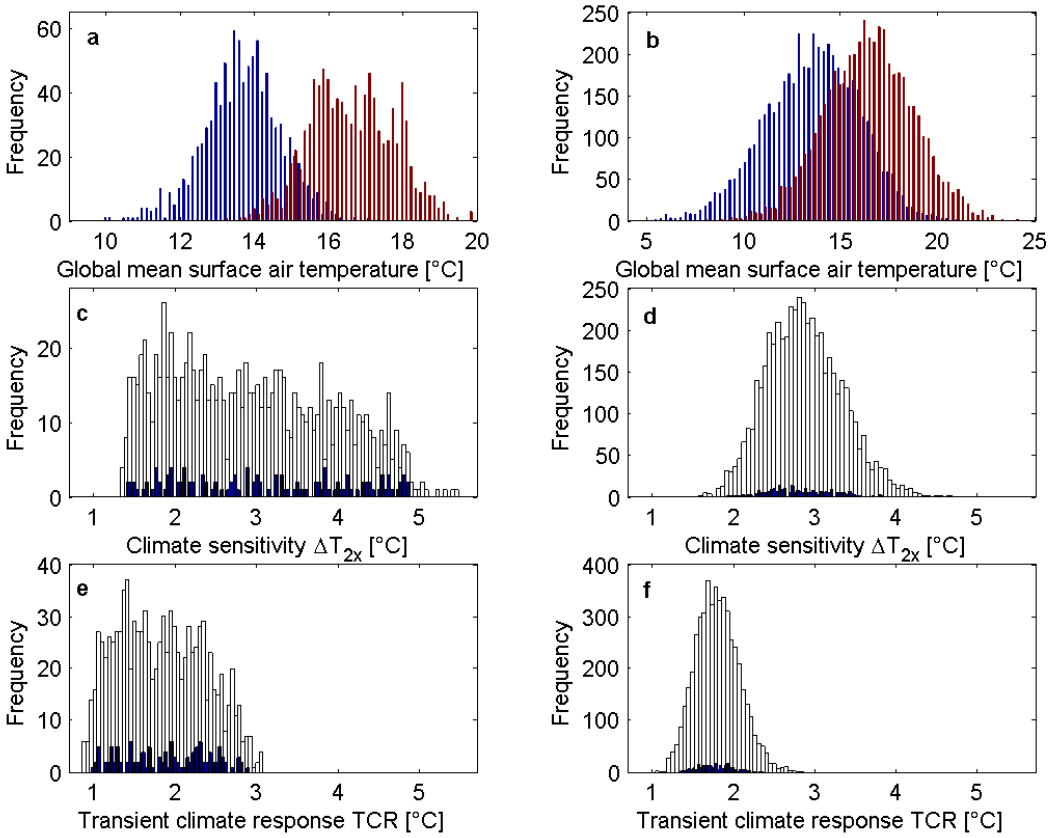

Fig. 5.1: Frequency distributions for pre-industrial and $2xCO_2$ climate characteristics (left: correlated ensemble, 1000 runs), right: uncorrelated ensemble (5000 runs)). **a, b**: simulated equilibrium global-mean surface air temperature for 280 p.p.m. (blue) and 560 p.p.m. CO_2 (red); **c**, **d**: corresponding distribution of climate sensitivity ΔT_{2x}, calculated as the difference of the two equilibria, and **e**, **f**: transient climate response TCR. Dark blue bars (c-f) denote model versions consistent with present-day data. The nearly uniform shape (c and e) mainly result from the chosen sampling scheme (see section 4.3).

Fig. 5.1a and b show the frequency distributions of the global-mean surface air temperature (SAT) inferred from the correlated (left) and uncorrelated (right) parameter ensemble. Because of a broad range chosen for each of the model parameters the range in covered global-mean temperature is large and comprises SAT values, which strongly deviate from the standard model version,

especially in case of the uncorrelated ensemble (Fig. 5.1b). The parameter correlation (see section 4.3) causes a more systematic sampling of those model versions which are not too far from the realistic pre-industrial climate state, but which at the same time yield a broad range of ΔT_{2x} values. This is reflected in the larger spread of inferred ΔT_{2x} values for the correlated than for the uncorrelated ensemble (Fig. 5.1c and d, white bars). The difference in the shape of the frequency distribution reflects the difference in the choice of the prior distribution (beta shaped for *UE*, uniform for *CE*) as well as the difference in the sampling scheme of the parameter space: random for *UE* (Latin Hypercube), systematic for *CE* (higher weighting of specific parameter combinations through the prescribed parameter correlation structure). Fig. 5.1e and f show the transient climate response (TCR), defined as the global-mean SAT increase, averaged over a 20 year period, centred at the time of CO_2 doubling (year 70 of a 1% CO_2 increase). This diagnostic also reflects the lag induced by ocean heat-uptake and is more directly relevant to climate change in the 21st Century than the equilibrium climate sensitivity.

5.1.1 Present-day climate constraints on climate sensitivity

It is still not well understood how model biases in simulation of modern climate affect climate sensitivity. Yet results from models, which produce a "realistic" modern climate state, might be preferable to "unrealistic" models. The strict and objective criteria of realistic model performance would be a requirement for model simulations to fall within the range of uncertainties of observed climate characteristics. However, even state-of-the-Art climate models (GCMs) reveal systematic errors in simulating different climate characteristics, which are often much larger than observation uncertainties (COVEY et al., 2003). A more subjective way to assess the degree of model realism is to accept as tolerable the magnitude of errors typical for other climate models. Because this is an implicit target for any climate model development and tuning, the selection of such subjective criteria mimics a suite of models, which will be treated by other modellers as suitable for climate studies. To constrain models with empirical data we use seven global climate characteristics, which we outline below. All of these characteristics (except for the ocean temperature) have been used in the second and third assessment report of the IPCC for model-data inter-comparison.

We considered as tolerable the following intervals for the annual means of the following climate characteristics which encompass corresponding empirical estimates: Global surface air temperature 13.1-14.1°C (JONES et al., 1999); area of sea ice in the Northern Hemisphere 6-14 mil km^2 and in the Southern Hemisphere 6-18 mil km^2 (CAVALIERI et al., 2003); total precipitation rate 2.45-3.05 mm/day (LEGATES, 1995); maximum Atlantic northward heat transport 0.5-1.5 PW (GANACHAUD and WUNSCH, 2003); maximum of North Atlantic meridional overturning stream function 15-25 Sv (TALLEY et al., 2003), volume averaged ocean temperature 3-5°C (LEVITUS et al., 2005). Thus the chosen ranges – while being somewhat subjective - represent to the first approximation typical scattering of simulations with different atmosphere-ocean GCMs (e.g. SAR and TAR IPCC reports) and encompass observational data of key present-day climate characteristics.

These consistency criteria reduce the original ensemble size by about 90% (95%) for the correlated (uncorrelated) parameter ensemble, which underlines that the parameter choices not only strongly affect the temperature response to CO_2 but also the present-day climate.

In case of the uncorrelated ensemble the present-day data-constraints reduce the range of ΔT_{2x}, whereas for the correlated ensemble the range remains essentially unaffected (Fig. 5.1c and d, dark blue bars). The reason for this difference is given by the difference in the sampling scheme: In the latter case the sampling was chosen to systematically select model versions, which cover a broad range of ΔT_{2x} and which at the same time are not too far from present-day climate. Thus the chosen correlated parameter combinations (*CE*) yield a subset of model versions, which span a broad range of ΔT_{2x} and which all are consistent with present-day climate characteristics. This result is in line with most recent findings of GCM studies (MURPHY et al., 2004; STAINFORTH et al., 2005), demonstrating that model versions with a high ΔT_{2x} cannot be ruled out by annual mean data of modern day climate. For our further analysis (chapter 5.2 and 5.3) we will mainly focus on the correlated model ensemble, as it yields a set of realistic model

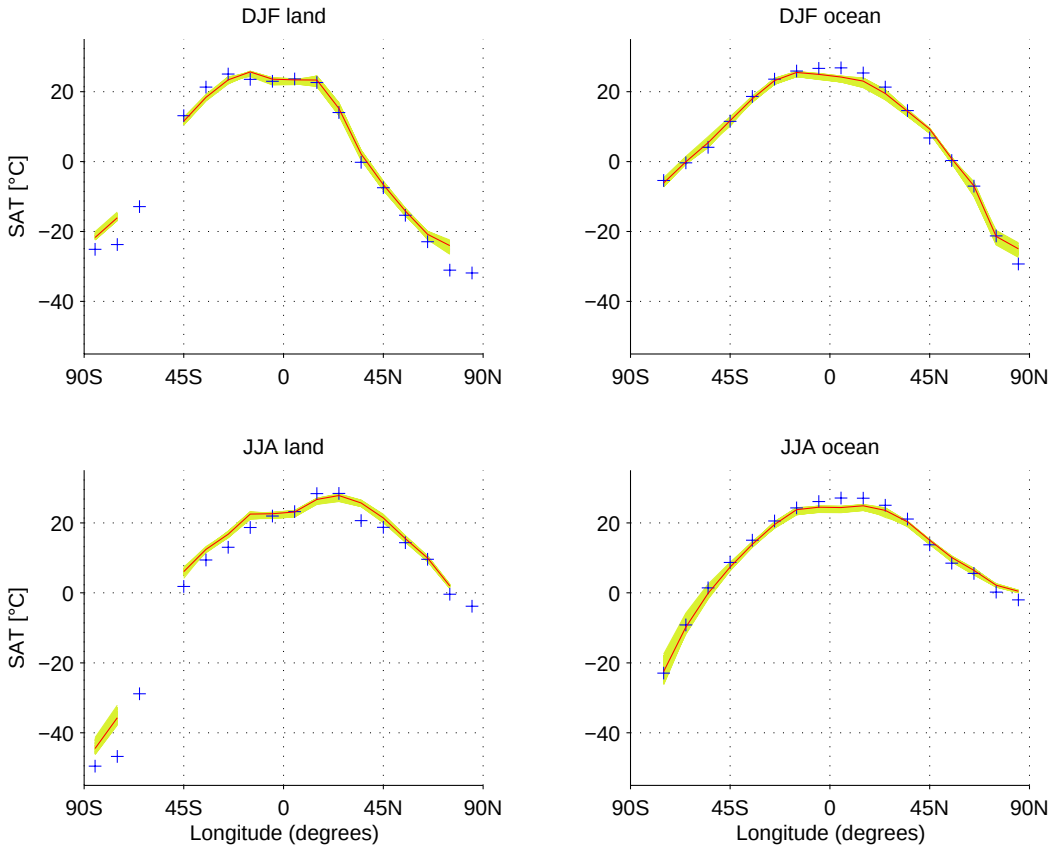

Fig. 5.2: Zonally averaged surface air temperature (SAT) over land and oceans, shown for northern hemisphere winter (upper panel) and summer (lower panel). The light-green lines represent the latitudinal profile of all present-day consistent model members from the correlated ensemble (123 runs), while the red line illustrates the profile for the basic CLIMBER-2 parameter combination. Blues crosses show an estimate from observational data (GUACA, 1993).

versions, which covers the ΔT_{2x} range of structurally different climate models used in the last IPCC report (1.5-4.5°C).

We tested if additional present-day data information (beyond global-mean climate characteristics) may further constrain the uncertainty range of climate sensitivity. For this purpose we focused – in analogy to Petoukhov et al. (2000) – on the model performance of the seasonally resolved latitudinal profile of zonally averaged surface air temperature, precipitation and global cloud cover. We analysed the spread in the simulation of these characteristics, inferred from the set of correlated model versions: A large spread would possibly allow us to reject unrealistic models and thus to constrain the range of ΔT_{2x} by using present-day climate constraints beyond global-mean data.

For all model versions a good agreement between simulated and observed zonally averaged temperature is seen, for both seasons as well as for land and ocean regions (Fig. 5.2). Largest deviations occur at high latitudes. Most notably the spread between different model versions is not very pronounced and is smaller than the deviation between the standard CLIMBER-2 model (red lines) from the observational data for many latitudes.

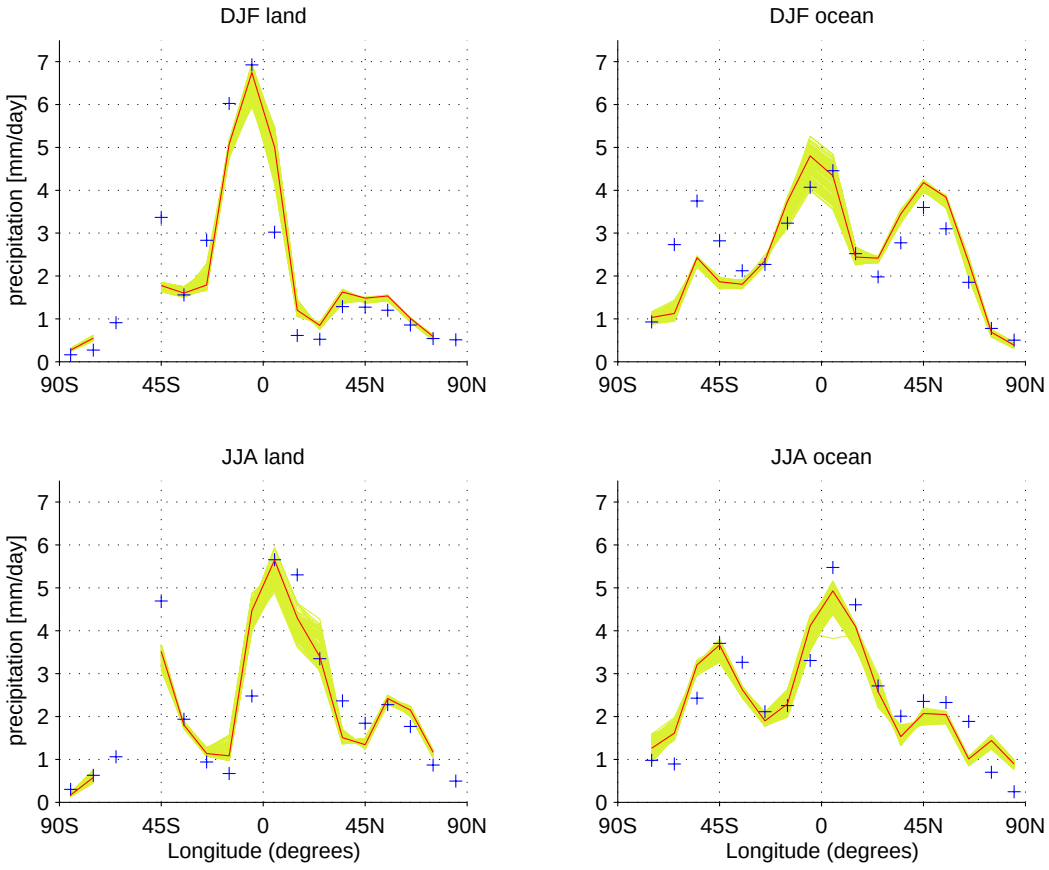

Fig. 5.3: Zonally averaged precipitation over land and oceans, shown for northern hemisphere winter (upper panel) and summer (lower panel). The light-green lines represent the latitudinal profile of all present-day consistent model members from the correlated ensemble (123 runs), while the red line illustrates the profile for the basic CLIMBER-2 parameter combination. Blues crosses show an estimate from observational data (JAEGER, 1976).

The main precipitation characteristics are captured by the model although some deficiencies are revealed, which comes as no surprise given the strong spatial and temporal variability of precipitation patterns and the relatively low resolution of the CLIMBER-2 model (PETOUKHOV et al., 2000). The spread between different model versions is larger than seen for the profile of surface air temperature (Fig. 5.2), yet smaller than the deviation between the standard model (red lines) and the empirical data at most latitudes.

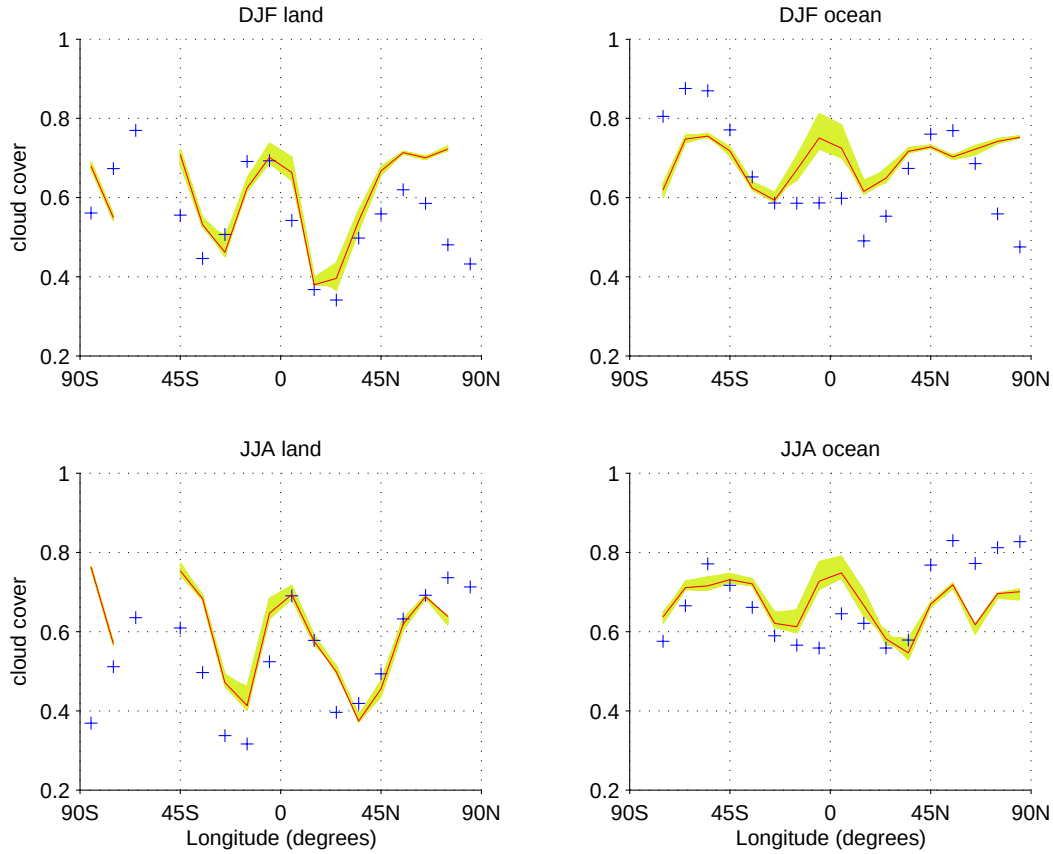

Fig. 5.4: Zonally averaged cloud cover over land and oceans, shown for northern hemisphere winter (upper panel) and summer (lower panel). The light-green lines represent the latitudinal profile of all present-day consistent model members from the correlated ensemble (123 runs), while the red line illustrates the profile for the basic CLIMBER-2 parameter combination. Blues crosses show an estimate from observational data (WARREN, 1988).

Simulated cloudiness reveals a similar behaviour to precipitation: The model captures the main spatio-temporal variability of total cloud fraction but reveals some systematic under- and overestimation at specific regions during the year. In this context it is worth mentioning that even comprehensive climate models suffer from a large bias in the representation of cloud cover (IPCC, 2001; COVEY et al., 2003). The spread among different model realizations, although pronounced at

certain latitudes (especially over low latitude sea areas), is comparatively small compared to the larger model-data discrepancy.

To conclude, the analysis of spatial and temporal present-day climate characteristics has revealed, that our ensemble of model versions realistically reproduces the zonally averaged latitudinal profile (over land and ocean, for summer and winter) of surface air temperature, and – with some larger degree of bias for specific regions – of precipitation and of cloudiness. The spread among CLIMBER-2 versions of different ΔT_{2x}, already constrained by global-mean present-day climate, is comparatively small for surface air temperature and more pronounced, when precipitation or cloudiness are considered. Regarding the model spread for further constraining our model ensemble, it turns out that this information does not help to effectively reduce uncertainty in climate sensitivity. This is because the spread among different model members is of comparable magnitude or even smaller than the model-data error for most latitudes. As we have compared our simulations with zonally averaged observational data, separated into summer (JJA) and winter (DJF) months, those results imply that the seasonal cycle does not offer an effective means of constraining our ensemble and thus of reducing uncertainty in the range of ΔT_{2x}. Yet if we had generated an ensemble of more extreme model versions such as Stainforth et al. (2005), we would assume to infer a larger spread among different ensemble members. For those models the annual cycle may well help to reject unrealistic model versions, as demonstrated by Knutti et al. (2006). We further should add that the use of advanced statistical methods, such as *fingerprinting* (HASSELMANN, 1993; ALLEN and TETT, 1999) helps to better constrain the present-day model performance for high resolution climate models.

From a theoretical viewpoint it can be questioned if the seasonal cycle is very helpful for effectively constraining the uncertainty range of ΔT_{2x}: Although the same feedbacks are acting, when the climate system is forced either by seasonal changes in solar insolation or by increasing CO_2 concentrations, the system is not expected to behave the same way. In case of the latter the forcing is homogeneously distributed and a large feedback contribution is expected to come from the tropics, whereas the seasonal cycle is very weak in low latitudes and thus may provoke a different net feedback.

It should be noted that the presented comparison of CLIMBER-2 results with present-day climate characteristics is by far not exhaustive and was only discussed qualitatively without further specification of quantitative goodness-of-fit criteria. Our aim was to demonstrate that for a set of key climate characteristics the present-day climate state does not prove to be effective in reducing uncertainty in future climate change.[8]

[8] For a more detailed comparison of the standard CLIMBER-2 model version with present-day climate characteristics see Petoukhov et al. (2000).

5.2 Simulation of the Last Glacial Maximum

The main focus of this thesis is on constraining the uncertainty range of climate sensitivity by comparing LGM ensemble simulations with paleo data (see next chapter). To provide a broad basis for interpreting our results we first analyse the simulated LGM climate response in this chapter. The key findings from those analyses are summarized in SCHNEIDER VON DEIMLING et al. (submitted).

Having analysed the range of simulated climate sensitivity we now will investigate the range of simulated LGM cooling. We focus our analysis on the correlated ensemble (CE) as it covers a larger spread in ΔT_{2x} and thus spans a broader range of possible LGM cooling. We will first discuss the applied glacial boundary conditions, illustrate their effect on the spatial radiative balance (radiative forcing), and then infer the range of simulated global LGM cooling. As the glacial experiment is no direct analogue for a future warming given the differences in the forcings, we explicitly analyse and discuss the impact of individual glacial forcings on the magnitude of dT_{LGM}. Finally we describe the typical regional characteristics of the simulated glacial temperature anomaly. This regional information will be used in chapter 5.3 for constraining the uncertainty range of ΔT_{2x} by using proxy data of regional temperature change.

5.2.1 Paleo-climatic background

Looking back into the recent Earth's history a period of a stable climate regime is seen during the last 10.000 years, referred to as the Holocene climate. Prior to that climate state conditions of an ice age world persisted for about 100.000 years, characterized by a much larger climate variability, the built-up of pronounced inland ice sheets covering large parts of northern America and Eurasia, and by a much colder mean temperature than today. The information inferred from different types of climate archives (paleo proxies) substantially contributed within the last decades to an enhanced knowledge of past climate conditions. It was especially the information about past climate changes archived in Antarctic ice cores (PETIT et al., 1999; STAUFFER et al., 2004), which has drawn a lot of attention to the issue of linking anthropogenic greenhouse gas increase and rising temperatures. The ice cores reveal an impressive correlation between inferred levels of greenhouse gas concentration and reconstructed temperature changes over the glacial cycles (covering a time period of several hundred thousands of years). As the main physical mechanisms, which have determined past climate evolution, are the same as those which will determine future climate change, the *paleo-calibration* method has been suggested (COVEY et al., 1996). Its aim is to analyse past climate history in the view of constraining uncertainty of future climate change.

The time period of around 21 kilo years before present, commonly referred to as the Last Glacial Maximum (LGM), is characterized by the maximum volume of the northern hemisphere ice sheets, along with a pronounced cooling over most of the globe. For that period, several regional temperatures have been

reconstructed, comprising marine and terrestrial proxies of low and high latitudes. Furthermore the main climate forcings of the LGM are relatively well known. Given this knowledge of past climate conditions, the LGM is a focus climate state for many modelling studies, offering the chance to test the performance of a climate model for boundary conditions considerably different from the present ones.

Most important the information inferred by analysing simulated glacial cooling can be used to constrain predictions of future climate change. Several studies (e.g. HOFFERT and COVEY, 1992; HANSEN et al., 1993) have estimated the magnitude of global LGM forcing and the global temperature anomaly dT_{LGM} to infer an estimate of *climate sensitivity* (ΔT_{2x}). The underlying assumption of a direct link between past and future temperature change implies that a bias in the assumed LGM forcing or in the temperature anomaly directly translates into a bias of inferred climate sensitivity. Thus an accurate estimate of dT_{LGM} is of crucial importance when determining the sensitivity of Earth's climate system to changes in the radiation budget, based on past climate changes.

Modelling studies as well as paleo data archives both offer a means of estimating dT_{LGM}, but may both reveal some caveats. Model based estimates of global LGM cooling depend on the climate sensitivity (i.e. on the feedback behaviour) of a given model and on the magnitude of the applied glacial forcings. Shortcomings also exist for proxy-based estimates of dT_{LGM} as the spatial coverage from proxy records is rather poor on a global scale. In the following we will use proxy-data from specific regions of the globe (section 5.2.2) to constrain the ensemble, i.e. to estimate what range of simulated global LGM cooling is consistent with reconstructed regional temperature change (section 5.2.4.2).

5.2.2 Data constraints from paleo proxies

Global coverage of paleo records is too sparse for reconstructing global LGM cooling with satisfactory accuracy. Yet for specific regions an estimate of large-scale regional temperature change can be inferred from proxies. Given the strong link between (large scale) regional and global temperature response, the inferred information about temperature change at specific regions of the globe can be applied to constrain the simulated magnitude of global LGM cooling. Furthermore our ensemble simulations suggest a similar strong link between past regional cooling and future global warming (chapter 5.3). The latter issue will be explored in the following chapter in the context of constraining the uncertainty range of climate sensitivity, while we will focus in this chapter on constraining the range of likely global LGM cooling.

When looking for the best region for applying the LGM data-constraints, several criteria have to be considered. Well-calibrated proxy-data need to be available and the response should not be affected too much by regional small-scale dynamics, which cannot be resolved by our coarse-resolution model. This might be the case for Greenland, where ice core data are available, but possibly comprise some strong local signature. A few geographically distinct Antarctic ice-cores provide temperature estimates from southern high latitudes, yet covering a comparably small region of the globe. Numerous sediment-data are available from tropical ocean sites, allowing large-scale averaging over the entire tropical

ocean belt (thus the importance of local processes is minimized and the relative importance of global forcings, i.e. the effect of well-mixed greenhouse gases, is maximized). Tropical land areas are smaller and more affected by regional factors; data coverage is sparse and temperature reconstruction complicated by uncertainties of potential lapse rate changes. Hence, we have chosen the tropical oceans as our most reliable test region and apply proxies from tropical land sites and Antarctica for checking the consistency of our results (section 5.2.4.2).

Reconstructed sea surface temperatures (SSTs) from various types of proxy-data have been discussed controversially over the past decades, particularly the magnitude of tropical temperature response. Yet in recent years the analysis of different reconstruction techniques has led to reject very low and high large-scale cooling (CROWLEY, 2000; LEA et al., 2003; NIEBLER et al., 2003). For deriving a robust SST data-constraint we use an objectively interpolated dataset (SCHÄFER-NETH and PAUL, 2003), which comprises a large set of sediment cores of stringent quality and age control (about 300 for the Atlantic). We focus on data from the tropical Atlantic (20°N-20°S), based on GLAMAP reconstructions (SARNTHEIN et al., 2003) that were derived from transfer functions of faunal assemblages of foraminifera. Accounting for reconstruction uncertainties of each data core and for uncertainty in the pattern of SST cooling, this dataset yields a range of averaged tropical Atlantic SST cooling of 3.0°±0.9° (2σ, see Appendix C for further detail). When considering an average over all ocean basins, slightly reduced SST anomalies would have to be applied for our analysis. A crucial issue of such an estimate is in how far the result is proxy-dependent. Geochemical SST reconstructions (Mg/Ca and alkenone methods) are in agreement with reconstructions from faunal transfer functions for low latitudes (BARD, 2001; ROSELL- MELE et al., 2004; BARKER et al., 2005). Systematic differences arise in the eastern equatorial Atlantic (especially in upwelling regions), where geochemical methods suggest a less pronounced maximum cooling (about 4°C, ROSELL- MELE et al., 2004; BARKER et al., 2005). We account for this possible bias by creating an alternative data set in limiting maximum tropical cooling of the original data-set to 4°C, and recalculate the mean and associated error. In the following, we present results from the first set only, which yields the largest uncertainty spread (see Appendix C).

5.2.3 Simulation design

Simulating the LGM climate crucially depends on the radiative forcing of the climate system (resulting from the pronounced difference between modern and glacial boundary conditions), and on the model sensitivity governing the amplification and dampening of this forcing by the model-inherent feedbacks. We have applied boundary conditions for greenhouse gas concentrations (an equivalent CO_2 concentration of 167 p.p.m.), northern hemisphere ice sheets (including a sea level lowering of 120 m) and orbital parameters that were specified in the framework of the *Paleoclimate Modelling Intercomparison Project* (PMIP-2, www-lsce.cea.fr/PMIP-2). Additionally we account for forcing contributions resulting from glacial dust and vegetation. We refer to this ensemble as *SIM_LGM_PMIP2* (see Table 1 for all performed experiments). As our climate model does not include a dust cycle, radiative effects of dust are prescribed as monthly top-of-the-atmosphere anomalies of the short-wave radiation, which

have been calculated for modern and LGM boundary conditions, including dust concentration changes, from several ECHAM-5 simulations (STIER et al., 2004), (M. Werner, pers. communication). Vegetation cover is prescribed from a CLIMBER-2 LGM simulation, run in interactive vegetation mode. Thereby, vegetation changes are treated in this study as an additional forcing rather than as a feedback.

In order to specify the contribution of the individual forcings to total LGM cooling we performed a factor analysis the following way (GANOPOLSKI, 2003): To separate the magnitude of CO_2 affected cooling from dT_{LGM}, we additionally performed an ensemble of simulations, for which we applied pre-industrial boundary conditions, but prescribe the CO_2 concentration to its glacial value of 167 p.p.m. (also accounting for glacial changes in CH_4 and N_2O which are not included in CLIMBER-2 radiative scheme). The difference in the simulated temperature between this "CO_2 only" experiment (SIM_CO_2, see Table 1) and the pre-industrial runs yields that fraction of the glacial cooling which is caused by CO_2 concentration changes. We further performed three additional ensembles by successively adding the glacial forcings of ice sheets (SIM_ICE), vegetation cover (SIM_VEG) and dust (SIM_DUST) and determine the impact of individual forcings by taking the difference between 2 successive ensembles. It should be noted that this methodology does not account for non-linearities in the system response. If we calculated the CO_2 affected cooling as the difference between the total LGM cooling and an ensemble of simulations, where all boundary conditions are set to glacial, but CO_2 fixed to its pre-industrial value of 280 p.p.m., we infer a slightly larger fraction of CO_2 induced cooling (see section 5.3.1).

5.2.4 Simulation results of the Last Glacial Maximum climate

In this section we will first analyse the strength in simulated radiative forcings that result from the prescription of the glacial boundary conditions. This enables us to compare our results with forcing estimates from GCMs. Special emphasize will be on the pronounced difference in the spatial patterns among the individual forcing agents. In this context the difference in the feedback strengths for all applied glacial forcings will be discussed and implications drawn for linking past climate history to future climate changes.

5.2.4.1 Analysis of the main glacial forcings

The alteration of continental ice sheet extent, atmospheric greenhouse gas and dust concentration, land-sea distribution and vegetation cover from modern values to those, which are representative for the LGM climate, constitute a pronounced forcing of the climate system. The large extent of northern hemisphere glacial ice sheets and the expanded land area due to lowered glacial sea level both increase the global surface albedo and thus result in a strong negative forcing. The reduction in greenhouse gas concentration results in a reduced atmospheric opacity to long-wave radiation and enhances the negative forcing. High glacial dust concentration can warm the climate, e.g. by reducing the albedo of snow-covered regions, and can cool the climate by reflecting more sunlight to space. In the global and annual mean the latter effect is assumed to

be much larger. The replacement of modern day by glacial vegetation types contributes to changes in the planetary surface and exerts for most regions a negative forcing by an increase in surface albedo, which is especially large in boreal latitudes of the northern hemisphere. Changes in glacial orbital parameters affect the spatial and seasonal distribution of incoming solar energy, but only contribute minor to the global magnitude of LGM radiative forcing.

For quantifying the strength of all considered main forcings we have extended the CLIMBER-2 code to allow for explicit calculation of the required radiative flux anomalies and have performed additional ensemble runs, which we describe in the following. We have estimated the perturbation of the energy balance by quantifying the magnitude of all main individual glacial forcings (ice sheets, greenhouse gases, dust, vegetation) from anomalies in the radiative fluxes between pre-industrial and LGM simulations. Solar forcing due to orbital changes is fairly well known and is included in the full set of glacial forcings for estimating the LGM cooling, but its forcing contribution is not analysed separately as its global magnitude is comparatively small for the LGM period (about 0.04 W/m^2, BROCCOLI, 2000).

The prescription of glacial ice sheets, vegetation and dust mainly affects the short-wave (SW) radiation balance and thus the corresponding radiative forcings are calculated in a different way than that of CO_2, which mainly affects the long-wave (LW) radiation balance. The radiative forcing of glacial ice sheets (RF_{ICE}) and vegetation cover (RF_{VEG}) have been quantified by calculating the radiative SW flux perturbance at the top-of-the-atmosphere (TOA). For that purpose we first have calculated the outgoing SW flux (R_{SW}) for each atmospheric grid cell during the last year of the present-day equilibrium state (year 3500) and then have re-calculated the perturbed SW flux (R'_{SW}) resulting from the prescription of either glacial ice sheets or vegetation, while fixing all other boundary conditions to their pre-industrial value and maintaining the surface and atmospheric quantities. For quantification of RF_{ICE} we have replaced present-day geography by glacial geography (including the effect of sea level lowering). In case of RF_{VEG} we have replaced the present-day vegetation distribution with that inferred from a CLIMBER-2 LGM run with interactive vegetation scheme. The TOA difference in SW fluxes ($R_{SW} - R'_{SW}$) between both experiments (present-day and perturbed run) yields the magnitude of radiative forcing for each grid cell.

The values of radiative forcing discussed in the following, represent the globally averaged annual mean of the radiative flux anomalies. Dust forcing has been calculated for modern and LGM boundary conditions, including dust concentration changes, from several ECHAM-5 simulations (M. Werner, pers. communication (2004); STIER et al., 2004). Those fields have been interpolated to fit the CLIMBER-2 resolution and are directly implemented as monthly TOA anomalies into our model's SW radiation scheme.

In accordance with GCM estimates of CO_2 forcing (RF_{CO2}) we calculated the LW radiative flux perturbance, resulting from a decrease in equivalent CO_2 concentration (280 p.p.m. to 167 p.p.m.), at the tropopause (see next section for further details). The results of all performed radiative forcing calculations for the full set of model versions are illustrated in the following figure.

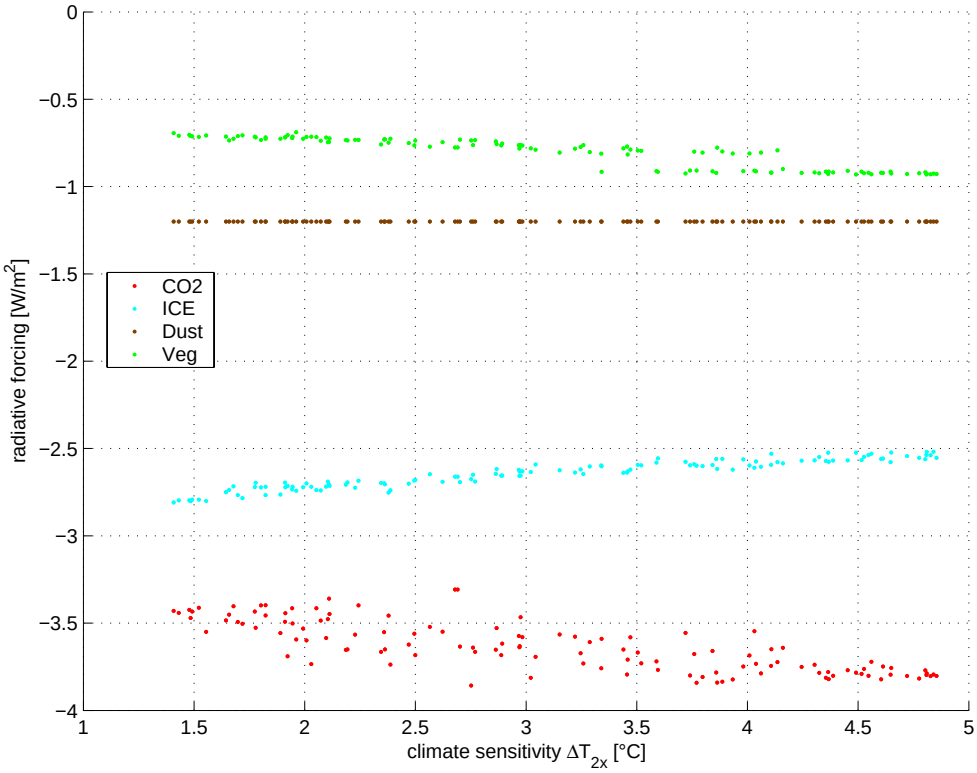

Fig. 5.5: Simulated global annual-mean radiative forcing for all main individual glacial forcing agents (red: CO_2, cyan: ice sheets, brown: dust, green: vegetation). Shown are estimates of all model versions (correlated ensemble), which are consistent with present-day climate characteristics. Besides dust forcing all estimates slightly depend on the set of chosen model parameters (see text).

In our simulations the largest contribution to global LGM radiative forcing results from the decrease in the concentration of greenhouse gases (RF_{CO2}). In this context it should be mentioned that our inferred magnitude of CO_2 radiative forcing is somewhat larger than best-guess estimates given by the IPCC (2001). Applying the proposed calculation scheme $RF_{CO2}=5.35*\ln(CO2_{LGM}/CO2_{MOD})$ (IPCC, 2001) we infer a mean estimate of –2.8 W/m^2. A slight overestimation in the magnitude of our inferred radiative forcing estimates (compared to GCMs) results from the fact that we omit the impact of SW flux perturbation, which slightly decreases the net effect of tropopause CO_2 forcing. Yet this effect is rather small (about 5%, CESS et al., 1993). Of higher importance is a likely bias in the radiative forcing calculation scheme between CLIMBER-2 and GCM inferred estimates. The magnitude of calculated forcing depends on the definition of tropopause height, which in turn depends on the vertical resolution of a given model (SHINE et al., 2003). Furthermore RF_{CO2} depends on the effect of stratospheric adjustment, which is likely to differ between GCMs and the CLIMBER-2 model with its simplified stratosphere representation.

Besides dust forcing, which has been directly prescribed as a SW radiative anomaly for all ensemble members, the calculated forcings depend slightly on the model sensitivity. This is the case as the broad range of perturbed parameters yields different realisations of present-day climate, with e.g. differing cloud cover or extent in snow covered regions. Those differences in the basic climate state

affect the magnitude of calculated radiative forcing and are the reason for the observed dependence between calculated radiative forcing and climate sensitivity.

The aggregate global strength of all considered glacial forcings accounts for about –7.5 to –8.0 W/m^2 for our ensemble, which is comparable to the study of Hansen et al. (–7.1±1.5 W/m^2, (1993)) and slightly larger than the estimate of Hoffert and Covey (–6.7±0.9 W/m^2, (1992)). Glacial dust and vegetation contribute globally about 2 W/m^2 to this amount and illustrate that those often neglected forcings should be included for a comprehensive simulation of the LGM climate state[9].

5.2.4.2 Global LGM cooling

The analysis of global-mean radiative forcing has revealed a radiative perturbation of the climate system, which is much larger than the radiative forcing resulting from anthropogenic emissions over the industrial period (IPCC, 2001). As the pronounced LGM climate forcings prevailed for a long time, the climate system could approach a climate state significantly colder than the present-day climate (for most regions of the globe).

The calculated difference in global-mean surface air temperature (SAT) between pre-industrial and glacial climate (dT_{LGM}) covers a range of 4.3-9.8°C in our ensemble simulations (Fig. 5.6, dark blue dots). This range is comparatively broad and can be further narrowed down as the simulated regional glacial cooling proves to be tightly linked to simulated global LGM cooling. We thus can constrain the range of dT_{LGM} by requiring consistency of simulated with reconstructed regional temperature change. For that purpose we focus on the subset of ensemble members, whose simulated tropical Atlantic SST cooling falls inside the discussed proxy-data range (3.0°±0.9°, see section 5.2.2) and constrain simulated global LGM cooling to 5.8±1.4°C. This range contains substantially larger cooling than recent PMIP-2 estimates (~4.1±1.0°C) (MASSON-DELMOTTE et al., 2006). The discrepancy partly can be explained by our simulated additional cooling through glacial dust content and vegetation cover. Its magnitude can be derived from Fig. 5.6, which shows the global cooling resulting from the prescription of the main individual forcings. The largest contribution comes from the combined effect of greenhouse gas (dT_{CO2}, red dots) and ice sheet forcing (dT_{ICE}, light blue dots), which together account for about 75% of total LGM cooling (this includes the effects of a lower sea level and ice sheet elevation on temperature).

The solid red line (Fig. 5.6) is calculated by assuming that the temperature response dT_{CO2} is directly proportional to the radiative forcing RF ($dT_{CO2}=\lambda*RF_{CO2,}$ with λ referred to as the *feedback parameter*). We thus simply have scaled dT by the ratio of glacial to 2xCO_2 forcing. High ΔT_{2x} model versions show slightly larger cooling than estimated from this linear approximation, which assumes the same strength of climate feedbacks for the glacial and modern climate. The validity of this assumption will be analysed in more detail in the following section, in view of

[9] The magnitude of forcing by glacial dust content is rather uncertain due to incomplete knowledge of its regional distribution and radiative properties. See section 5.3.4.2 for a short discussion about the uncertainty of forcing contributions from glacial dust content.

the dependency of λ on the background climate.

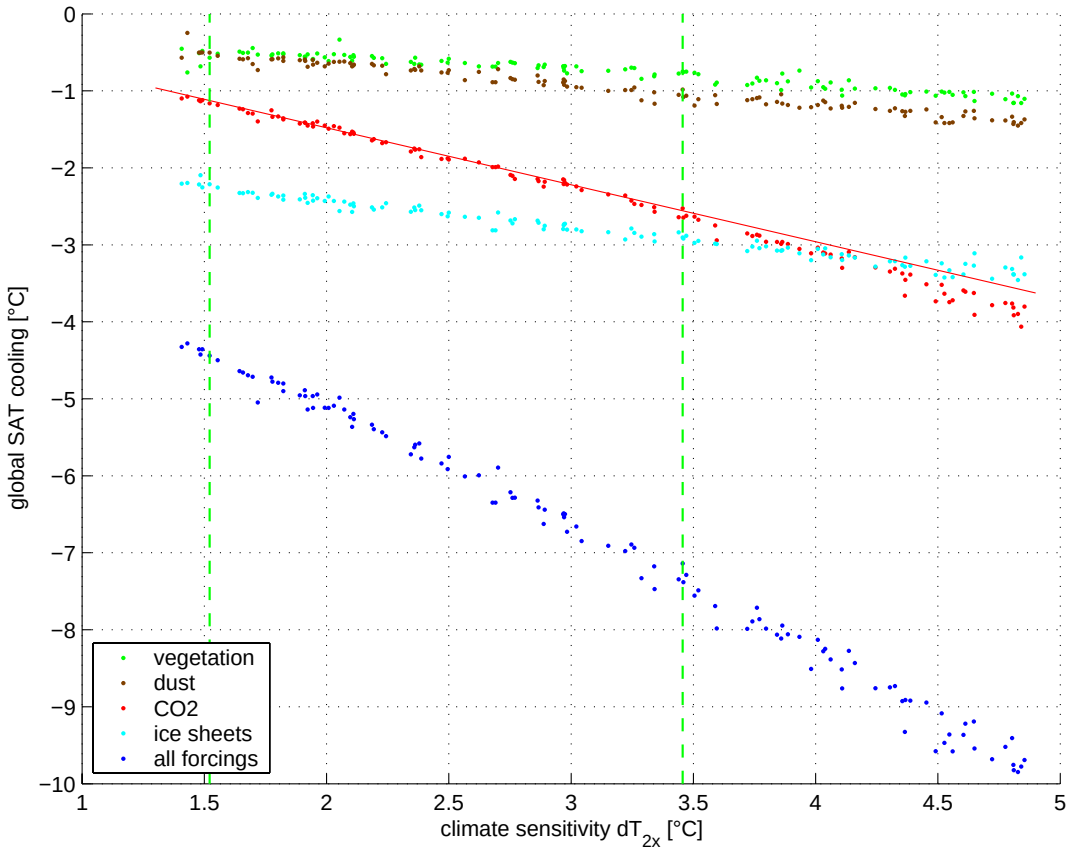

Fig. 5.6: Contribution of individual forcings to global LGM cooling. Shown is the magnitude of simulated global annual-mean SAT cooling between the pre-industrial and LGM climate, arising from the prescription of all main glacial forcings (dark blue dots). Additionally the change in SAT for individual forcing components is illustrated (green: vegetation, brown: dust, red: CO_2, cyan: ice sheets). The solid red line represents a theoretical approximation, which assumes a linear relation between the temperature anomaly resulting from lowered CO_2 levels and CO_2 radiative forcing (see main text). Vertical green lines indicate the range of model versions, consistent with a tropical Atlantic SST cooling of 3.0°±0.9°C.

As mentioned before, many LGM modelling studies neglect the forcing impact of glacial dust content and vegetation cover. Fig. 5.6 illustrates that this omission results in an underestimation of global LGM cooling by about 1.5°C for a midrange climate sensitivity of 3°C for our simulations. Orbital changes do not significantly contribute to global cooling and are not separately shown in the above figure.

The individual glacial forcings are of different nature, and differ not only in magnitude but as well in their spatial distribution. Its impact on the simulated global temperature response becomes apparent in the slope and intercept of the

regression lines through the individual ensembles in Fig. 5.5 (lines not explicitly shown). Concerning the intercept all regression lines are close to zero with the exception of the ensemble representing the cooling impact of ice sheets (light blue dots), which has an intercept at –1.8°C. Further simulations reveal that about 0.6°C of this magnitude can be explained by the change in Earth's surface level through the prescription of LGM ice sheets and sea level lowering. The additional 1.2°C result from albedo changes mainly of the ice sheets and demonstrate that this strongly inhomogeneous forcing yields a different temperature response compared to the response following an homogeneously distributed forcing such as CO_2 (see next section).

How are our estimates of global LGM cooling affected by uncertainties in the glacial forcings? If we repeated our analysis of estimating dT_{LGM} for e.g. the assumption of slightly increased ice sheet forcing, we would constrain the same range of dT_{LGM}, but from a set of models with lower climate sensitivities, as long as the latitudinal profile of the glacial temperature anomaly remains unchanged. Yet if e.g. this stronger high latitude forcing only marginally affects the tropical SST decrease (our focus area to constrain the ensemble) but strongly increases high latitude cooling, we then would infer a larger estimate of dT_{LGM}. To check for this uncertainty we replaced the ICE-5G (PELTIER, 1994) by the ICE-4G ice sheet reconstruction (PELTIER, 2004), which yields a slightly larger ice sheet forcing (globally about 0.5 W/m^2). Applying again the tropical SST constraint our new constrained ensemble covers model versions of lower climate sensitivity, but the inferred dT_{LGM} is almost identical for both experiments. Thus the impact of uncertainty in the glacial forcings is of crucial importance, when the range of likely climate sensitivities is to be estimated (as performed in the following chapter), but does not strongly affect our estimate of global LGM cooling.

We now will proceed with testing the robustness of our inferred dT_{LGM} range against our choice for a tropical paleo proxy constraint, which is based on reconstructions from low latitude foraminifera. Recent studies have shown that reconstructed tropical SSTs from geochemical methods agree with estimates derived from faunal transfer functions (ROSELL- MELE et al., 2004; BARKER et al., 2005). Systematic differences arise especially in upwelling regions, where geochemical methods suggest a less pronounced maximum cooling. However, as we discuss a large spatial mean cooling, those differences are not crucial for our analysis.

Would our estimate of global LGM cooling have to be revised if we used proxy information from different regions to constrain dT_{LGM}? Assuming a tropical (30°S-30°N) land cooling of 4-6°C (FARRERA et al., 1999), we infer a range of slightly larger dT_{LGM} (6.5±1.1°C). Ice-core data from Antarctica (about 8±2°C surface cooling (VIMEUX et al., 2002; JOUZEL et al., 2003) constitute a strong test for the simulated latitudinal temperature profile. This additional, independent constraint yields an estimate for global LGM cooling of 5.9±1.3°C, which is highly consistent with our tropical SST based estimate.

Given the consistency of dT_{LGM} estimates, which we infer from proxies from different regions of the globe, our results suggest a best-guess for global LGM cooling close to 6°C, with about 1.5°C of the temperature anomaly resulting from cooling contributions from glacial dust content and vegetation cover. As we have mentioned before this range includes substantially larger cooling than suggested by recent PMIP-2 models (MASSON-DELMOTTE et al., 2006) and points to a systematic underestimation of LGM cooling for those studies.

5.2.4.3 *Examination of invariance of the feedback parameter λ*

Having analysed the magnitude in radiative forcing and glacial cooling for all individual forcing agents, we now can estimate the individual feedback strengths for the Glacial and compare those values with the feedback strengths, inferred from the CO_2 doubling experiment. We thus can interpret climate sensitivity estimates, inferred from paleo-calibration studies (COVEY et al., 1996) that estimate ΔT_{2x} from past changes in global-mean temperature and radiative forcing.

We therefore analyse the feedback parameters, which describe the ratio of global-mean surface temperature change to global-mean forcing, for the total LGM response (λ_{LGM}), as well as for each of the individual glacial forcings (λ_i).

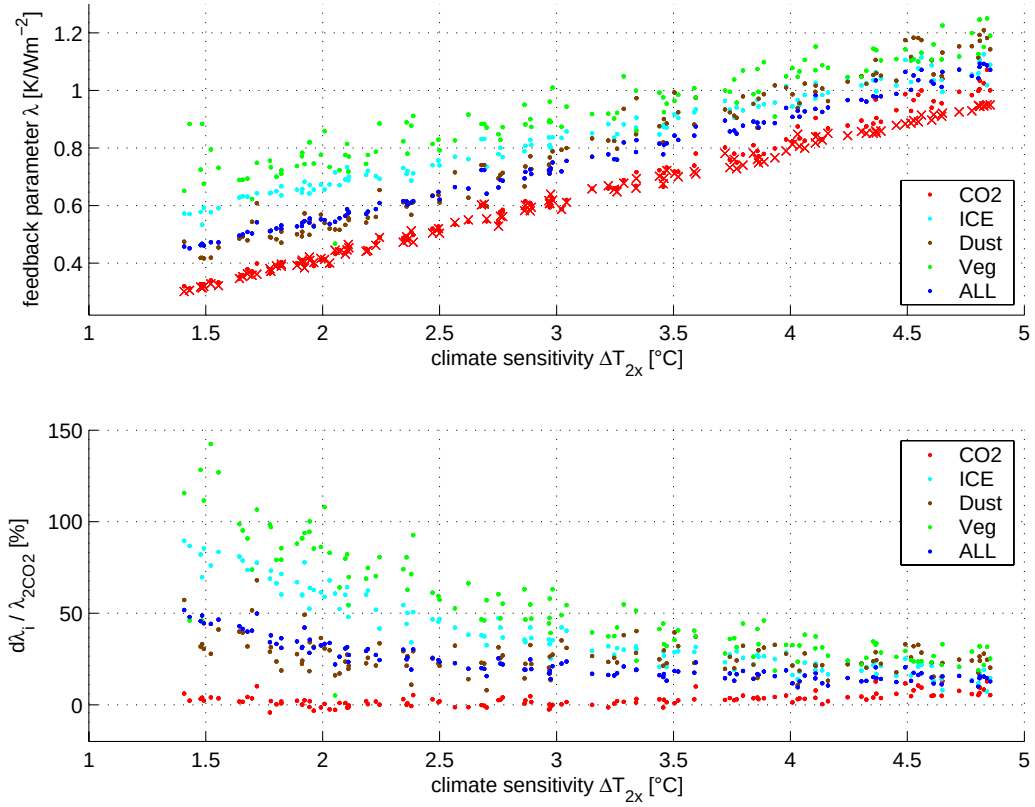

Fig. 5.7: Feedback parameter λ inferred from different experiments. The red dots (red crosses) represent the magnitude of λ inferred from the homogeneously distributed glacial CO_2 forcing ($2xCO_2$ forcing). All other model results are inferred from the inhomogeneous forcings of glacial ice sheets (cyan), vegetation (green), and dust (brown). The dark blue dots illustrate the feedback parameter for the LGM simulation with all feedbacks acting. All values are inferred from the correlated ensemble of present-day consistent model versions. The lower panel illustrates the percentage deviation of λ_i from λ_{2CO2}.

Estimates of λ inferred from the inhomogeneously distributed forcings (ice sheets[10], vegetation, dust) indicate systematically larger values compared to λ_{2CO2} (Fig. 5.7). Especially for low sensitivity model versions the feedback parameter for vegetation and ice sheet forcing is pronouncedly larger than the feedback parameter inferred from the doubling of CO_2 experiment. HANSEN et al. (1997) found that the temperature response due to a forcing located at high latitudes is larger than for a forcing at low latitudes. This is in line with our λ estimates for ice sheet and vegetation forcing, which both represent high northern latitude forcings. The temperature response to dust forcing is not that obvious to analyse, as the implemented dust forcing shows a rather pronounced spatial and seasonal variability. In this context the partitioning of forcing over ocean and land may be an important aspect for further analysis.

The conclusion we draw from the above figure is that the feedback parameter λ may well depend on the forcing distribution: For strongly inhomogeneous forcings (especially in case of a pronounced weight in high latitudes) our model ensemble suggests that the feedback parameter is larger than for the homogeneous $2xCO_2$ experiment. The strong deviation of the individual feedback parameters λ_i from λ_{2CO2} especially for low sensitivity model versions results from the large difference in the lapse rate feedback between the $2xCO_2$ and the glacial experiments and will be discussed in chapter 5.4.

Furthermore the comparison between both CO_2 forcing experiments allows us analysing the impact of the background climate on the magnitude of λ. The magnitude of λ_{CO2} is similar for the $2xCO_2$ experiment (a doubling from 280 to 560 p.p.m., red crosses in Fig. 5.7) to the glacial experiment (lowering of 280 p.p.m. to 167 p.p.m., red dots). For model versions with a climate sensitivity in the lower half of the considered ΔT_{2x} range the feedback parameter is almost identical, yet for sensitivities in the upper half a systematic bias arises, indicating that the feedback parameter λ_{CO2} is slightly larger for the glacial climate (about 10%).

We should mention that we infer slightly larger magnitudes for the CO_2 radiative forcing (RF_{CO2}) than compared with best-guess estimates from GCMs. Yet our larger value for CO_2 radiative forcing does not necessarily imply that our radiation scheme overestimates the effect of CO_2, because the differences can arise from difference in the treatment of stratospheric adjustment (see section 5.2.4.1). Thus when comparing our feedback parameters with GCM estimates, the slightly larger magnitude of CO_2 radiative forcing in our analysis should be taken into account.

To conclude, our results reveal systematically larger feedback strengths for the glacial climate, mainly resulting from the larger temperature response for inhomogeneous than for homogeneous (CO_2) forcing. The majority of model versions reveal a feedback parameter (λ_{LMG}) which is about 10-20% larger than the feedback parameter inferred from CO_2 doubling (λ_{2CO2}), whereas this discrepancy increases with decreasing model sensitivity in our ensemble. The implication for paleo-calibration studies, which estimate ΔT_{2x} from past changes in global-mean temperature and radiative forcing, is a tendency for overestimating the magnitude of climate sensitivity.

---

[10] For calculation of λ_{ICE} and λ_{LGM} the additional global cooling, caused by an increase in glacial height level (lower sea surface), has been removed.

5.2.4.4 Spatial characteristics of LGM forcing

We will use information about *regional* LGM temperature anomalies to constrain the uncertainty range of climate sensitivity (chapter 5.3). Thus this analysis crucially depends on a realistic simulation of large-scale regional cooling and we will discuss the spatial temperature response in the next section. For a better interpretation of the inferred spatial cooling we illustrate in the following figure the pattern of the non-homogeneously distributed glacial forcings.

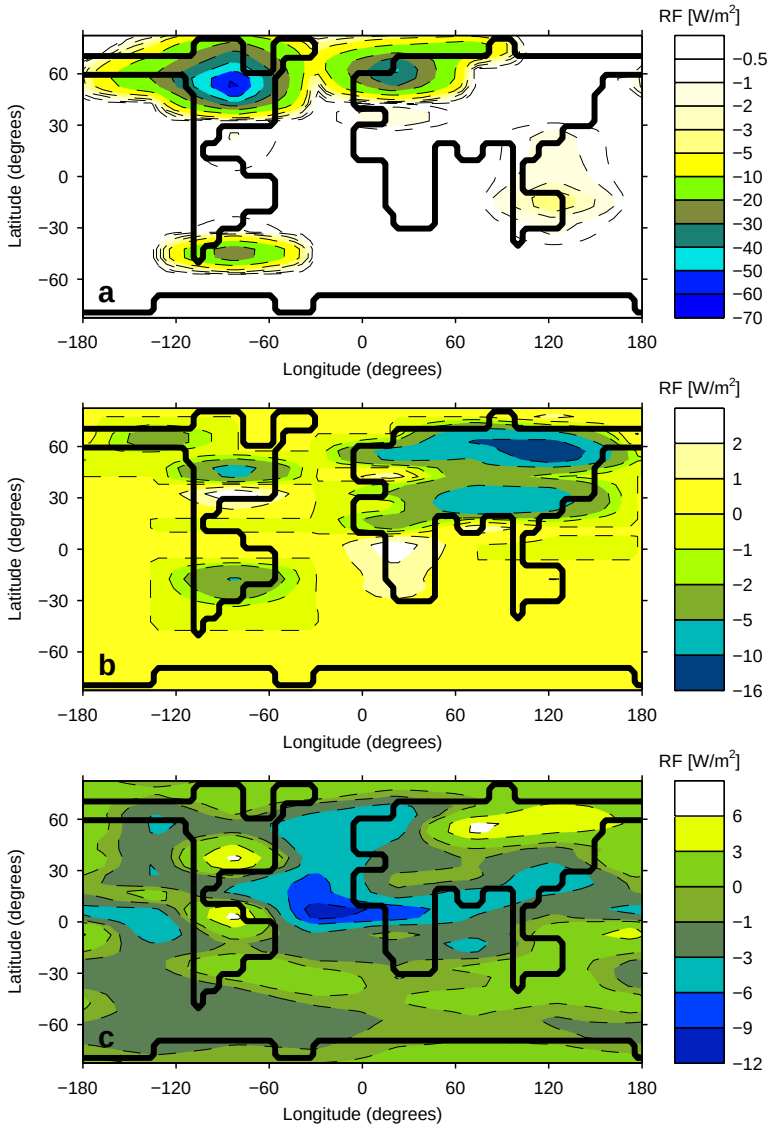

Fig. 5.8: Spatial LGM forcing. Shown is the annual mean radiative forcing for glacial ice sheets (a), vegetation cover (b), and dust (c). All values represent the ensemble mean of model versions constrained by tropical proxy-data. Note that apparent geographical overlap between ice sheet and vegetation forcing results from the facts that due to a coarse spatial model resolution some grid cells are only partially covered by ice sheets, and in these grid cells both, ice sheets and vegetation forcing, are nonzero. Another reason for the apparent overlap is the used graphical interpolation, which causes a smoothing of the contour lines.

By far the largest regional contribution to the glacial cooling results from the pronounced forcing over northern hemisphere ice sheets, which reaches maximum values up to –70 W/m^2 over southern Laurentide ice sheet (Fig. 5.8a). A smaller, yet not negligible effect comes from the substitution of ocean by land areas as a consequence of the lower glacial sea level. This effect is especially pronounced for shelf regions in southern America, yielding a comparatively large forcing contribution for this area.

Vegetation forcing (Fig. 5.8b) reveals large negative forcing in the northern hemisphere, which results from the strong albedo change in boreal latitudes through the conversion of forest into tundra. Besides its strong negative forcing effect, glacial vegetation patterns also exert a positive forcing with maximum values up to 4 W/m^2 in our simulations for specific regions. The difference in the inferred forcing strength among ensemble members is largest in the vicinity of forcing maxima with a maximum standard deviation of 1.2 W/m^2 (0.9 W/m^2) for ice sheet (vegetation) forcing[11]. The apparent geographical overlap between ice sheets and vegetation forcings results from the coarse spatial model resolution, as some grid cells are only partially covered by ice sheets, and in these grid cells both, ice sheets and vegetation exert a forcing. Furthermore the applied graphical tool, which interpolates the calculated CLIMBER-2 grid box values to a finer grid in order to smooth the model results, additionally contributes to the overlap of those both forcings for specific regions (Fig. 5.8).

The most pronounced inhomogenity in the forcing pattern is seen for glacial dust (Fig. 5.8c), which covers a range of large negative to large positive forcing. Furthermore it reveals a strong seasonal variation, resulting in a positive global forcing for one month of the year. The spatial distribution of CO_2 forcing is not explicitly shown as this homogeneously distributed forcing shows comparatively little spatial variability (HEWITT and MITCHELL, 1997).

5.2.4.5 Regional LGM cooling

The strong inhomogenities seen in the glacial forcings suggest a strong imprint in the spatial pattern of LGM cooling. Its characteristics can be inferred from the following figure, for global SAT cooling (dT_{LGM}), as well as for the SAT cooling following the prescription of the individual forcings.

The total LGM cooling is by far strongest over the northern hemisphere ice sheets with maximum cooling about 28°C, moderate tropical cooling (with larger cooling over land areas than over the oceans) and pronounced Antarctic cooling. The spatial inhomogenity clearly reveals the imprint of the applied boundary conditions, whose effect on the temperature anomaly is shown in Fig. 5.9c-f for each individual forcing. Similar to the impact of glacial ice sheets (Fig. 5.9c), vegetation change exerts a pronounced cooling of high northern latitudes (although of much smaller amplitude, Fig. 5.9e). The CO_2 forcing shows a rather uniform temperature response with a characteristic amplification of the cooling towards the poles (Fig. 5.9d). The strongly inhomogeneous pattern of glacial dust forcing (with positive and negative forcing contributions) yields a net cooling, with

[11] The magnitude of dust forcing does not depend on the model version (see details in section 5.2.4.1). Thus the standard deviation is only given for ice sheet and vegetation forcing.

largest anomalies in the northern Atlantic sector.

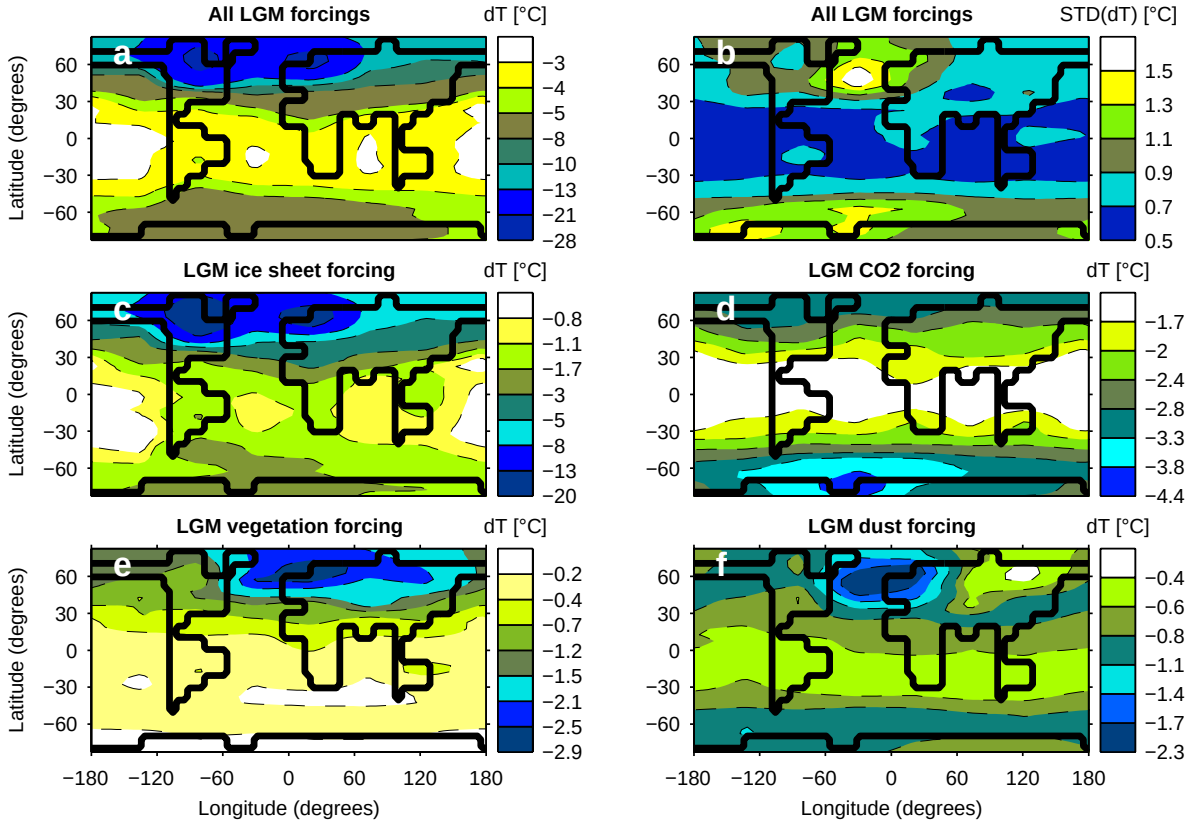

Fig. 5.9: Spatial LGM cooling. Shown is the annual SAT temperature anomaly (glacial / pre-industrial) resulting from the prescription of all main forcings (a), and from individual forcings of ice sheets (c), CO_2 (d), vegetation (e) and dust (f). All data represent the mean values for the ensemble constrained by tropical SST proxy-data. The spread from the mean is illustrated in (b).

Fig. 5.9b illustrates the standard deviation of all ensemble members that are shown in Fig. 5.9a. A maximum spread of SAT decrease is seen in Antarctica and in the North Atlantic, which can be interpreted by the difference in the extent of sea ice area and its impact on the temperature signal through the sea-ice albedo feedback. Especially the North-Atlantic region reveals to be sensitive to individual glacial forcings. As the extent in sea ice is tightly coupled to the location of North-Atlantic convection sites, a change in the location of those sites may well be seen in the temperature signal. Analysing the change in overturning strength in our ensemble we indeed infer a change in ocean circulation manifested in a reduction of NADW (North Atlantic Deep Water) for several ensemble members, for which we subsequently have implemented vegetation (SIM_VEG) and dust (SIM_DUST) forcing (see section 5.3.1 for a more detailed analysis of the impact of ocean circulation changes).

The conclusions we draw from the comparison of the glacial forcing and temperature anomaly patterns are that i) regional forcing may well determine regional climate change (as e.g. is the case for glacial ice sheets), but ii) that the maximum of forcing and temperature response do not have to strictly coincide (as

e.g. is the case for glacial dust and vegetation). The analysis of dust forcing further reveals that, although its main forcing is more confined to tropical regions, it well affects high latitude climate, as can be seen from the poleward amplification of the temperature response (Fig. 5.9f).

5.3 Constraining uncertainty in climate sensitivity by paleo data

In chapter 5.1 we have inferred the range of ΔT_{2x} from an ensemble of 1000 model versions (correlated ensemble), which span a broad range of different feedback strengths as a consequence of the simultaneous perturbation of 11 model parameters. We have shown that this range is only weakly reduced if data constraints from present-day climate are applied. As a next step we have run the same ensemble of model versions for LGM boundary conditions and inferred the ranges of global and regional glacial temperature change (chapter 5.2). In the following we will now combine the simulation results of those experiments and investigate the potential of LGM proxy-data in view of reducing uncertainty in the range of ΔT_{2x}. The crucial question to be explored in this context is whether there is a set of model versions, all being consistent with present-day climate data, which yield a LGM cooling inconsistent with reconstructed glacial temperatures. If the reason for inconsistency is a too low or too high model sensitivity then we could reduce the uncertainty range of ΔT_{2x}. An important aspect of our approach is that we perform both, the CO_2 doubling and the LGM experiment for each model and thus automatically account for differences in feedbacks and climate response between colder and warmer climates. We do not need to assume the same sensitivity to CO_2 changes for LGM conditions as for CO_2 doubling; we thus avoid an important problem that arises in purely data-based estimates of ΔT_{2x}.

In the following sections we will first explore, which regions are well-suited for constraining ΔT_{2x} by paleo data (section 5.3.1), we then proceed with the analysis of the relationship between simulated regional glacial cooling and $2xCO_2$ warming (section 5.3.2), discuss our methodology for constraining ΔT_{2x} (section 5.3.3) and evaluate the robustness of our inferred ΔT_{2x} ranges (section 5.3.4). The main findings presented in this chapter are summarized in SCHNEIDER VON DEIMLING et al. (accepted).

5.3.1 Choice of well-suited regions for model-data comparison

When looking for the best region for applying the LGM data-constraints, several criteria have to be considered. Well-calibrated proxy-data need to be available and the response should not be affected too much by regional small-scale dynamics, which cannot be resolved by our coarse-resolution model. As we want to constrain the model response to a doubling of atmospheric CO_2 content, GHGs should be an important forcing in the region and ideally the model response would show a pronounced spread among ensemble members for those regions such that only a well-defined subset of model versions will pass the consistency test with paleo data.

We have discussed the availability of paleo archives in the previous chapter (section 5.2.2). We now investigate the choice of best regions in the modelling context. In doing so we consider the simulated change in surface air temperature (SAT) between the pre-industrial and glacial climate (Fig. 5.10a) and analyse its standard deviation among all ensemble members for different regions of the globe (Fig. 5.10 b).

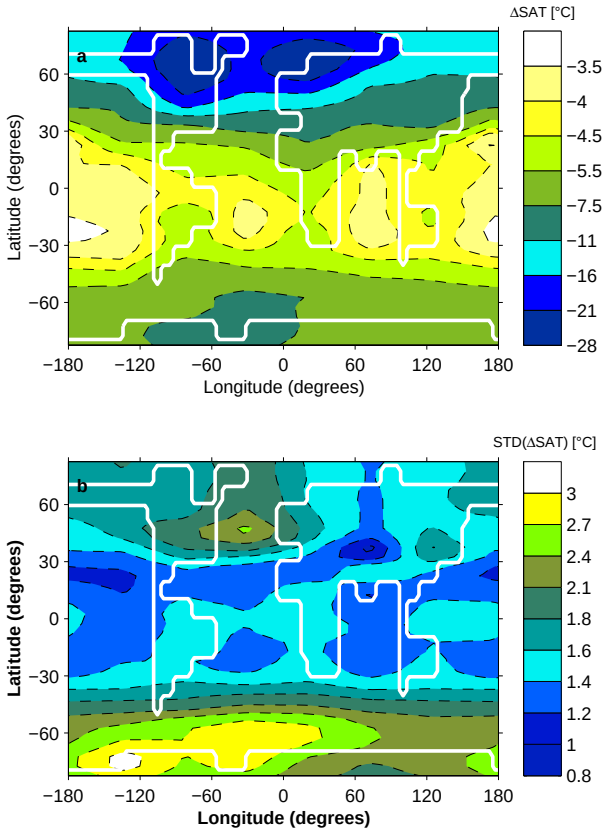

Fig. 5.10: Regional mean SAT cooling. The upper panel (a) shows the annual mean SAT anomaly between the LGM and pre-industrial climate for all present-day consistent ensemble members, the lower panel (b) shows the corresponding standard deviation among those model versions.

In contrast to the LGM simulations discussed in the previous chapter (SIM_LGM_PMIP2) the above figure shows the simulation results for our standard LGM runs (SIM_LGM, Table 1). Both experiments slightly differ in view of the prescribed glacial GHG concentration (180 p.p.m. for SIM_LGM, 167 p.p.m. for SIM_LGM_PMIP2) and ice sheet reconstruction (ICE-4G for SIM_LGM, ICE-5G for SIM_LGM_PMIP2). In section 5.3.4 we will constrain our model ensemble by focusing on the standard LGM runs and will use the LGM simulations from the previous chapter (SIM_LGM_PMIP2) to discuss the robustness of our inferred ΔT_{2x} ranges in view of the applied boundary conditions.

The comparison of Fig. 5.10 with Fig. 5.9a shows that the magnitude and spatial characteristics of SAT cooling is very similar in both ensembles. Maximum cooling occurs at high northern latitudes in the vicinity of the pronounced glacial ice sheets, moderate cooling is inferred for tropical regions and for high southern latitudes the poleward amplification of the cooling response yields a strong LGM cooling. Fig. 5.10b shows the standard deviation in simulated SAT anomaly of all present-day consistent model runs. In contrast to the corresponding figure of the previous chapter (Fig. 5.9b) we here show the spread before we have further constrained the ensemble by paleo data. Thus Fig. 5.10b informs about those regions, where the simulated temperature anomaly deviates strongest among different present-day consistent model members. In the modelling context those regions would be ideal for effectively constraining the ensemble. Fig. 5.10b suggests that this is the case for Antarctic regions and the Northern Atlantic. Yet one has to further consider the degree of confidence in the simulation of glacial

cooling of those areas. In this view the Northern Atlantic region should be discarded as the pronounced model spread is caused by a change in the location of deep water formation, which reveals a pronounced model dependency.

The analysis of the glacial forcings in the previous chapter has shown that the contribution of the individual forcings to regional cooling may differ strongly from region to region. As we want to constrain the temperature increase following a doubling of atmospheric CO_2 concentration (ΔT_{2x}), the region for constraining the model ensemble should reveal a strong GHG forcing signal in the simulated LGM temperature anomaly. The factor analysis performed (section 5.2.3) offers a means to estimate which regions suggest the largest imprint of CO_2 forcing. Yet this analysis method does not account for possible non-linearities in the model response. In order to infer an improved estimate of the fraction of LGM cooling attributable to lowered CO_2 concentrations, we performed two additional ensembles, in which (i) CO_2 has been lowered to its glacial value (180 p.p.m., implicitly accounting for CH_4 and N_2O changes) while keeping all other boundary conditions fixed to pre-industrial values (SIM_CO_2_LGM, Table 1), and – to account for non-linearities – (ii) all boundary conditions have been set to LGM conditions, but CO_2 fixed to its pre-industrial value of 280 p.p.m. (SIM_abCO_2_LGM). In the first case we calculate the contribution of CO_2 to LGM cooling as the difference between this ensemble (SIM_CO_2_LGM) and the pre-industrial runs in accordance with the factor analysis. In the latter case we calculate the CO_2 contribution as the difference between the second ensemble (SIM_abCO_2_LGM) and the ensemble with all LGM forcings contributing to the temperature response. The magnitude of inferred CO_2 induced SAT cooling is shown for both experiments in Fig. 5.11.

The ratio of CO_2 attributable cooling to total LGM cooling reveals a pronounced spatial imprint of the inhomogeneously distributed glacial forcings. The more distant from the northern hemisphere ice-sheets, the larger is the relative effect of CO_2, reaching maximum values of about 50% in large areas of the southern hemisphere. Although the patterns in Fig. 5.11a and Fig. 5.11b look rather similar they reveal a systematic difference between both experiments: For the case, where the ratio of CO_2 attributable SAT cooling was inferred from the colder climate state (b) the fraction of dT_{CO2}/dT_{LGM} is slightly larger for most regions of the globe (Fig. 5.11c). Additionally changes in the ocean circulation pattern (meridional overturning in the Atlantic sector) show a different imprint for both simulation sets. For the first experiment, where the boundary conditions were set to pre-industrial values besides CO_2, the overturning strength is only weakly affected by the change in CO_2 concentration, whereas in the latter case, where all boundary conditions were set to glacial climate (besides CO_2), we infer a change in the overturning strength for most ensemble members: We reveal a slight weakening in NADW (about 1-5 Sv) in combination with a southward shift of the location of deep water formation. As a consequence the sea-ice area extends further southwards and explains the larger CO_2 induced cooling in this area (Fig. 5.11c), caused by an increased sea-ice albedo feedback. An effect of opposite sign is seen in Antarctica. This can be explained by the teleconnection induced by the so-called *bipolar seesaw* (CROWLEY, 1992; STOCKER, 1998): A reduction in the strength of NADW yields a reduced northward oceanic heat transport. This decrease leads to a warming in the Southern Ocean and over Antarctica.

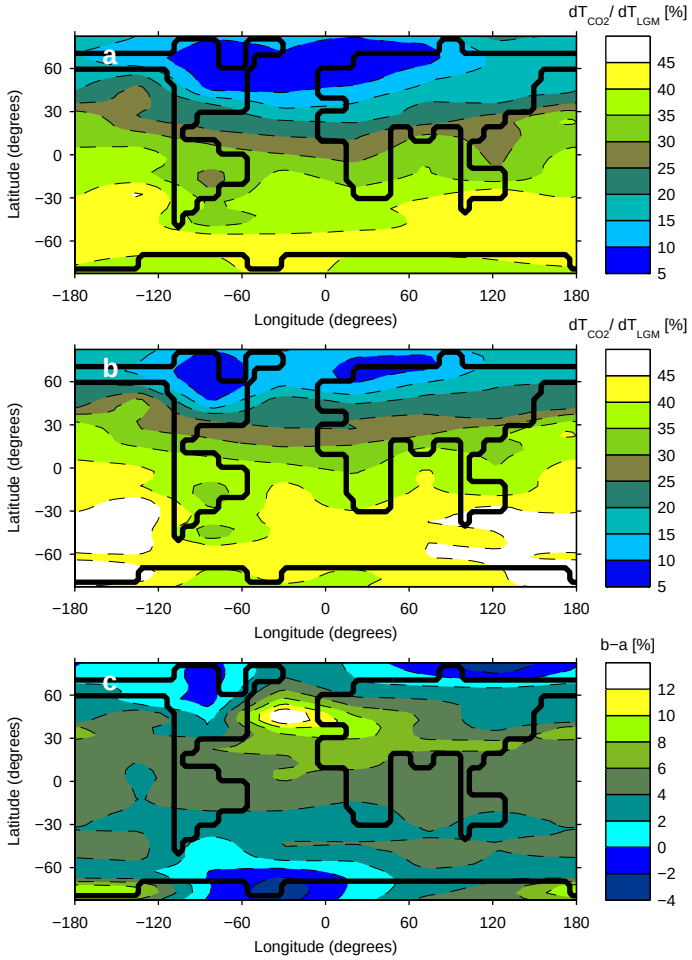

Fig. 5.11: Ratio of CO_2 attributable SAT cooling to total LGM SAT cooling. Panel (a) and (b) show the percentage of LGM cooling, caused by the glacial drop in the concentration of GHGs, for the ensemble mean of all present-day consistent model versions. Simulation results from (a) were inferred from an additional ensemble with prescribed glacial CO_2 content while keeping all other boundary conditions fixed to pre-industrial values, for (b) all boundary conditions were set to LGM conditions, but CO_2 fixed to its pre-industrial value. The difference (in %) between both experiments (b-a) is illustrated in the lowest panel (c).

To conclude, it can be seen that the magnitude of CO_2 attributable cooling depends to a certain extent on the background climate[12], and on the type of experiment that was used to estimate dT_{CO2}, as it may contain a strong regional imprint of changes in the ocean circulation in our simulations. Additionally the exact value of dT_{CO2} depends on the chosen model version as can be seen in the following figure, which shows the fraction of CO_2 attributable cooling for our focus regions to constrain the ensemble.

[12] Globally averaged dT_{CO2} amounts 35% for SIM_CO_2_LGM and 39% for SIM_abCO_2_LGM.

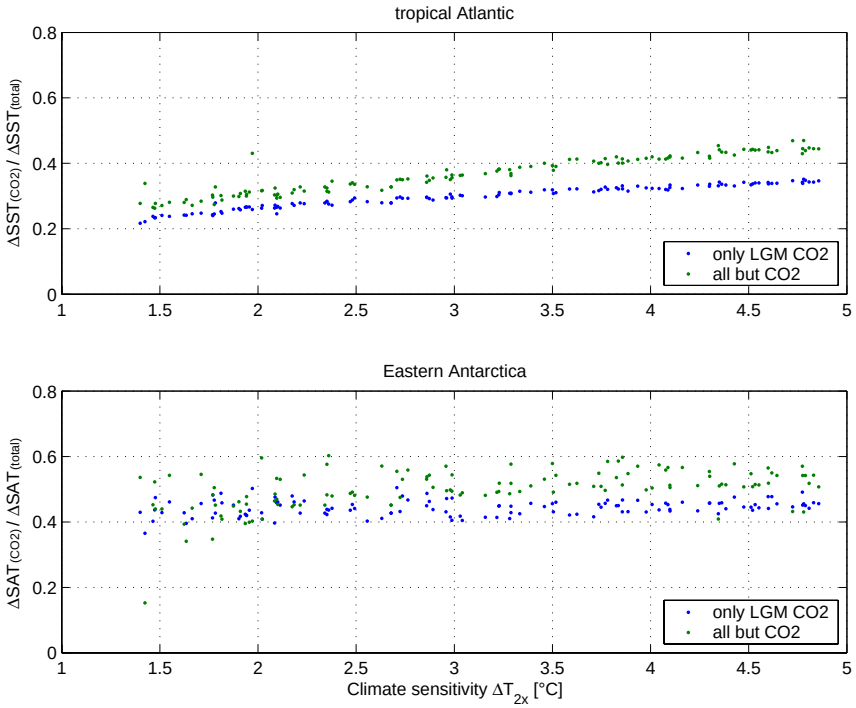

Fig. 5.12: Fraction of LGM cooling attributable to CO_2 lowering. Shown is the ratio of annual mean LGM cooling, attributable to CO_2 concentration changes, to total LGM cooling (tropical Atlantic SSTs: upper panel, Eastern Antarctic SAT: lower panel). Blue dots represent model results obtained for changes in CO_2 content only (SIM_CO_2_LGM), green dots for prescribing all glacial forcings but CO_2 (SIMabCO_2_LGM).

With increasing model sensitivity the fraction of CO_2 attributable LGM cooling is increasing. This dependency is more pronounced for the tropical SSTs (Fig. 5.12, upper panel) than for the Antarctic region (Fig. 5.12, lower panel), which might be explained by the larger difference in the lapse rate feedback among model versions for low latitudes than for high latitudes (see next chapter).

In order to compare the ratio of CO_2 attributable tropical SST cooling to total LGM cooling with GCM based studies, which have neglected dust and vegetation forcing, we performed a third ensemble. Those additional simulations are equivalent to SIM_CO_2_LGM but disregard forcing of LGM dust and vegetation changes (SIM_CO_2_PMIP). The resulting ratio of dT_{CO2}/dT_{LGM} spans a range consistent with results from Shin et al (2003), and slightly smaller than estimated by Kim et al (2004).

To come back to the question, which areas show a large imprint of GHG forcing in the simulated LGM cooling, the analyses performed suggest that the northern high latitudes are dominantly affected by the presence of large continental ice sheets, with GHGs contributing only minor to the signal. This makes them less suited despite the availability of Greenland ice-core data. Yet the high latitudes of the southern hemisphere reveal a strong GHG signal and a comparatively large model spread. Thus Antarctic ice core archives (remote from the area of a possibly strong signal caused by changes in the overturning characteristic) seem to be the best choice for a model-data comparison in the modelling context. On the other hand the Antarctic region is isolated regarding its location,

comparatively small compared to the tropical ocean area, where a large amount of high quality sediment cores offers a means for inferring large scale LGM cooling for a broad region of the globe. Furthermore the confidence in reconstructed tropical SSTs can be improved by inference from independent methods (e.g. from foraminifera or from geo-chemical proxies). Given those arguments we decided to focus our further analysis on the tropical Atlantic region for constraining the model ensemble by paleo data. We use reconstructed Antarctic temperatures to check consistency of our ΔT_{2x} estimates, inferred from low and high latitude proxies.

5.3.2 Linkage of regional LGM cooling and global CO_2 warming

In the following we will illustrate the relation between simulated regional LGM cooling and global $2xCO_2$ warming. This relation is the backbone of our analysis and is shown in Fig. 5.13 for four key regions, where proxy-data are available. The effectiveness of our approach to constrain the uncertainty range of ΔT_{2x} will crucially depend on how strong this link between simulated past glacial cooling and $2xCO_2$ warming proves to be.

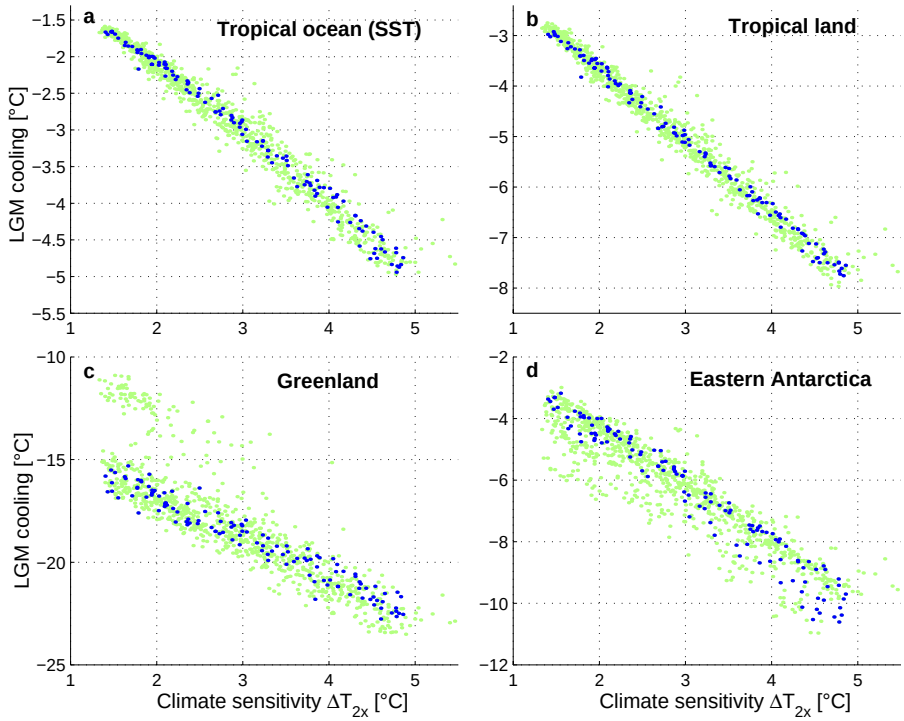

Fig. 5.13: Dependence of LGM cooling (relative to the pre-industrial climate) on ΔT_{2x} for different regions. Shown is **a**, annual mean of average (20°N-20°S) global tropical SST cooling; and annual mean average SAT cooling for **b**, tropical land (30°N-30°S), **c**, Greenland, **d**, eastern Antarctica. Green points represent the entire ensemble (1000 runs, SIM_LGM), blue points only model versions consistent with present-day climate (123 runs).

The strong correlation between ΔT_{2x} and LGM cooling is striking (Fig. 5.13): The larger the sensitivity of a given model version to CO_2 doubling, the larger the simulated LGM cooling. For those models, which are consistent with present-day data (blue dots), a quasi-linear relationship between ΔT_{2x} and LGM cooling is inferred. This close link is not dependent on the exact choice of the present-day data constraints and will be the basis for our approach of constraining ΔT_{2x} in the next section. Implications of structural uncertainty and the issue of model dependence of this strong relation will be discussed in section 5.3.4.1.

5.3.3 Applied methodology for constraining uncertainty in climate sensitivity

To infer an estimate of ΔT_{2x}, which is consistent with reconstructed regional LGM temperature data, one could go back to the unconstrained model ensembles, proceed according to Bayes' formula and present the most extreme values for ΔT_{2x} quantiles as robust estimates. However, we would like to make use of the relations displayed in Fig. 5.14: A suggested linear relation between LGM cooling and ΔT_{2x}. For that purpose we apply an "interval method", which allows to derive statistically robust estimates of ΔT_{2x}, and which proves to be even more conservative than a Bayesian procedure. We describe this method in the following.

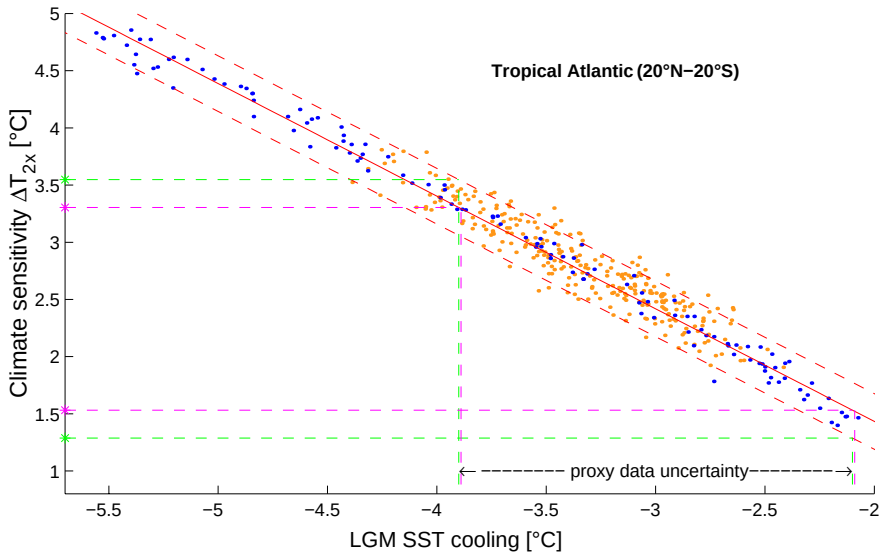

Fig. 5.14: Inferring ΔT_{2x} from LGM data. Simulated annual mean tropical Atlantic SST cooling (averaged from 20°N-20°S) is shown for correlated (blue dots) and uncorrelated parameter ensembles (orange dots). The red curve shows the linear fit to the correlated ensemble, the red dotted lines represent the fit-error, conservatively estimated from the uncorrelated ensemble as the 5-95 percentile of the spread of deviations from the fit. Only runs consistent with present-day data are shown. Purple (green) dashed lines illustrate the range of ΔT_{2x} (including fit-error bounds) consistent with a mean tropical Atlantic SST cooling of 3.0±0.9°C.

Our preferred region to constrain the model ensemble is the tropical Atlantic (20°N-20°S), as motivated in section 5.2.2. For all other regions discussed in the following the method is applied the same way. We first approximate the inferred relationship between ΔT_{2x} and tropical LGM SST cooling by a linear regression (Fig. 5.14, solid red curve). The fit uses the simulation results of the correlated ensemble (blue dots, SIM_LGM), which covers a broad range of ΔT_{2x}. We then read the ΔT_{2x} range from the fit-curve (pink asterisks), which is consistent with the reconstructed glacial SST cooling (3.0±0.9°C). We account for the additional uncertainty in ΔT_{2x} caused by deviations from the fit. This is realized by choosing the 5-95 percentile of the deviation spread (represented as red dashed lines), estimated from the uncorrelated ensemble (orange dots, SIM_uncor_LGM), as it provides larger deviations than for the correlated ensemble and thus yields a more conservative uncertainty measure. Using the fit and the spread estimate, we then determine ΔT_{2x} ranges (green asterisks), which are consistent with mean tropical Atlantic SST cooling. A methodology to constrain the transient climate response (TCR) can be found in Appendix A.

The application of the proposed interval scheme for the tropical SST paleo constraint yields a range of 1.3-3.5°C for ΔT_{2x} (0.9-2.1°C for TCR). This range is notably smaller than estimates of previous ensemble-based studies (FOREST et al., 2002; KNUTTI et al., 2002; MURPHY et al., 2004; STAINFORTH et al., 2005), and even smaller than that estimated by the IPCC (HOUGHTON, 2001). Yet our estimate of the ΔT_{2x} range does so far not account for uncertainty in the model structure, in the radiative forcing, and does not include paleo information from other regions. A detailed analysis of those factors will be presented in the next section.

5.3.4 Uncertainties affecting the estimate of climate sensitivity

Our constrained ΔT_{2x} range crucially depends on a) the universality of our inferred quasi-linear relationship between future warming and past cooling, thus on the model structure, b) the applied glacial boundary conditions, and c) the reliability of reconstructed paleo temperatures. All of those factors determine the broadness in the inferred range of ΔT_{2x}, and will be discussed in the following.

5.3.4.1 Model structure

Our model results suggest a strong correlation between simulated regional LGM cooling and 2xCO_2 warming. The key question in view of the robustness of our results is whether the close correlation of regional LGM cooling with ΔT_{2x} (Fig. 5.13) is specific to our model, or whether it is valid more generally. Physical reasoning makes a close link between mean glacial tropical cooling and ΔT_{2x} plausible. Mean glacial tropical cooling largely reflects lower CO_2 values, and is as such the inverse of an increased CO_2 experiment. A similar study with a multi-model ensemble would help to clarify the importance of processes not resolved by our model (e.g. ENSO). Simulations with comprehensive climate models realised within the PMIP-2 project will be published in the near future and will help to judge the degree of model dependency of our results.

The shape, location and the uncertainty of the strong relation proposed in Fig. 5.14 depend on the model used and how or which processes are resolved or parameterised in the model. In contrast to the close linear relationship found in CLIMBER-2, Annan et al. (2005) find a much weaker correlation of glacial SST and climate sensitivity in an atmospheric GCM coupled to a slab ocean. They infer deviations of the individual simulations from a linear approximation about five times larger than in our model. We take this larger spread as a measure for uncertainty when using structurally different models and enlarge our inferred spread estimate by a factor of five. The resulting upper limit of ΔT_{2x} is shifted by 1°C towards larger sensitivities. Additional to uncertainty in the spread an offset in the regression line (Fig. 5.14) may introduce a further bias. At this stage there are too few model realisations with fully-coupled comprehensive climate models to quantify this effect.

We can compare our results with preliminary simulation results from the PMIP-2 project. For this purpose we refer to our ensemble, in which forcing contributions from glacial dust and vegetation patterns have been omitted (SIM_CO_2_PMIP) for consistency with PMIP-2 boundary conditions. As the only two available PMIP-2 simulations fall inside our considered uncertainty range when we only double our inferred spread estimate, we assume to rather overestimate than underestimate the impact of structurally different models on our results by having enlarged the spread by a factor of five.

In the modelling context the crucial issues for determining CO_2 sensitivity from an inverse glacial experiment are (i) what fraction of tropical glacial cooling is due to CO_2 and how much is due to other forcings and horizontal energy transport, and (ii) whether there are strongly asymmetric feedbacks for warming and cooling not correctly captured by our model. Concerning (i), we have included uncertainty in aerosols, glacial ice sheets and GHG concentrations (see next section) – and we note that the horizontal energy transport out of the tropics in other models is unlikely to be considerably outside the range covered in our ensemble, which yields a range of 1.4-2.0 for the ratio of global to tropical SAT cooling. Concerning (ii), processes not captured by our model (e.g., ENSO-dynamics) may play a role, but this would only change our ΔT_{2x} estimate if such processes affect the mean SST of the tropics in a strongly asymmetric way for LGM and CO_2 doubling. Hence it remains to be cleared in how far a multi-model ensemble shows a much wider spread than seen in Fig. 5.14. Note that derivations of ΔT_{2x} purely based on paleo-data (e.g. LEA (2004) implicitly assume a symmetry between warming and cooling and a fixed fraction of glacial cooling attributable to CO_2.

5.3.4.2 Glacial forcings

Although the main LGM forcings are relatively well known, uncertainty in the individual forcing strengths remains. This is especially the case for the impact of glacial dust (aerosol) content due to incomplete knowledge of its regional distribution and radiative properties (CLAQUIN et al., 1998; SOKOLIK and TOON, 1999). Uncertainty in the magnitude of aerosol forcing is one of the main reasons why it is not possible to effectively constrain the range of ΔT_{2x} by comparing simulated 20th Century warming with observational data. This is because a combination of high climate sensitivity models with large negative aerosol forcing yields a moderate temperature response, consistent with observations. Yet for the LGM climate the problem of aerosol shielding is not a problem for constraining the upper limit of ΔT_{2x}: A large negative dust aerosol forcing

reinforces the global cooling and enhances the GHG induced temperature change[13]. Thus a large uncertainty in the quantification of maximum negative aerosol forcing leads to large uncertainty in the lower bound of climate sensitivity for studies focusing on the LGM cooling, whereas it leads to large uncertainty in the upper bound for approaches, that constrain ΔT_{2x} by focusing on the anthropogenic warming.

For testing the sensitivity of our inferred climate sensitivity range to changes in the prescribed dust forcing we first evaluate the impact of a possible overestimation of dust forcing on ΔT_{2x} by running an identical ensemble with the dust radiative anomaly reduced by 50% (SIM_LGM0.5). This weaker radiative forcing yields a slightly reduced contribution to the simulated glacial cooling, as can be seen for our focus regions in the following figure.

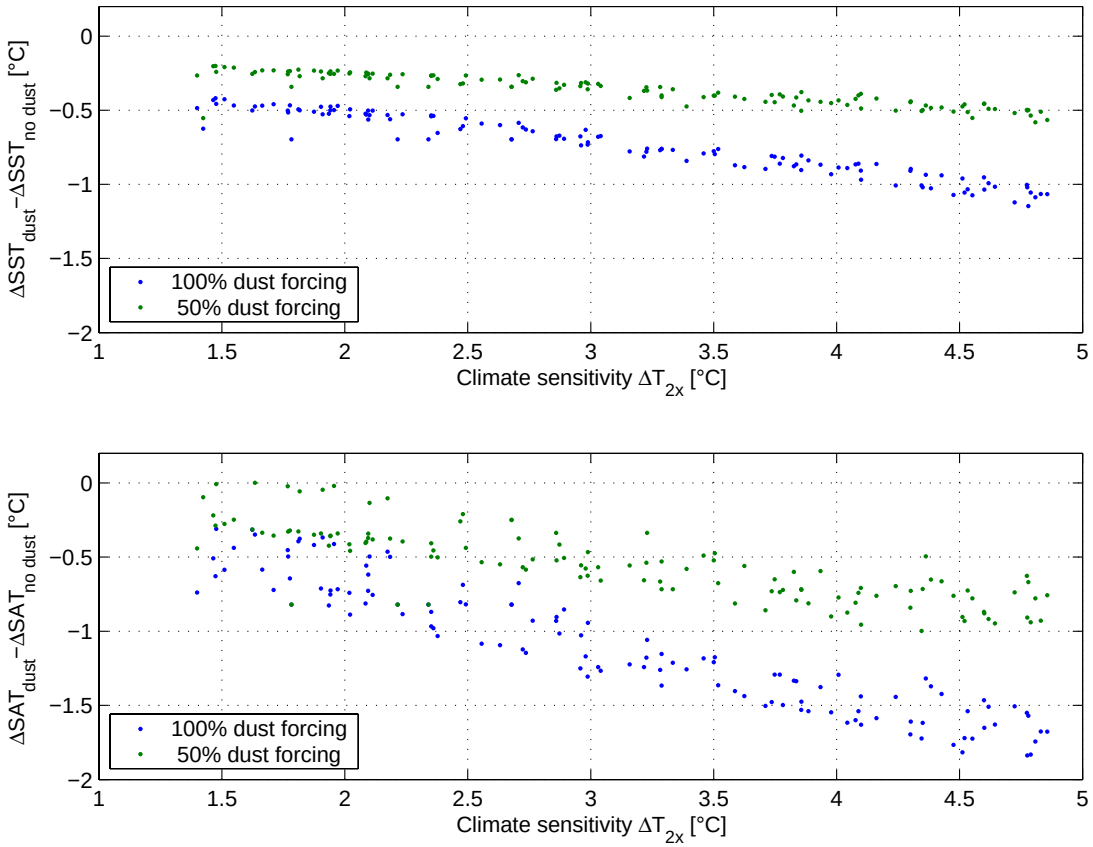

Fig. 5.15: Additional glacial cooling through dust forcing. Shown is the difference in LGM cooling between model versions, which account for dust forcing (green dots: 50% dust forcing, blue dots: 100% dust forcing) and the same model versions without being forced by glacial dust, illustrated for tropical Atlantic SST decrease (upper panel) and Eastern Antarctic SAT decrease (lower panel).

[13] Dust may as well constitute a positive forcing by lowering snow and ice albedo. As we focus our analysis on regions remote from the area of high northern latitudes, this effect is not considered in our analyses: Due to the far distance from the main dust sources the increase in Antarctic glacial dust content is much weaker than inferred from Greenland ice cores (Mahowald et al.,1999).

The implementation of the radiative impact of glacial dust (100% scenario, SIM_LGM) implies an additional global forcing of about –2.1 W/m^2 for the tropics (0.3 W/m^2 for eastern Antarctica), which translates into an additional cooling of about 0.5-1.0°C (0.4-1.8°C) for mean tropical Atlantic SST (eastern Antarctic SAT). For the scenario of 50% dust forcing (SIM_LGM0.5) the additional cooling is almost half the size for most model members.

A much stronger forcing than realized by our 100% scenario seems unlikely, or one would expect a stronger correlation between tropical SSTs and dust in the atmosphere over a complete glacial cycle: Ice and sediment cores indicate a drastic increase of dust deposition rate at the MIS4/MIS3 boundary (around 60 kyr B.P.), while SST cooling in the tropics is rather moderate at that time. Multivariate analysis of tropical SST and Antarctic dust concentration (LEA, 2004) provides an upper estimate for the impact of dust on glacial temperature. Moreover, when accounting for the fact that only part of the glacial SST signal should be attributed to the increase in dust concentration and that changes in dust concentration coincide with CO_2 drop, ice-sheet growth and sea level lowering, the effect of dust on LGM cooling is smaller than estimated by multivariate analysis (LEA, 2004). Regarding our estimate of ΔT_{2x}, the considered uncertainty in dust forcing (a reduction by a factor of two) leads to a small shift (about 0.3°C) of the ΔT_{2x} range to larger values.

In addition to the impact of uncertainty in the magnitude of dust forcing we consider uncertainty in glacial ice sheet forcing. The key determinant is the spatial extent of the imposed ice sheets, which can be well constrained by moraine signatures. The total ice sheet volume is accurately known from sea level lowering. Uncertainties remain concerning the exact shape and albedo of the ice sheets. We therefore reduced the standard model parameters of ice sheet albedo by 10% and derived an increase of the upper ΔT_{2x} limit of 0.5°C. The sensitivity of our results to changes in the ice sheet shape was investigated by replacing Peltier's ICE-4G ice sheet reconstruction (PELTIER, 1994), which we use for our standard LGM design (SIM_LGM), through ICE-5G (PELTIER, 2004), with most pronounced differences between the two in the Eurasian region. The difference for tropical Atlantic SST cooling between those two experiments is rather small (0.15-0.25°C for most model members).

The concentration of glacial GHGs is rather well known from trapped air bubbles in ice cores, which contain information about past atmospheric compositions. To quantify the impact of (comparatively small) uncertainty in GHG forcing on our ΔT_{2x} estimate we re-run the ensemble for an *equivalent*[14] CO_2 concentration of 170 p.p.m., which is closer to the PMIP-2 design than our standard experiment with 180 p.p.m. (SIM_LGM), which is more at the lower end of recent estimates of glacial-interglacial GHG concentration changes. This additional decrease of 10 p.p.m. lowers the upper limit of ΔT_{2x} by 0.1°C.

Uncertainty in orbital and vegetation forcing, which both are small compared to the uncertainty in the remaining forcings, are not considered for our further analysis. In the following we comprise the forcing uncertainty of glacial dust content, ice sheets and GHG concentration by discussing a minimum and a maximum scenario of glacial radiative forcing (SIM_lowRF and SIM_highRF, see

[14] This concentration yields the same radiative forcing as the sum of individual GHG forcings resulting from changes in CO_2, CH_4 and N_2O concentrations.

Table 1). We run those two ensembles for the discussed differences in the glacial boundary conditions and then apply our methodology of constraining the uncertainty range of climate sensitivity.

Focusing on the tropical Atlantic SST constraint (3.0±0.9°C), our results suggest a range for ΔT_{2x} of 1.2-3.3°C in case of the assumption of maximum LGM forcing, and an increased range of 1.8-4.3°C for minimum LGM forcing. As described in section 5.3.3, our intervals represent conservative estimates of 5-95% quantiles.

Are those results robust if we repeat our analysis for alternative regions to constrain the model ensemble? We will investigate this further aspect in the next section.

5.3.4.3 Paleo data

The uncertainty range of our climate sensitivity estimates depends on the reliability of the applied paleo-data. For the reasons given in section 5.2.2, our data constraint is strongest for reconstructed tropical SSTs (based on Atlantic sediment cores). The fact that fundamentally different proxy reconstructions (such as transfer function and geo-chemical methods) yield consistent results for most regions of low latitudes, as e.g. suggested by first results of a huge multi-proxy inter-comparison project (MARGO, KUCERA et al., 2005), enhance the credibility in the considered SST paleo-temperature estimates.

Nevertheless it is instructive to also consider other data types and regions. Tropical land data are subject to larger uncertainty (3.5-7°C cooling) (FARRERA et al., 1999; PINOT et al., 1999), but yield similar estimates of ΔT_{2x}. Ice-core data from Antarctica (about 5.4±1.4°C cooling above the temperature inversion, and 8±2°C surface cooling, VIMEUX et al., 2002; JOUZEL et al., 2003; WATANABE et al., 2003) constrain ΔT_{2x} independently from low latitudes, showing highly consistent results with tropical SST based estimates (Fig. 5.16, note the small difference between solid and dashed blue intervals). In this context we should mention that our model-data comparison for Eastern Antarctica is not biased by an overestimate of altitude changes in the ice sheet, which would result if one assumed a pronounced increase in Antarctic ice sheet height during the LGM. We only apply changes in ice sheet altitude due to sea level lowering (120m) for Eastern Antarctica. The comparison of ice-core temperatures from Greenland (18-20°C surface cooling, DAHL-JENSEN et al., 1998) with our model simulations again yields consistent ΔT_{2x} estimates (Fig. 5.13c), but this should not be over-interpreted given the small size of Greenland and the coarse model resolution. Overall, the fact that very different absolute temperature changes in high and low latitudes all yield very similar estimates of ΔT_{2x} gives additional credence to our results.

We have assembled the effects of the choice in paleo data constraints (tropical or Antarctic) and of both forcing scenarios, discussed in the previous section, in Fig. 5.16. The comparison of our inferred ΔT_{2x} ranges (blue intervals) with recent ensemble studies, which have constrained climate sensitivity by he comparatively small warming signal of the last hundred years (upper four intervals), suggest that our approach reveals to be effective in constraining the uncertainty of model sensitivity. Our upper limit of ΔT_{2x} is almost consistent with the upper end of the IPCC estimate of 4.5°C. It may seem counterintuitive that our lowest limit of paleo consistent ΔT_{2x} (interval 1a) is lower than the lower limit constrained by present-

day data (vertical dashed green line). This discrepancy results from the applied interval method to constrain the ensemble, which is based on a conservative interpolation of the model behaviour (see section 5.3.3).

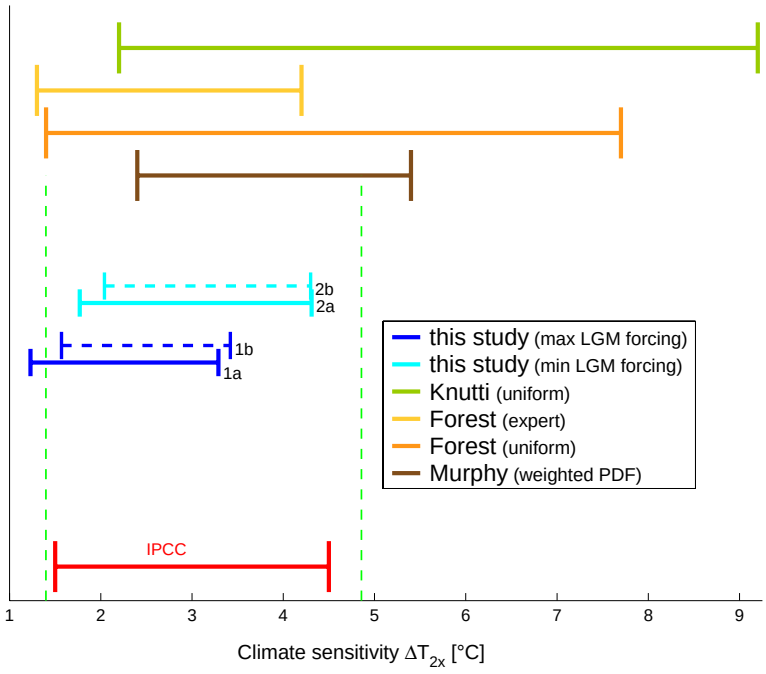

Fig. 5.16: Climate sensitivity estimates. The dark (light) blue intervals represents the 5-95% range of ΔT_{2x} consistent with LGM cooling for a minimum (SIM_lowRF) and maximum (SIM_highRF) assumption of glacial forcing, illustrated for mean tropical Atlantic SST cooling (3.0±0.9°C, solid lines) and Antarctic cooling (5.4±1.4°C, dashed lines). Vertical green dashed lines represent the ΔT_{2x} range resulting from the present-day data consistent parameter ensemble without applying LGM constraints. Other recent ΔT_{2x} estimates (5-95%, FOREST et al., 2002; KNUTTI et al., 2002; MURPHY et al., 2004 (weighted PDF)) are shown for comparison (see legend).

If our model failed to realistically simulate the latitudinal profile of LGM cooling then we would expect that our inferred ΔT_{2x} ranges from low and high latitudes diverge to some degree. The comparison of the solid blue intervals in the above figure (tropical SST constraint) with the dashed blue intervals (Antarctic constraint) illustrates that our estimates of climate sensitivity of both regions are highly consistent and suggest that our model ensemble realistically covers the main latitudinal characteristics of LGM cooling.

To summarize, our analyses of different factors contributing to the uncertainty range in ΔT_{2x}, we state that the largest contribution to the spread in climate sensitivity comes from the applied proxy-data (about 1.6°C), a slightly smaller contribution from uncertainty in radiative forcing (about 1°C) and the lowest contribution from uncertainty in the model spread (about 0.5°C, which might be as large as 2°C if we assume structural uncertainties to be pronounced).

5.3.5 Implications

Our most important result is perhaps that we confirm, based on a new methodology, the most likely value for ΔT_{2x} being between 2.5 to 3ºC. This estimate is in agreement for the best-guess of most-recent studies (KERR, 2004), which resulted from bottom-up approaches based on a physical understanding of radiative forcing and feedbacks, as well as from analysis of the observed climate evolution in the 20th Century. However, those studies have found it difficult to confirm the upper limit of 4.5ºC given by the IPCC, suggesting that higher values are possible (see Fig. 5.16, upper four intervals). This is no positive evidence for higher values but a lack of evidence for ruling those out. Nevertheless, it is important to constrain the upper limit, to help society evaluate the worst-case risks involved in future GHG emissions.

We conclude that the tropical cooling during the LGM as reconstructed with increasing accuracy from various types of proxy-data, can provide a constraint on the upper limit of ΔT_{2x}. The effectiveness of such a constraint will crucially depend on the question how strong the link between simulated glacial cooling and future warming (ΔT_{2x}) proves to be, when an ensemble of structurally different models is considered. Simulation results from inter-comparison studies (such as PMIP-2) will allow for a first step towards quantifying this uncertainty. Assuming that our inferred close relationship between LGM cooling and CO_2 warming represents a universal characteristic seen as well in comprehensive climate models, and assuming that the *mean* tropical Atlantic SST cooling during the LGM (averaged from 20°N-20°S) was in the range of 3.0±0.9ºC, we then infer the range of consistent climate sensitivities. When additionally accounting for uncertainty in the glacial forcings our method gives a 5-95% range of 1.2-4.3°C (up to about 5.3°C if structural uncertainties are accounted for) for the climate sensitivity to CO_2 doubling (0.9-2.6°C for the transient climate response TCR). These results are corroborated by ΔT_{2x} estimates being based on reconstructed Antarctic cooling (5.4±1.4°C, inversion level).

The promising outcome of our study suggests that further investigations with multi-model ensembles will be worthwhile, especially in the view of a successful first multi-thousand-member GCM ensemble (STAINFORTH et al., 2005), to analyse the importance of structural uncertainties for our methodology applied for constraining the uncertainty range of climate sensitivity.

5.4 Analysis of simulated model feedback strengths

The IPCC uncertainty range for climate sensitivity (1.5-4.5°C) is based on the comparison of the simulated temperature response ΔT_{2x} from different GCMs for the same forcing scenario ($2xCO_2$). The difference in ΔT_{2x} estimates from those models mainly results from differences in their simulation of the model-inherent feedback cycles. The broadness of the spread in the simulated feedback strengths thus is a good indicator of the degree to which our results are model-independent and shall be explored in this chapter. We do this by quantifying the strengths of all individual feedbacks[15] (of water vapour, clouds, lapse rate, albedo) for our ensemble of different model versions and compare these with results derived from comprehensive climate models. The crucial question is: Do we cover in our CLIMBER-2 model ensemble the feedback characteristics of different GCMs? A further main aspect, explored in this chapter, is the dependence of the feedback strength on the background climate. Is the feedback parameter, inferred from estimates of past temperature change and radiative forcing, a good measure for the expected climate response to future forcing?

We begin our analysis by describing the applied methodology of calculating the feedback components, which is based on the theoretical derivations presented in chapter 2.

5.4.1 Feedback calculation

Different methods have been applied in the past to quantify the feedback strength of a given climate model (WETHERALD and MANABE, 1988; CESS et al., 1990; SODEN et al., 2004)). Here we apply the *offline top of the atmosphere (TOA) radiation* method, which has been pioneered by Wetherald and Manabe (1988). The advantage of this method is, that it enables to directly calculate the differential behaviour in the radiative fluxes (at the TOA), which result from a change in internal climate variables (i.e. in water vapour, cloud, albedo and lapse rate). The radiative perturbation derived, normalized by the change in global-mean temperature, then can be taken as a direct measure of the feedback strength. Yet this method has not been applied to a large set of climate models because it is computationally expensive and difficult to implement (SODEN et al., 2004). In contrast to comprehensive climate models, the computational efficiency of CLIMBER-2 allows us to apply this method to a large ensemble of model versions and thus enables us to analyse the spread in individual feedback strengths for a set of models, covering a broad range of different climate sensitivities. As we use this method consistently for all ensemble members, our results do not suffer from a possible bias due to different assumptions made for the feedback calculations, as is the case for GCM inter-comparison studies (COLMAN, 2003a).

[15] We use the term “feedback” in the following for referring to the indirect feedbacks described in section 2, unless we explicitly refer to direct or indirect feedback components.

To derive the strengths of the considered model feedbacks we have extended the CLIMBER-2 model code for applying the offline calculation method. In the following the calculation scheme will be exemplified for water vapour feedback, and is applied the same way for the calculation of the remaining feedbacks. We first perform a perturbed run (e.g. *2x*CO_2) and store the temporally and spatially resolved equilibrium fields of water vapour for each grid cell. We then perform a standard (*1x*CO_2) equilibrium run and determine the outgoing long-wave (LW) and short-wave (SW) radiative fluxes at the TOA (R_{LW} and R_{SW}) for each grid cell. In the next step we re-run the radiative code of LW and SW radiation for the last year of the 1xCO_2 integration offline with the water vapour fields substituted by the restored fields from the perturbed run (2xCO_2) and again determine the fluxes R'_{LW} and R'_{SW} during each time step for each grid cell. The difference in the radiative TOA fluxes ($R'_{LW} - R_{LW}$) and ($R'_{SW} - R_{SW}$) between the standard and the perturbed run – divided by the change in global-mean surface temperature ΔT_S between both experiments – then yields the water vapour feedback *WV* for both radiation bands:

$$WV_{LW} = \frac{R'_{LW} - R_{LW}}{\Delta T_S} \quad \text{and} \quad WV_{SW} = \frac{R'_{SW} - R_{SW}}{\Delta T_S} .$$

When we show the magnitude of water vapour feedback *WV* in the following figures, we refer to the annually and globally averaged sum of LW and SW feedback contributions. The same applies for cloud feedback, whereas albedo feedback only affects the net SW radiation and lapse rate feedback only affects the net LW radiation.

5.4.2 Feedback analysis of correlated and uncorrelated model versions

We first have quantified the feedback strengths of water vapour, clouds, lapse rate and albedo for the correlated parameter ensemble, which covers a broad range of climate sensitivities between 1.3-5.5°C. The radiative perturbation was calculated between the pre-industrial climate state (CO_2 280 p.p.m.), and the perturbed equilibrium climate of doubled CO_2 concentration (560 p.p.m.). For taking account of possible non-linearities in the response, we have further performed the same experiment but with the control and perturbed climate swapped (exchanged). When we describe the *mean* feedback strength in the following, we refer to the average value over both experiments.

For analysing the difference in the simulated feedback strengths, resulting from the introduction of parameter correlations (see section 4.3), we have additionally performed the same set of simulations for the uncorrelated parameter ensemble. The results of those analyses are presented in Fig. 5.17, which shows the spread in individual mean feedback strengths for correlated and uncorrelated model versions.

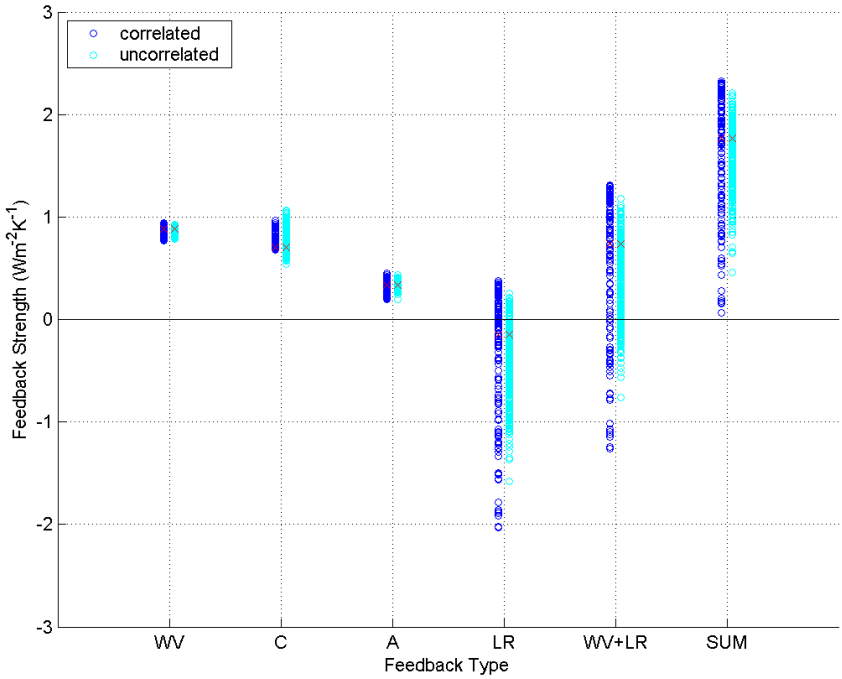

Fig. 5.17: Range of simulated model feedbacks for correlated (dark blue) and uncorrelated (cyan) parameter ensembles. Shown are the mean feedbacks strengths for all individual global feedback components (WV: water vapour, C: cloud, A: albedo, LR: lapse rate). Additionally the range of the combined effect of water vapour and lapse rate (WV+LR) and the sum of all feedbacks (SUM) are shown. Positive values indicate an amplification of an initial radiative perturbation, negative values a weakening. All model versions shown are consistent with pre-industrial climate constraints.

Largest positive feedback contributions to the aggregate feedback strength (i.e. the sum of all feedbacks) comes from water vapour and clouds, followed by a smaller contribution of albedo. Lapse rate feedback extents from slightly positive to largely negative values. The sum of all feedbacks covers a broad range of feedback strengths and is larger for the correlated than for the uncorrelated ensemble. This finding reflects the difference in the simulated climate sensitivity range.

The difference especially at the high end does not seem as pronounced as one would expect from the large difference in the spread of simulated climate sensitivities from both ensembles. Yet it should be noted that at the high end an even small increase in the sum of all feedback provokes a much larger change in the temperature than at the lower end due to the non-linear relation between the feedback parameter and the system gain (Fig. 2.1). Furthermore the simulated temperature response depends on the feedback strength *and* on the magnitude of radiative forcing. We account for the fact, that the radiative forcing is itself subject to uncertainty (CESS et al., 1993; IPCC, 2001) and allow for a spread in this quantity. By perturbing model parameters, which affect the tropopause height and the direct radiative forcing of CO_2 (see App. B) we span a range of 4.4-5.2

W/m^2 (4.2-5.5 W/m^2) for the correlated (uncorrelated) ensemble[16]. As a consequence of the introduction of parameter correlations, model versions with a large feedback sum are preferentially combined with large radiative forcing values. This effect adds to the differences in the spread of the feedbacks and thus explains the much larger spread in climate sensitivity for correlated model versions compared to the uncorrelated ensemble.

The spread in individual mean feedback strengths is comparable or larger for the correlated ensemble compared to the uncorrelated ensemble, besides the cloud feedback, for which a broader range is inferred for uncorrelated parameter sets. Yet when the analysis of cloud feedback is performed for LW and SW components separately then the spread is largest for the correlated ensemble. As LW and SW components offset each other to a larger degree for model versions from the correlated parameter set, the spread of the net cloud feedback is smaller than for the uncorrelated ensemble.

To summarize, the comparison of the correlated and the uncorrelated parameter ensemble has revealed that the ranges of individual feedback strengths are not pronouncedly different between both ensembles and show – besides cloud feedback – a broader spread in the correlated ensemble. As a consequence, the spread in the aggregate feedback strength is larger for the correlated ensemble and partly explains the difference in the spread of climate sensitivity between both ensembles. The other part results from a systematic difference in combining feedback strengths with radiative forcings: In case of the correlated ensemble large values of the aggregate feedback strength are systematically combined with large radiative forcings, whereas the combination is realized randomly for the uncorrelated parameter ensemble.

5.4.3 Linear approximation of the system response

So far we have only accounted for linear feedback contributions. Yet it may turn out that these characteristics describe the simulated temperature response only insufficiently, and that non-linear feedbacks can not be neglected to explain the spread in ΔT_{2x}. We explore this issue in the following by comparing the magnitude of simulated climate sensitivity with an estimate of ΔT_{2x} based on the linear system approximation as outlined in chapter 2:

Having quantified the aggregate mean feedback strength (*F)* and the magnitude of radiative forcing (*RF*) we can determine the expected change in equilibrium surface temperature by applying equation 2.13 ($dT_S = \frac{RF}{\lambda_0^{-1} - F}$). In the following we test the validity of this approach, assuming that the model response can be approximated by a linear superposition of all individual feedback strengths. The radiative forcing RF is realized by doubling the atmospheric CO_2 concentration from 280 to 560 p.p.m.

Fig. 5.18 shows the magnitude of the global temperature change ΔT_{2x} (abscissa),

[16] Those ranges include slightly larger values than inferred from GCMs. See section 5.2.4.1 for a critical discussion about this discrepancy.

which is calculated by applying the linear approximation versus the simulated global temperature change (ordinate), which is equal to the climate sensitivity of a given model version.

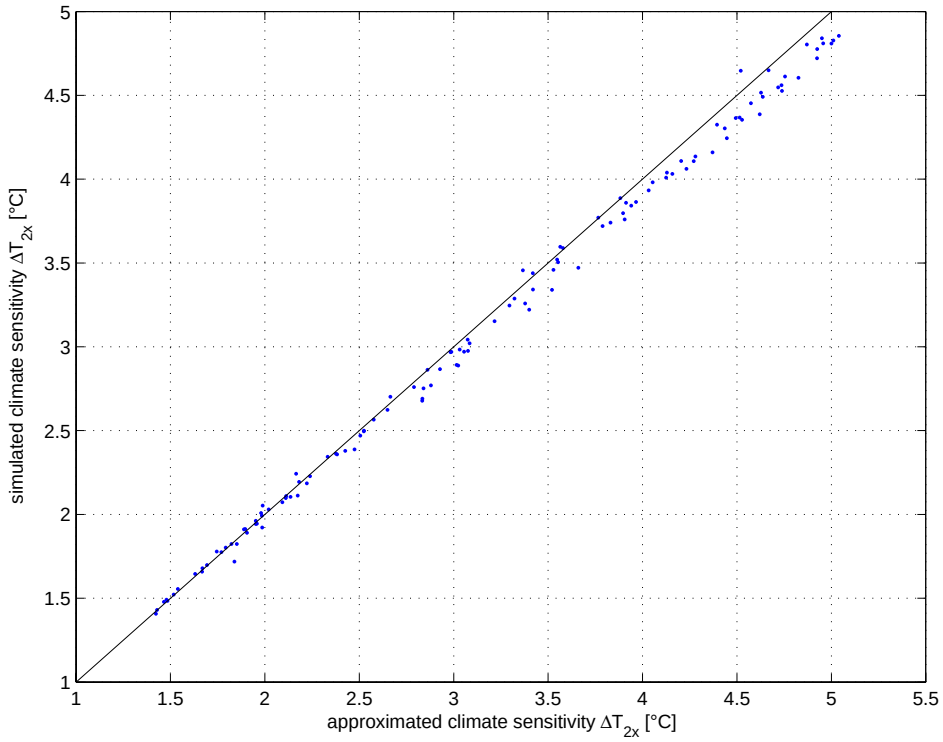

Fig. 5.18: Comparison of approximated and simulated change in global-mean equilibrium surface temperature for a doubling of CO_2. Approximated temperature responses have been inferred by assuming that the system response can be described by a linear superposition of all individual model feedbacks (equation 2.13). Feedback strengths and simulated temperature changes have been inferred from model versions of the correlated parameter ensemble (constrained by present-day data).

If the calculated change in global-mean temperature ΔT_{2x} was equal to the simulated temperature response, then all dots would lie on the solid line. Deviations from that line thus indicate how accurately the approximation describes the real (simulated) change in equilibrium temperature. As can be seen from Fig. 5.18, those deviations are rather small for model versions with a low climate sensitivity and slightly increase with increasing temperature response.

According to equation 2.13, the calculation of the temperature change requires knowledge of the magnitude of radiative forcing RF, of the sum of all indirect feedbacks (referred to as *SUM* in the following) and of the direct surface temperature feedback λ_0. The first two are directly determined with the described offline calculation routine, while the latter is more difficult to calculate for a complex model. This feedback (surface temperature feedback) is only weakly model-dependent (COLMAN, 2003b) and we use a value of λ_0^{-1}=3.34 W/m^{2}K, which represents the mean from seven GCMs reported in Colman (2003a).

Differences between the calculated and simulated temperature response may

arise from a bias in the estimate of λ_0 or in the aggregate mean feedback strength, which may result from the omission of non-linear feedback contributions in the calculation scheme. As the direct temperature feedback λ_0 depends on the mean vertical temperature profile, an assumption of a fixed value of this feedback may introduce a slight bias in the estimate of its strength. We expect that this feedback varies slightly in our ensemble as we generate a set of model versions with slightly different global lapse rates for the basic climate state.

The impact of non-linear feedback contributions to the system response will be explored in the following. For minimizing a bias in the estimate of the individual feedback strengths, due to non-linearities in the system response, we have performed two types of simulations. We first have calculated the feedbacks from a control climate of 280 p.p.m. and a perturbed climate state of 560 p.p.m. (*standard experiment, STD*) by calculating the difference in the radiative top of the atmosphere LW and SW fluxes $R^{STD}_{LW,SW}|_{CO2=280}$ and $R'^{STD}_{LW,SW}|_{CO2=560}$. Then we have normalized the flux difference by the difference in global-mean temperature for inferring the feedback strength. In an *inverse experiment (INV*) we have calculated the feedbacks for the same parameter ensemble from a set-up with both climate states swapped ($R^{INV}_{LW,SW}|_{CO2=560}$ and $R'^{INV}_{LW,SW}|_{CO2=280}$). As e.g. the magnitude of cloud feedback depends on the albedo of the underlying surface type, a change in the albedo affects the size of the inferred cloud feedback. Thus this feedback might be expected to depend to a certain extent on the climate state.

Fig. 5.19 shows the individual feedback strengths for the correlated (upper panel) and the uncorrelated (lower panel) parameter ensembles for both experiment types. The range of covered feedback strengths for the basic experiment (dark blue circles) is very similar to that for the inverse experiment (cyan circles). This implies that differences in the basic climate state do not lead to pronounced differences in the inferred individual feedback strengths for a *2x*CO_2 forcing scenario. This is also the case for the cloud feedback, which – at least at a global scale – does not show a strong dependency on the type of experiment (standard or inverse). Yet when considering the feedback behaviour for the transgression from the glacial to the pre-industrial climate, the difference between both experiment types is more pronounced (not shown).

The similarity between approximated and simulated temperature responses (Fig. 5.18) and the similarity in the range of the inferred feedback strengths from the standard and inverse experiment (Fig. 5.19) suggests that non-linear feedback components do not crucially contribute to the global equilibrium surface temperature response in case of a *2x*CO_2 forcing. Yet this finding does not mean that non-linear feedbacks may not arise in the system. The results rather suggest that – if strong non-linear feedbacks exist – they mutually compensate when analysing the net global feedback strength (see section 5.4.5 for a discussion of non-linear feedback behaviour in the system). We thus may indeed approximate the simulated global temperature response (ΔT_{2x}) by the sum of all individual linear feedbacks and conclude that we can explain the spread in climate sensitivity by quantifying those components.

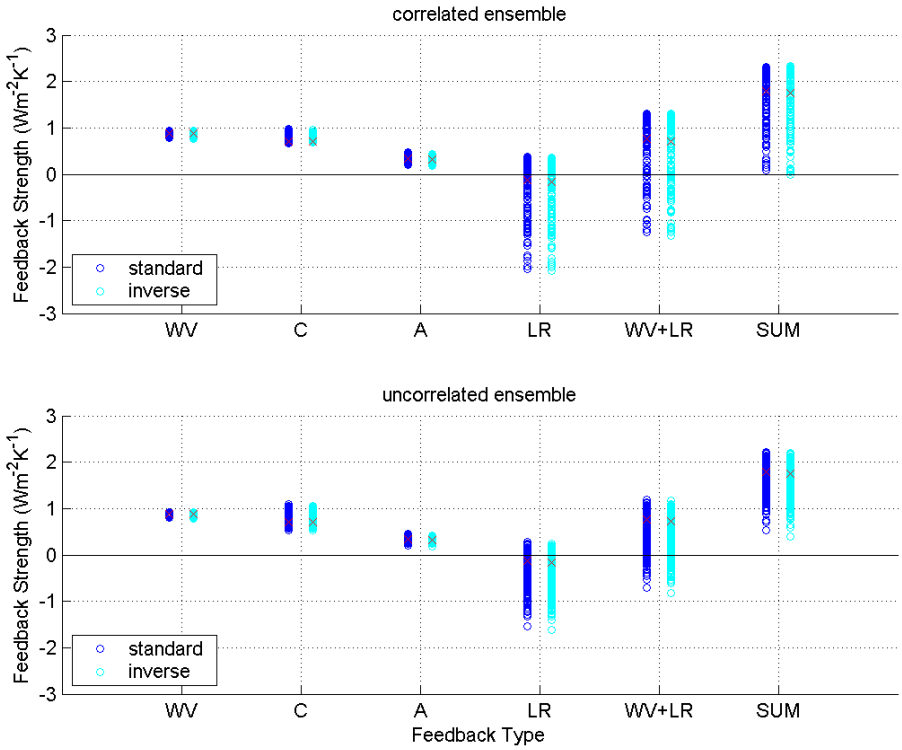

Fig. 5.19: Individual global feedback strengths for *standard* (dark blue circles) and *inverse* (cyan circles) experiments. In the first case the feedbacks have been calculated for a basic climate state of 280 p.p.m. CO_2 and a perturbed state of 560 p.p.m. CO_2, in the second case the feedback calculation was performed while the basic and perturbed states have been swapped. All model versions are consistent with pre-industrial climate constraints.

5.4.4 Comparison with GCM results

In the following we will compare our results from the correlated parameter ensemble with feedback estimates derived from different GCMs. Colman et al. (2003a) compared the feedback strengths of eleven[17] atmospheric GCMs coupled to mixed layer oceans for a *2x*CO_2 scenario. A very recent study was performed by Soden and Held (SUBMITTED) who analysed the transient feedback behaviour of coupled ocean-atmosphere GCMs, which are used in the 4th assessment report of the IPCC for 21st Century climate change experiments. We will refer to the first study as *C03*, to the latter as *SH05*.

[17] This number includes seven different GCMs with four of them being counted twice as different versions of the same model are analyzed.

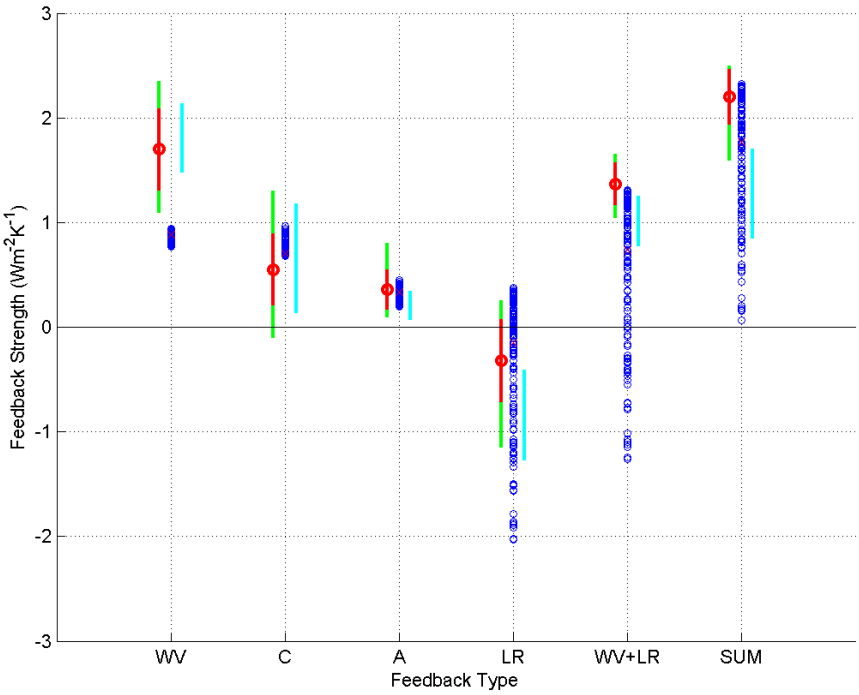

Fig. 5.20: Comparison of CLIMBER-2 with GCM results. Shown are the ranges of the mean feedback strengths for the correlated parameter ensemble (blue circles) next to the ranges inferred from two GCM inter-comparison studies (Colman (2003a) (*C03*): red circle: mean values of 11 GCMs, red range: $\pm 1\sigma$, green: full range; Soden and Held (submitted) (*SH05*): cyan: full range). All CLIMBER-2 model versions are consistent with pre-industrial climate characteristics.

The estimated individual feedback strengths from our model ensemble by and large agree with estimates of comprehensive climate models (Fig. 5.20). Yet at the same time some systematic difference between our results and those from *C03* and *SH05* become apparent and shall be discussed in the following.

Most obvious is the difference between CLIMBER-2 and GCMs in the simulated water vapour feedback strength, which covers larger values in both GCM inter-comparison studies than in our ensemble (Fig. 5.20). Observational constraints indicate that some of high end GCMs may overestimate the strength of this feedback (MINSCHWANER and DESSLER, 2004). Yet SODEN et al. (2005) show consistency between simulated and observed water vapour feedback characteristics for latest generation GCMs and do not question model versions with a water vapour feedback as high as 2 W/m^{2}K. Thus a comparison with comprehensive climate models indicates that our ensemble of model versions yields comparatively low values of this feedback and that we do not cover a large spread of models with pronouncedly different water vapour feedback. Yet it has been shown in many climate modelling studies that for models with a large tropospheric moistening (more positive water vapour feedback) also a large tropospheric warming (more negative lapse rate feedback) is derived, such that inter-model differences in water vapour feedback largely offset each other (SODEN and HELD (SUBMITTED); COLMAN, 2003a). As a consequence the

combined effect of water vapour and lapse rate should be considered when discussing the contribution of individual feedbacks to the aggregate uncertainty (SODEN and HELD, (SUBMITTED); HANSEN et al., 1984; HELD and SODEN, 2000; COLMAN, 2003a). We do this by discussing the spread in the sum of those two feedbacks ("WV+LR") and conclude that our ensemble covers the lower two thirds of the combined feedback range from *C03* and fully includes the range from *SH05*.

Concerning the simulated cloud feedback our range is consistent with *C03* and *SH05* but the spread is not as pronounced as in those studies. Albedo feedback is positive for all of our ensemble members, lower in magnitude compared to water vapour and cloud feedback and consistent with GCM results.

In view of ranking the importance of uncertainty in individual feedbacks the largest spread results from differences in lapse rate behaviour in our ensemble, whereas in *C03* and *SH05* the largest spread comes from uncertainty in cloud behaviour. However we should note in this context that we generate model versions with a climate sensitivity as low as 1.3°C, which approximately corresponds to the temperature response of the direct surface temperature feedback and thus the sum of all indirect feedbacks has to be close to zero (see section 2.2). This can be only achieved by a large negative contribution of the lapse rate feedback as all other feedbacks yield positive contributions. The set of considered GCMs does not include model versions with a climate sensitivity below 2°C and thus does not include models with a very large negative lapse rate feedback as covered in our ensemble.

The most important aspect for our analysis in view of constraining climate sensitivity (chapter 5.3) is that we span in our ensemble almost the entire plausible range inferred from GCMs for the sum of all feedbacks as can be seen in Fig. 5.20. Yet the uppermost end of the aggregate feedback strength from *C03* is not covered by our simulations. Our ensemble thus does not explicitly include model versions with a maximum feedback strength as large as in *C03*. Yet the effect of this discrepancy on our results in view of constraining climate sensitivity (chapter 5.3) is minimized by our applied methodology of rejecting unrealistic model versions: We have inferred a linear relationship between LGM cooling and $2xCO_2$ warming and thus can extrapolate the range of covered climate sensitivities (and thus of covered feedback strengths). For future studies it will be worthwhile to check in how far this extrapolation proves to be valid for high sensitivity model versions.

The sum of all feedbacks shows a systematic difference between both GCM inter-comparison studies (Fig. 5.20). This may be due to the fact, that the feedbacks in one study represent the system behaviour for equilibrium changes (*C03*) while in the other study the transient system response has been analysed (*SH05*). A further difference is given by the use of a simple mixed layer ocean in one study (*C03*) and the use of a fully-coupled ocean in the other study (*SH05*). Thus in view of similarity of our results with both inter-comparison studies, our inferred feedback strengths should be more similar to *C03* in view of the considered change in the climate state, and should be more similar to *SH05* in view of the impact of ocean dynamics on the results.

5.4.5 Feedback analysis of the glacial climate

An approach to infer the sensitivity of the Earth system to changes in the radiation balance is to focus on past climate changes, and to estimate the magnitude of past global cooling ΔT and global radiative forcing RF. The feedback parameter λ, defined as the ratio of $\Delta T/RF$, then can be taken as a measure for the sensitivity. This concept is the basis for the *paleo-calibration method* (COVEY et al., 1996), which has been applied for different epochs in the geologic past. Of crucial importance for such an approach is the assumption that the feedback parameter is approximately the same when inferred from past climate conditions or from scenarios of future climate change.

In the following sections we will review the validity of this assumption by comparing the inferred feedback strength from our $2xCO_2$ simulations with the LGM simulations. For this purpose we have performed two additional experiments. We firstly repeated the feedback calculations for two climate states, which are representative for the climate of the Last Glacial Maximum (LGM, see chapter 5.2): A basic climate state of 170 p.p.m. CO_2 and a perturbed climate state of 230 p.p.m. CO_2, while all further boundary conditions (continental ice sheets, dust concentration, vegetation cover, solar insolation) are the same as for the LGM simulations presented in previous chapters of this thesis. Thus the only forcing for this experiment (referred to as "*LGM*-CO_2" in the following) is given by the change in glacial CO_2 concentration. The mean feedback strength is determined analogously to the *2x*CO_2 experiments by repeating the calculation routine with the control and perturbed climate state swapped and taking the average over both ensembles.

The second set of calculations was performed to analyse the feedbacks, which determine the pronounced temperature change between the LGM and the pre-industrial climate (referred to as "*LGM-PI*") in the following. The radiative forcing for this experiment is given by the full set of glacial forcings (ice sheets, CO_2 concentration, dust, vegetation, solar insolation). Again the control (LGM) and perturbed (pre-industrial) climate states have been swapped and the mean feedback strengths determined by averaging over both ensembles. The resulting mean feedback strengths for the doubling of CO_2 experiment (*2x*CO_2) as well as for the glacial simulations (*LGM-PI* and *LGM*-CO_2) are shown in Fig. 5.21.

The comparison of the three performed experiment types shows that the individual feedback behaviour can reveal some pronounced differences. The magnitude of the difference among feedback strengths depends on the feedback type and on the experiment. The range of realized water vapour feedback strength is rather similar in all experiments and suggests that this feedback acts approximately linearly in our model with a tendency of a slightly larger magnitude for a warmer climate. Cloud feedback reveals a pronounced dependency on the climate state and on the forcing type: It is systematically larger for the warmer temperature regime (*2x*CO_2) than for the glacial experiments, whereas the *LGM-PI* (cyan circles) yields lower values than the *LGM*-CO_2 experiment (green circles). A similar behaviour (but of opposite sign) can be inferred for the albedo feedback[18], which proves to be systematically larger in a colder climate (HEWITT and MITCHELL, 1997).

[18] Regarding the *LGM-PI* experiment, the calculated magnitude of radiative forcing of glacial ice sheets has been subtracted from the albedo feedback.

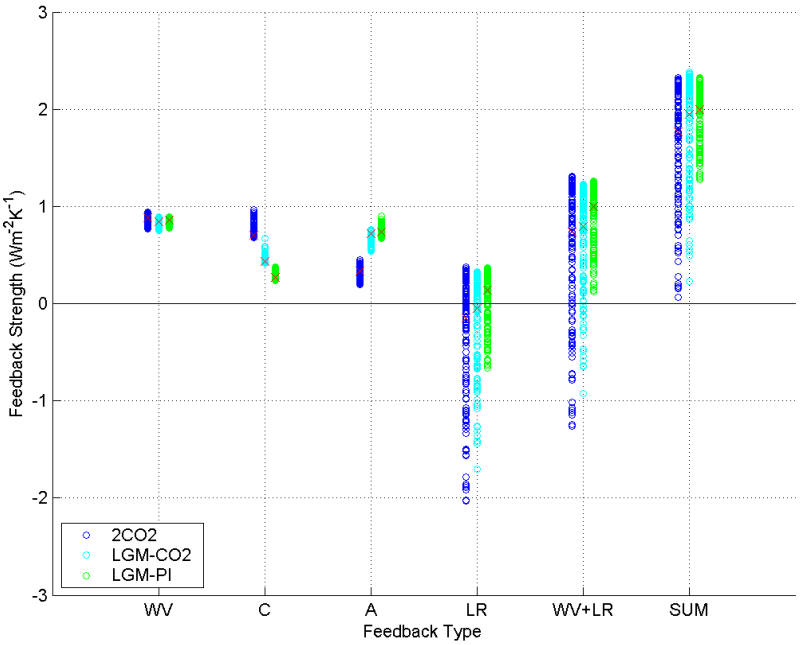

Fig. 5.21: Dependence of the feedback strengths on the climate state and forcing pattern. Shown are the individual mean feedback strengths for the correlated ensemble for a *2x*CO_2 and for two glacial scenarios. In case of the first glacial experiment (*LGM-PI*) the transgression from the glacial to the pre-industrial climate is analysed (full set of glacial forcings), whereas in the second experiment (*LGM*-CO_2) only changes in the CO_2 content (from 170 p.p.m. to 230 p.p.m.) constitute the forcing. All model versions are consistent with pre-industrial climate characteristics.

Concerning the cloud feedback behaviour, a meaningful interpretation of the results requires a detailed analysis of several factors which all determine the strength of the resulting feedback. The investigation of global cloud cover in our model ensemble has revealed that changes in cloud coverage are rather small for all experiment types. Yet this characteristic might not be a very informative predictor of cloud feedback behaviour, as the final feedback strength crucially depends on *where* those changes occur (a latitudinal redistribution of clouds may not change global cloud coverage, but may strongly modify the magnitude of cloud feedback). Additionally changes in cloud height and in cloud optical thickness are further important aspects for the understanding of the global net cloud feedback.

The lapse rate feedback is consistent at the upper range for all experiment types, whereas at the lower range some pronounced difference in the feedback strength among the experiments can be seen. A general tendency for a less pronounced negative lapse rate feedback is inferred for the glacial simulations. The reason for this deviation might be seen in the parametrisation of the lapse rate profile: A large negative feedback contribution comes from tropical regions with a large value of surface air specific humidity q_s, which enters the parametrisation scheme squared. For the colder glacial temperature regime q_s is reduced and thus the

negative specific humidity term in the parametrisation scheme is reduced as well (see equation (2) in PETOUKHOV et al. (2000)).

A further systematic bias is seen between both LGM experiments. In case of the *LGM-PI* experiment, model versions with a strong negative lapse rate feedback (below –1 W/m^2) are not realized. This might be explained in view of the difference in the spatial forcing pattern between the *LGM-PI* and the *LGM*-CO_2 experiment. Lapse rate feedback shows a pronounced latitudinal dependency: It is negative for tropical regions, increases with latitude and reaches large positive values for high latitudes. In case of model versions with a global negative lapse rate feedback the latitudinal profile is shaped such that the negative feedback contribution exceeds the positive contribution. Obviously the global lapse rate feedback depends on the latitudinal distribution of the forcing, which differs between *LGM*-CO_2 and *LGM-PI.*

How does the inferred difference in the individual feedback behaviour between the performed experiments affect the magnitude of the aggregate feedback strength? The upper half of the sum of all feedbacks is comparable for all three experiment types, with a slight bias towards larger values for the glacial climate (Fig. 5.21). The lower half is similar for the *2x*CO_2 and *LGM*-CO_2 experiment, whereas for the *LGM-PI* experiment the total range is reduced, mainly due to the difference in the spread in lapse rate feedback.

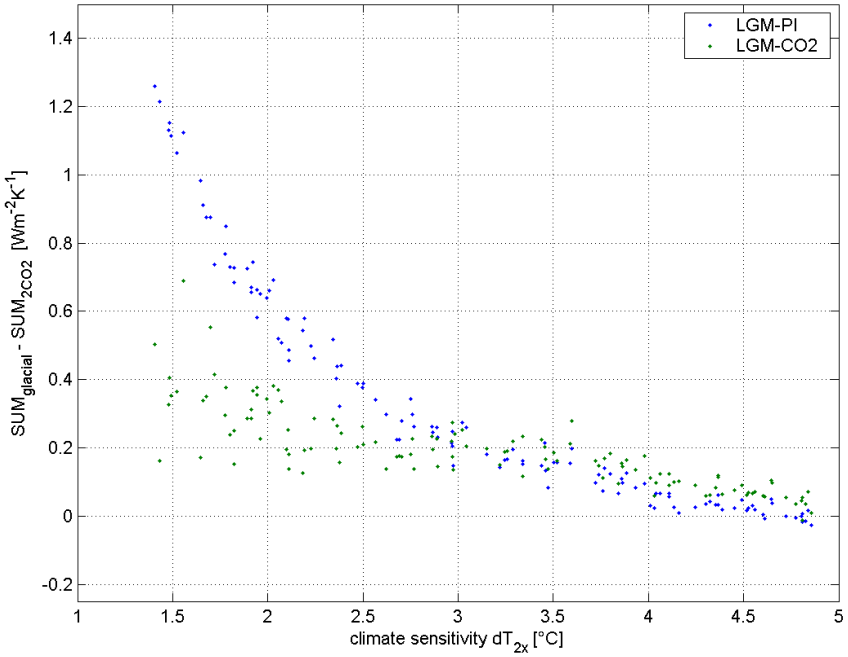

Fig. 5.22: Difference in the feedback behaviour between the *2x*CO_2 experiment and the glacial experiments. Shown is the difference in the aggregate mean feedback strength (SUM) between the experiments *LGM-PI* and 2xCO_2 (blue dots) and between *LGM*-CO_2 and 2xCO_2 (green dots) for each model version from the correlated parameter ensemble (only pre-industrial consistent model members). The climate sensitivity (abscissa) of a given model version represents the change in equilibrium surface temperature inferred from a doubling of CO_2 from 280 p.p.m. to 560 p.p.m.

A more detailed analysis reveals that the difference in the sum of all feedbacks between the *2x*CO_2 experiment and the glacial simulations is largest for low sensitivity model versions and that this difference is much more pronounced for the *LGM-PI* experiment than for the *LGM*-CO_2 experiment (Fig. 5.22).

The difference in the aggregate mean feedback strength between the glacial and the *2x*CO_2 experiments is positive for almost all model versions and implies that the feedback strength is systematically larger for the glacial simulations. Although the difference in the aggregate feedback strength is largest for low sensitivity model versions, its impact on the difference in the simulated temperature response is the more pronounced the larger the magnitude of the feedback sum due to the non-linear relation between the feedback factor and the system gain (see Fig. 2.1). The systematic difference in the feedback strengths for the Glacial and for CO_2 doubling thus corroborates our findings in section 5.2: A tendency for systematically larger feedback parameters λ_{LGM} than λ_{2CO2}, with the difference being most pronounced for low sensitivity model versions.

Finally we analyse which feedback components cause the difference between the 2xCO_2 and glacial climate. We therefore illustrate the contribution of individual feedbacks to the aggregate mean feedback strength in Fig. 5.23. Because albedo feedback is larger in the glacial experiments (compared to 2xCO_2), whereas cloud feedback is smaller, we analyse the combined contribution of both feedbacks to discuss its net effect. Fig. 5.23 shows that for low sensitivity model versions the combined feedback of cloud and albedo is smaller for the glacial experiments than for the 2xCO_2 runs, resulting in a weakening of the aggregate feedback strength for *LGM-PI* and *LGM*-CO_2, whereas for high sensitivity models the opposite behaviour is inferred (an increase in the aggregate feedback strength). The difference in simulated lapse rate feedback is most pronounced for low sensitivity model versions, and reveals to be larger in the glacial experiments than in the 2xCO_2 simulation. With increasing model sensitivity this difference decreases sharply. The contribution of water vapour feedback is not explicitly shown, as changes in this feedback are rather small for the different experiment types in our simulations (Fig. 5.21).

Thus the inferred difference in the aggregate feedback strength between the glacial *and* 2xCO2 simulations can be mainly explained by differences in simulated lapse rate feedback for low sensitivity model versions. The combined cloud and albedo feedbacks crucially determine the difference in the sum of all feedbacks for high sensitivity model versions. Yet those findings about the weight of individual feedback components on the aggregate feedback strength should be seen in the context of the model used and of the parameter perturbations chosen.

To conclude, the analysis of the individual mean feedbacks has revealed that the individual feedbacks show some dependency on the climate state and on the forcing pattern. Especially lapse rate feedback suggests a pronounced sensitivity to the forcing pattern for low sensitivity model versions in our model ensemble.

A slightly larger sum of the feedbacks for both glacial experiments compared to the 2xCO_2 simulations suggests an increase in the feedback strength for the glacial climate, in line with GCM based results (e.g. HEWITT and MITCHELL, 1997). This implies that paleo-calibration studies, that infer the sensitivity of the climate system to CO_2 doubling from estimating the strength of the feedback parameter λ from the glacial climate, tend to overestimate the magnitude of climate sensitivity ΔT_{2x}. As we use the LGM climate to constrain the set of realistic model versions,

but determine the climate sensitivity ΔT_{2x} from the doubling of CO_2 simulations, our approach does not suffer from the same caveat.

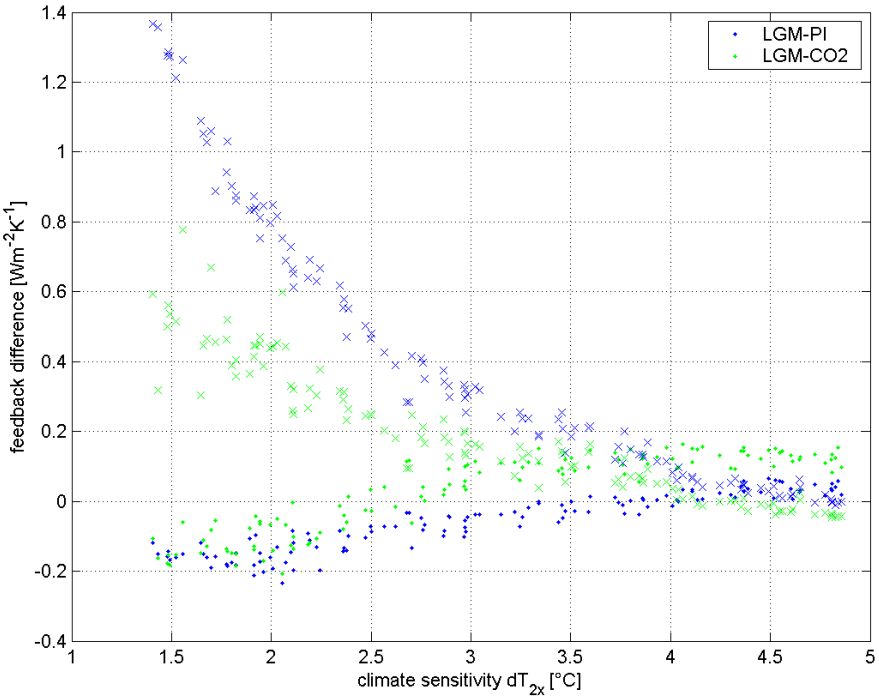

Fig. 5.23: Contribution of individual feedbacks to the discrepancy in the aggregate mean feedback strength. The difference in the magnitude of individual feedbacks between the 2xCO_2 and both glacial experiments (*LGM-PI*: blue, *LGM-*CO_2: green) is shown for the combined albedo and cloud feedback (dots) as well as for lapse rate feedback (crosses). Positive (negative) values indicate a larger (smaller) feedback in the glacial experiments than in the doubling of CO_2 simulations.

The detailed analysis of the individual model feedbacks presented in this chapter helps to interpret the impact of our applied parameter perturbations on the model performance. Ideally we would have generated an ensemble of model versions, which covered the entire plausible range of GCM feedback behaviour. Our results suggest that we have constructed a large set of CLIMBER-2 models with different realizations of the individual feedbacks, but that the spread e.g. in water vapour and cloud feedback is not as large as inferred from a set of comprehensive climate models. Yet when accounting for correlations among individual feedbacks (as is the case for water vapour and lapse rate feedback) we infer a larger degree of consistency between our results and GCMs. Future CLIMBER-2 ensemble studies with an extended experimental design for parameter perturbations and structural extensions will have to show whether additional realistic climates with vastly different feedback spreads could be constructed. In any case, we expect the sort of ensemble-based feedback analysis may represent a prototype for future uncertainty analyses suitable for inter-model comparison: The quantification of feedback strengths allows for physical interpretations, revealing

how the subjective choice of perturbing specific model parameters affects the main feedback cycles of a given climate model.

6 Summary and Conclusions

The analysis presented here has demonstrated that one can significantly reduce uncertainty in climate sensitivity ΔT_{2x}, the change in equilibrium global-mean surface temperature for doubling CO_2 concentrations, by accounting for information about past climate changes. For this purpose, we focused on the strong climate signal provided by the pronounced difference between the pre-industrial climate and the Last Glacial Maximum (LGM) to effectively constrain the model sensitivity. We do this by comparing simulated LGM cooling with information inferred from proxy-data. To the best of our knowledge, this work represents the first such experiment what systematically combines an ensemble of fully-coupled climate models with proxy-based knowledge about regional LGM cooling. In the following we outline our results in view of the experimental simulation design (section 6.1) and then present the main simulation results of our study (section 6.2).

6.1 Construction of model ensembles

The ensemble simulations presented in this thesis required a set of extensive preparatory steps before undertaking our analysis. Those steps are outlined in this section, which is rather technical, whereas the main simulations results are presented in the following section.

In the framework of this thesis we performed ensemble simulations in the order of some thousand model runs for a fully-coupled (ocean-atmosphere) design. The prerequisite for the feasibility of such type of simulation experiments was the availability of an efficient climate model. Furthermore the model had to allow for generating a set of different model versions by perturbing specific model parameter to modify the main atmospheric feedbacks (water vapour, clouds, lapse rate, and albedo).

The model of intermediate complexity, CLIMBER-2, appeared to be well-suited for our purposes, but had to be extended for enabling the simulation experiments presented. In contrast to simplified climate models, climate sensitivity is not a tuning parameter for CLIMBER-2, so we had to find a way of modifying this key model characteristic. We achieved this goal by extracting a set of 9 atmospheric parameters, that are most influential on the model inherent feedback strengths and whose value is subject to uncertainty. Additionally we decided to account for uncertainty in ocean-mixing processes and enlarged the set by two further parameters that describe the horizontal and vertical ocean diffusion scheme. We then specified the range of plausible values for all eleven parameters.

The realisation of simulations in an ensemble framework requires specification of how individual parameter values are chosen and how they are combined with each other. Given the large dimensionality of our parameter space we implemented an efficient Monte-Carlo scheme (Latin Hypercube Sampling) and performed an ensemble of 5000 CLIMBER-2 equilibrium simulations of pre-industrial and $2xCO_2$ climate, while simultaneously perturbing the set of 11 model

parameters. This experiment allowed us to estimate the spread of ΔT_{2x} realized in our model set. From a Bayesian perspective that assumes a non-informative, nevertheless particular prior distribution, then governing the Monte-Carlo sampling density. The resulting range of 2.0-3.8°C appeared too narrow for the aim of covering the feedback behaviour of a set of different General Circulation Models (GCMs). We thus modified the Latin Hypercube scheme to be more efficient in sampling a broader range of ΔT_{2x}. We achieved this by introducing positive and negative correlations among the atmospheric parameters, thus replacing the random combination of parameter values (uncorrelated ensemble) with a systematic scheme (correlated ensemble). The resulting ΔT_{2x} range proved to be much broader (1.3-5.5°C) and could be drawn from a much smaller ensemble size (1000 models).

We also sought to provide a set of models for the realistic simulation of the LGM climate. An important requirement for such a task involves accounting for all the main glacial forcings. The standard CLIMBER-2 model does not incorporate a module for the simulation of the glacial dust cycle. However we regarded this forcing to be important for our analysis and decided to *prescribe* the radiative effects of glacial dust content, which we inferred from a set of GCM simulations.

The majority of model extensions was required to calculate the forcing strengths, that resulted from changes in CO_2 concentration, ice sheet extent, and vegetation cover, as well as for the calculation of the models' inherent feedback strengths (resulting from changes in water vapour, clouds, lapse rate and albedo). For this purpose we applied the *offline calculation scheme*, used in many other studies, which allowed us to compare our inferred feedback strengths with other models.

6.2 Ensemble-based analysis of uncertainty in climate sensitivity

After the above outlined model extensions have been applied, we were in a position performing CLIMBER-2 ensemble simulations for $2xCO_2$ and LGM experiments in order to investigate the central question of this study:

To what extent can data constraints from observed present-day climate and from reconstructed LGM temperatures potentially narrow down the uncertainty range of climate sensitivity?

We initiated our analysis by exploring the effectiveness of present-day data to constrain the model ensemble. We defined a set of seven global-mean data constraints, which serve to separate realistic from unrealistic model versions. The ranges of those constraints were chosen to approximately represent the typical scattering of atmosphere-ocean GCM simulations and encompass observational data of key present-day climate characteristics. The outcome was that a large number of models revealed to be inconsistent (more than 90%) with observational data. But importantly this pronounced reduction in the set of model members did not lead to a distinct reduction in the uncertainty range of ΔT_{2x}. In line with ensemble-based GCM studies (MURPHY et al., 2004; STAINFORTH et al., 2005) our results indicate that it is possible to construct model versions of large climate sensitivity, which all are consistent with global-mean data of present-day climate.

We further investigated the potential of additional present-day data constraints to reduce the spread in climate sensitivity by exploring the latitudinal and seasonal model behaviour of zonally averaged surface air temperature, precipitation, and cloud cover. The set of models versions being consistent with modern global-mean data (123 of 1000 model members), revealed a good agreement with observational data for the latitudinal and seasonal model performance. The magnitude of model-data discrepancy, analysed for different latitudes and for summer and winter season, proved to be generally larger than, or of comparable magnitude to the spread among individual ensemble members. We thus concluded that adding data constraints for the seasonal cycle or for the latitudinal profile would not help to effectively narrow down the uncertainty range in climate sensitivity. This result contradicts a very recent ensemble-based study, suggesting that the seasonal cycle provides an effective means of reducing uncertainty in ΔT_{2x} (KNUTTI et al., 2006). Yet the authors of this study base their conclusion on a set of extreme model versions, which show climate sensitivities up to 11°C (STAINFORTH et al., 2005). Our ensemble of present-day consistent models reveals an upper limit of 4.9°C. If we enlarged this ensemble to include model versions of similar extreme climate sensitivity, we would also expect a strong reduction in the uncertainty range when accounting for data information of the seasonal cycle.

Thus the application of present-day data constraints has revealed, for the set of our CLIMBER-2 model versions, that uncertainty in ΔT_{2x} mainly remains unaffected. As a next – and central – step we investigated the potential of the pronounced temperature difference between the pre-industrial climate and the LGM to narrow down this uncertainty. The choice to focus on the LGM climate state seemed promising for our purposes as (i) the change in climate and greenhouse gas (GHG) concentrations is large, (ii) the main glacial forcings are reasonably well long, and (iii) lasted for a long time such that the climate system was in near-equilibrium. This approach to constraining climate sensitivity is not new in itself, but has been realized so far (to the best of our knowledge) either only in the framework of single model realizations or based exclusively on estimates of past climate change inferred from proxy-data. Our approach combines both methods and additionally allows us to account for uncertainty in the model response by performing the analysis for an ensemble of climate model versions with different climate sensitivities.

The starting point for our approach was to define a robust and effective data constraint, based on reconstructed LGM temperatures. The requirement for availability of well-calibrated proxy-data and large-scale representativeness of those data brought us to focus on the tropical Atlantic, where a large amount of high quality sediment cores cover a sufficiently broad region for inferring a robust estimate of large-scale mean LGM cooling. Additionally, we included estimates of tropical land and Antarctic cooling into our considerations in order to evaluate the impact of alternative proxies on our results.

We could have directly applied the defined data constraints for the set of simulated LGM climates with the aim of constraining uncertainty in ΔT_{2x}. Yet we wanted to provide a broad basis to judge the realism of our glacial simulations and thus analysed the simulated LGM climate response in detail first. For that purpose, we have performed a factor analysis, which allows us to quantify the impact of individual glacial forcings on the simulated temperature anomaly. The calculation of the forcing strengths, resulting from the prescription of glacial ice sheets, lowered GHG concentrations, atmospheric dust content and vegetation cover, revealed a global-mean radiative forcing of about 7.5-8.0 W/m^2 (in line with

comparable LGM studies and slightly larger than studies that omit forcing contribution from glacial dust content and vegetation cover). Our results indicate that the largest forcing is to be attributed to the prescription of glacial ice sheets and decrease in GHG concentrations (together they amount for about 75% of total radiative forcing), while dust and vegetation contribute an additional 2 W/m^2, and we conclude that it is important to include those two forcings for a comprehensive simulation of the LGM climate.

By requiring consistency of simulated mean tropical cooling with our specified tropical Atlantic SST proxy range (3±0.9°C) we can constrain the spread of global-mean LGM cooling (dT_{LGM}) to 5.8±1.4°C. This range proved to be robust when uncertainties in the radiative forcing were accounted for and consistent with estimates of dT_{LGM}, which we inferred from constraining the model ensemble by tropical land and Antarctic proxy-data. An important finding is that our range includes substantially larger cooling than estimated by recent modelling studies from the *Paleoclimate Modelling Intercomparison Project* (PMIP-2) (MASSON-DELMOTTE et al., 2006) and points to a systematic underestimation of LGM cooling for those studies. Results from our performed factor analysis indicate that this underestimate is in the order of 1.5-2.0°C due to the omission of dust and vegetation forcing. An important implication arises for studies that constrain the uncertainty range of ΔT_{2x} by LGM cooling but which omit glacial dust and vegetation forcing (e.g. ANNAN et al., 2005): Climate sensitivity is likely to be overestimated by an amount of about 1°C, as models have to be more sensitive to yield a temperature cooling consistent with paleo data.

In the context of PMIP-2 model results a further aspect is worth mentioning: A set of those models has revealed a systematic underestimation of high latitude LGM cooling. Our analysis of the spatial distribution of the glacial forcing and related temperature anomaly patterns has on the one hand shown that regional forcing may well determine regional LGM cooling (as e.g. inferred from ice sheet forcing). On the other hand, the analysis of dust forcing has revealed that this forcing, which is confined to low latitudes (and thus may be regarded as irrelevant for the discussion of Antarctic and Greenland temperatures), shows a polar amplification of the temperature response and may well affect high latitude cooling. The interesting implication regarding models underestimating high latitude cooling is: To what extent is this underestimate due model deficiencies – and to what extent is it due to prescribing an incomplete set of forcings?

The explicit quantification of the magnitude in simulated glacial forcing and related global LGM temperature response has allowed us to determine the feedback parameter λ (the ratio of global temperature change to radiative forcing), and to compare its magnitude with that inferred from the doubling of CO_2 simulations. Our results indicate a systematically larger feedback strength acting in the Glacial: Most model versions reveal a feedback parameter, which is about 10-20% larger (compared to λ_{2CO2}) when inferred from the LGM climate, while this estimate increases up to 50% for low sensitivity model versions. A few modelling studies allow a comparison with our results: Broccoli et al. (2000) infer a very similar value for λ_{LGM} and λ_{2CO2}, Hewitt and Mitchell (1997) estimate a larger glacial feedback parameter in line with our results (about 15%), whereas Stouffer and Manabe (2003) infer a much larger increase in the feedback strength for a colder climate. We conclude that the difference between λ_{LGM} and λ_{2CO2} is strongly model dependent, but is likely to reveal a tendency for a larger value of λ for the Glacial: Our analyses of the feedback parameters, determined separately for each individual LGM forcing agent, suggest that this is mainly the case as the inhomogeneously distributed forcings yield a larger temperature response than

the homogeneous CO_2 forcing. Our findings thus imply that the feedback parameter λ may well depend on the forcing pattern and that the climate sensitivity is not the same when estimated from a $2xCO_2$ experiment or when inferred from the LGM climate. This kind of analysis is helpful for the interpretation of *paleo-calibration* studies, which aim to determine ΔT_{2x} by estimating the ratio of past global temperature response to past global forcing: Without accounting for the likely difference in the feedback strength between past cooling and future CO_2 warming those studies may overestimate the magnitude of ΔT_{2x}. In this context it is important to clarify that the difference in the feedback strength is no caveat for our approach to constrain climate sensitivity. We explicitly calculate the climate sensitivity from the $2xCO_2$ experiment and perform the LGM simulations to constrain the set of realistic model versions. The outcome of this experiment is discussed in the following.

The task of constraining the uncertainty range of ΔT_{2x} with paleo-proxies requires defining regions for which the simulated cooling can be compared with data. Therefore we analysed those areas that are best suited for a model-data comparison under certain premises: The first premise was, that GHG forcing is an important forcing for the region. We have calculated the magnitude of LGM cooling that is attributable to changes in CO_2 content. Our results indicate a strong CO_2-affected cooling signal for large regions of the Southern hemisphere, where GHGs contribute up to 50% to total LGM cooling. A second issue for the choice of a strong paleo constraint concerned the broadness of the spread in simulated LGM cooling among different model versions. Regions that reveal a large spread would be favourable to constrain the ensemble as they would ideally allow only a well-defined subset of model versions to pass the consistency test with paleo data. Our simulation results have clearly shown that the Antarctic region meets these requirements. Yet this area of the globe is small compared to the large tropical region (and a realistic simulation is complicated by its isolated location). Furthermore, some Antarctic regions have revealed a strong signal caused by changes in the ocean circulation, which constitute a large, model-dependent imprint. Given the progress in tropical SST temperature reconstruction methods and the broad coverage of tropical sediment cores, especially in the Atlantic sector, we decided to focus on this region for constraining our model ensemble and to apply reconstructed Antarctic cooling for testing the robustness of our results.

Concerning the effectiveness of our approach in constraining climate sensitivity with information about regional LGM cooling, the crucial question is: How strongly is the simulated regional glacial cooling linked to the magnitude of ΔT_{2x}?

One of the key results of our study is that we found this link to be indeed very pronounced for the set of CLIMBER-2 model versions. We inferred a strong correlation between tropical as well as high latitude cooling and climate sensitivity. Focusing on the subset of model versions consistent with present-day climate, we could infer a quasi-linear relationship between ΔT_{2x} and LGM cooling. Based on this key finding, we have formulated an *interval method* for constraining the set of model versions by LGM proxy-data, resulting in robust estimates of 5-95% quantiles for ΔT_{2x}. The method is based on a linear regression of simulated regional LGM cooling and climate sensitivity – and allows for uncertainty in this strong relation by defining a conservative estimate of the spread around the regression line.

The requirement for consistency of simulated mean tropical Atlantic SST cooling with reconstructed temperatures from paleo proxies (3±0.9°C) narrowed down

the ΔT_{2x} range of 1.3-4.9°C (inferred from present-day climate constraints) to 1.3-3.5°C. This estimate of ΔT_{2x} covers a smaller range compared to the spread of 1.5-4.5°C, given by the Intergovernmental Panel on Climate Change (IPCC, 2001). Our interval is so far only based on considering uncertainty in paleo data and in model parameters (i.e. in the feedback strengths). To test the robustness of our results we have made considerable effort to account for uncertainty i) in the model structure, ii) in the glacial radiative forcing, and iii) further investigated the impact of constraining our ensemble by proxy data from different regions of the globe.

The key question with relation to model structure uncertainty is whether the strong correlation between regional LGM cooling and climate sensitivity is specific to our model or whether it is valid more generally. This question remains open until a set of comparable simulations with fully-coupled comprehensive climate models is available. Yet a first step in this direction can be undertaken by comparing our findings with preliminary results of LGM simulations from the PMIP-2 project. For that purpose, we have run our ensemble for identical boundary conditions (i.e. we neglected dust and vegetation forcing). So far only two models allow for a comparison: One of them clearly falls inside the range of our proposed relationship between tropical cooling and ΔT_{2x}, while the other is slightly outside (we have to double the estimate of the spread around our linear regression line for consistency with our results). A recent study with an atmospheric GCM coupled to a slab ocean has performed an ensemble experiment similar to ours, but inferred a much weaker correlation of glacial SST cooling and climate sensitivity (ANNAN et al., 2005). We have estimated the impact of a spread as large as discussed in this study on our results and found an increase in the upper limit of ΔT_{2x} by about 1°C.

Uncertainty in glacial radiative forcing is another important issue in light of the robustness of our inferred climate sensitivity range. We have represented its impact by accounting for uncertainty in the forcing exerted by glacial dust content, ice sheets and GHG concentrations and formulated a scenario of minimum and maximum LGM forcing. The additional ensemble simulations we undertook suggest a ΔT_{2x} range of 1.2-3.3°C (maximum forcing: 7.6-8.2 W/m^2) and 1.8-4.3°C (minimum forcing: 7.2-7.7 W/m^2). Yet we can not exclude the possibility that we have covered a too narrow uncertainty range for LGM forcing, but emphasize that we already account for a factor two in uncertainty of glacial dust forcing. As most dust experts would agree on a general cooling effect of glacial dust for tropical regions, we do not believe that large uncertainty in the magnitude of dust forcing strongly challenges our upper estimate of climate sensitivity, which was inferred by assuming a comparatively weak effect of dust forcing (0.6 W/m^2 globally). One would have to assume a positive global dust forcing for inferring pronouncedly larger estimates of the upper limit in climate sensitivity than inferred from our simulations. We conclude that uncertainty in radiative forcing adds about an additional degree to the uncertainty range of ΔT_{2x} and infer a range of 1.2-4.3°C for climate sensitivity, accounting for uncertainty in model feedback strengths, in reconstructed tropical SST cooling, and in the magnitude of LGM radiative forcing.

We undertook a final step to evaluate the robustness of our results by analysing the consistency among ΔT_{2x} estimates, which we inferred from different regions. As proxies from tropical land sites and from Greenland ice cores are subject to large uncertainty and may reveal a strong imprint of small-scale dynamics, we have discussed those regions only qualitatively. We pointed out that our tropical

SST constrained ΔT_{2x} estimate is supported by reconstructed cooling of those regions. We applied our interval scheme for simulated Antarctic cooling and constrained our ensemble with reconstructed temperature anomalies from Antarctic ice cores (5.4±0.4°C above the inversion level). The results from this experiment yield highly consistent ΔT_{2x} estimates and suggest that our model versions capture realistically the main latitudinal profile of LGM cooling. The fact that very different absolute temperature changes in high and low latitudes all yield very similar estimates of ΔT_{2x} gives additional credence to our results.

In terms of ranking the importance of the discussed uncertainties for the spread in climate sensitivity, we infer the largest contribution from the applied proxy-data (about 1.6°C), a slightly smaller contribution from uncertainty in the radiative forcing (about 1.0°C) and the smallest contribution from uncertainty in the model spread (about 0.5°C, which will increase up to 2.0°C if we assume structural uncertainties to be large).

An important finding of our study is that we apply a new methodology to constrain uncertainty in climate sensitivity and confirm the most likely value for ΔT_{2x} to be between 2.5 to 3ºC. This estimate agrees with the best-guess of most recent studies (KERR, 2004), based on a physical understanding of radiative forcing and feedbacks, as well as on the analysis of observed 20th Century temperature evolution. The promising outcome of our analyses demonstrates that information of reconstructed past temperature changes can help to efficiently constrain the uncertainty range of climate sensitivity. The set of model versions, which passes the LGM consistency test, suggests a ΔT_{2x} range almost identical to the IPCC estimate (1.5-4.5°C) and must be extended up to 5.3°C, if we assume structural uncertainties to be large. This is an important result as it helps limiting the likely range of future warming, and further helps to better interpret recent estimates of ΔT_{2x} that largely exceed the upper limit of IPCC: The large uncertainty range from those studies (FOREST et al., 2002; KNUTTI et al., 2002; MURPHY et al., 2004; STAINFORTH et al., 2005) demonstrates that it seems not possible to formulate a strong test for model sensitivity behaviour, based on observational data from present-day climate or on 20th Century warming .

The comparison of our results with the small number of alternative model studies of comparable experimental design has suggested that our method might underestimate structural model uncertainty. To be in a position to interpret our results in terms of a physical understanding and better evaluate the degree of model independence of our results, we have complemented our analysis with a detailed study of the feedback performance for the set of different CLIMBER-2 model versions. For this purpose, we implemented an *offline calculation scheme* to calculate the feedback strengths resulting from changes in water vapour, clouds, lapse rate and albedo.

We began our analysis by focusing on the doubling of CO_2 experiment ($2xCO_2$) and compared the difference in inferred feedback strengths for model versions from the correlated and uncorrelated model ensemble. Those two model sets reveal a pronounced difference in the spread of simulated ΔT_{2x} and thus suggest a different spread in the simulated feedback behaviour. The results of our calculations indicate that this difference can be attributed mainly to a larger spread in lapse rate feedback for the correlated ensemble. One may ask whether the information about the individual feedback strengths is a useful indicator for the *simulated* temperature change following a radiative perturbation of the climate system. It may turn out that non-linear feedback contributions, which are not accounted for in our calculation scheme, are of crucial importance for the

interpretation of simulated climate sensitivity. We explored this issue and concluded that the net effect of non-linear feedback contributions, arising from differences in the background climate, is small regarding the $2xCO_2$ experiment. We may thus describe the simulated temperature change as a linear superposition of all individual linear feedback components. This kind of analysis proved to provide indeed useful information to answer the crucial question: Which feedbacks contribute to what extent to the spread in climate sensitivity?

A comparison of calculated *individual* feedbacks has revealed that the largest positive contributions to the aggregate feedback strength (i.e. the sum of all feedbacks) result from changes in water vapour and clouds. Albedo feedback is about half as strong and spans a similarly broad range as water vapour and cloud feedback. The largest uncertainty in the aggregate feedback results from the broad spread in simulated lapse rate feedback, which covers a range from large negative to positive values. Those results can be compared with a set of different GCM simulations. By and large our results accord well with those models, yet some systematic differences became apparent. Obviously our model ensemble does not include model versions with a large water vapour feedback. Compared to GCM results, the spread in this feedback is comparatively small, and we state that our chosen experimental design did not allow for a broader range. Yet many GCM studies have shown that water vapour and lapse rate feedback are strongly anti-correlated and it has been suggested to comprise those two feedbacks for analysing the weight of individual feedback components. Following this directive, we state that the sum of water vapour and lapse rate feedback between our study and GCM estimates strongly overlaps. Our most important conclusion is that our ensemble of model versions spans almost the entire plausible range for the aggregate feedback strengths inferred from a sampling of more complex models. We are thus confident to have based our analysis on a set of model versions that reveal a broad range of plausible feedback strengths.

We completed our study with a feedback analysis of the LGM climate. For this purpose we performed two additional experiments. The first one is similar to the $2xCO_2$ experiment regarding the applied forcing (we increase CO_2 from 170 p.p.m. to 230 p.p.m.), but the background climate corresponds to the LGM climate state (experiment type I). The second experiment calculated the feedbacks, applying all glacial forcings, from the difference between pre-industrial and LGM climate (experiment type II). The results of those experiments revealed some well-pronounced differences in the performance of the individual feedbacks: While water vapour feedback shows only little dependency on the experiment type, the calculated strength in cloud and albedo feedback differs systematically in those simulations and reveals a pronounced non-linear behaviour concerning its dependency on the background climate and on the forcing type: The albedo effect is stronger in a colder climate, caused by larger contributions of sea ice and snow cover, and is more efficient when strongly inhomogeneous forcings are involved (as is the case for experiment type II). Cloud feedback shows the same systematic behaviour as albedo feedback, but of opposite sign. Lapse rate feedback reveals a strong dependency on the model sensitivity: For models with a low climate sensitivity, both LGM experiments reveal a lapse rate feedback that is not as negative as for the $2xCO_2$ simulations (especially experiment type II). For model versions with a large ΔT_{2x}, the strength in lapse rate feedback is rather similar among all experiments. Those results are helpful for the interpretation of our LGM simulations, which revealed a larger feedback parameter λ_{LGM} (compared to λ_{2CO2}): The pronounced difference in the lapse rate feedback explains the difference in λ for low sensitivity model versions,

whereas the pronounced increase in albedo feedback explains the larger glacial feedback strength seen for high climate sensitivity model versions.

Our results thus support the often-stated assumption that the albedo feedback becomes more important in the Glacial. Yet at the same time, the analysis of the individual feedbacks illustrates that albedo feedback alone may not explain the reason for an increase in the glacial feedback parameter, as changes in the remainder of feedback components are of equal importance.

6.3 Outlook

The analysis of the individual model feedbacks has revealed on the one hand, that our experiment was successful in view of generating a large set of model versions, which cover the aggregate feedback behaviour of more complex models. On the other hand, those analyses have shown some systematic difference in the strength and spread of individual feedback components between our ensemble simulations and GCM results, especially a less pronounced spread in water vapour and cloud feedback. Furthermore, modification of the lapse rate feedback turned out to be a very efficient means for modifying the model sensitivity. The large spread in this feedback crucially contributes to the spread in climate sensitivity in our model ensemble. It should be the objective for future CLIMBER-2 experiments to generate a similar (or even larger) spread in the aggregate feedback strength, but from an experimental design attaching stronger weight to the spread in water vapour and cloud feedback. In this context it will be worthwhile (if not mandatory) to apply *structural* model extensions to allow for more flexibility in the modification of those two feedbacks. Concerning the robustness of our results from constraining the uncertainty range of climate sensitivity, the crucial question to be answered by such an improved experiment will be: Is it possible to construct model versions with a pronounced asymmetric feedback behaviour for glacial cooling and CO_2 warming that is not covered in the set of model versions presented in this thesis? If this turns out to be the case, then we have to accordingly modify our estimate of ΔT_{2x}.

Appendix

A. Constraining uncertainty in the Transient Climate Response

For constraining the uncertainty range of TCR, we can not apply the same interval scheme as used for our methodology to constrain ΔT_{2x}: The linear relationship between LGM cooling and equilibrium warming does not hold for the transient model response. Therefore, for TCR, we replace the linear fit (see Fig. 5.14) by the more general function type $f(x)=a*(x-x_0)^b$ (with $f \leftrightarrow$ TCR, $x \leftrightarrow$ LGM cooling) and furthermore allow the standard deviation σ of the residuals to vary with x as a quadratic function $\sigma(x)$. In fact we observe σ to mildly expand at the tails of the fit. We determine the coefficients of that function as a maximum likelihood estimate, assuming a Gaussian distribution of the residuals for each x. Both fitting procedures (the one for f(x) as well as for $\sigma(x)$) are performed with the correlated ensemble that is more informative in the tails of $\sigma(x)$. However, as for the linear fitting procedure, we would like to obtain a conservative estimate in the sense that the uncorrelated ensemble displays larger values of σ. Hence we assume the same shape $\sigma(x)$ for the uncorrelated ensemble, but allow for an overall upscaling $c*\sigma(x)$, c being estimated from a quadratic fit. In summary, we have generalised the linear fitting f(x) including constant $\sigma(x)$ to a nonlinear fit f(x), $\sigma(x)$, yet ensuring that the average $\sigma(x)$ is obtained from the uncorrelated ensemble.

One may ask what would be the consequences if one applied this nonlinear procedure to the estimates of ΔT_{2x} as well. We have tested for that and found only minor changes in the derived intervals. The bounds of the intervals are shifted at maximum by 0.2°C to the extremes in one case (for tropical constraints) and much less otherwise. Hence we conclude that our results derived for ΔT_{2x} are very robust against the choice of fitting curve. As a final remark on our results for TCR we would like to stress that this study is designed to constrain a characteristic of equilibrium temperature change. To effectively constrain the range of TCR, transient data information should be included in the analysis.

B. Expert derived parameter ranges

In our study the range of simulated ΔT_{2x} is affected by accounting for uncertainty in eleven model parameters, nine representing atmospheric characteristics (affecting parametrisations of cloud optical depth, height of clouds, lapse rate, tropopause height) and two describing mixing processes in the ocean. For each run all parameters have been simultaneously perturbed over the following expert derived ranges (values in {brackets} denote the standard setting for CLIMBER2.3).

Ocean parameters: horizontal and vertical ocean diffusivity k_H: 200-5000 {2000} m^2/s, k_V: 0.1-1.0 $*10^{-4}$ {0.3 $*10^{-4}$} m^2/s at top, 1.1-2.0 $*10^{-4}$ {1.3 $*10^{-4}$} m^2/s at

ocean bottom (vertical profile after Bryan Lewis)

Optical depth of cloudiness: $ODc=(1-Rcc)*(OD_1-OD_2*\cos(latitude)^2) + Rcc*OD_3$, with Rcc relative amount of cumulus clouds, OD_1: 9.0-11.5 {10.2}, OD_2: 6.6-8.4 {7.7}

Tropopause height: C_t: 0.74-0.76 {0.75} (see equation (3) from PETOUKHOV et al. (2000)); a further parameter (ACO_{21}: 0.3-0.65 {0.5}) has been perturbed, which affects the value of integral transmission function of atmosphere (D) in eq. (3).

Lapse rate: a_q: 625-4440 {1110} $(kg/kg)^{-2}$; Γ_0: 4.7-5.2 $*10^{-3}$ {$5.0*10^{-3}$} K/m; Γ_1: 3.6-4.4 $*10^{-5}$ {$4.0*10^{-5}$} m^{-1} (equation (2) (PETOUKHOV et al., 2000))

Height of stratiform clouds: c_1: 0.165-0.200 {0.185} (equation (34), PETOUKHOV et al., 2000)

Radiative forcing of CO_2: $A'CO_2$: 0.70-0.76 {0.755} (equation (6.7) from V.Petoukhov, A.Ganopolski, M. Claussen, 2003, PIK report No.81).

The modification of all feedback parameters results in changes of the sum of all feedbacks (water vapour, cloud, lapse rate and albedo), spanning a minimum-maximum range of 71% (63%) of the mean value for the correlated (uncorrelated) ensemble. Parameter variations, which affect the CO_2 radiative forcing, result in a range of 16% (28%) of the mean forcing.

C. Quantification of paleo-data uncertainties

To estimate the uncertainty range (2σ) for mean tropical SST cooling, we consider the error contributions from a) large-scale patterns in the ocean data temperature field, which hamper a direct comparison with a coarse resolution model, and b) the statistical error for each reconstructed paleo temperature value.

We refer to an interpolated data set (SCHÄFER-NETH and PAUL, 2003) from which we use the variance $V=(1.41°C)^2$ as the starting point to estimate an uncertainty range for the spatial mean of the data field. In order to do so, we need to consider the correlation structure of the individual error sources. The data were interpolated using a kriging method (SCHÄFER-NETH et al.,), which basically takes into account data points in the vicinity of a location to be reconstructed, weighted by the ocean correlation structure. This results in a spatially smoothed correlation structure of the interpolated oceanic temperature field, with only b) being affected by the smoothing. The most extreme version of smoothing (compatible with the requirement that a) is not affected) would result in a spatial clustering of b) on the same scale as a). That simplifies the discussion as then we can estimate $2\sigma \approx 2\sqrt{(V/(N-1))}$, where N is given by the number of uncorrelated Atlantic ocean areas between 20°N and 20°S. With a correlation length of ~10-15° we obtain a rough estimate of $N \approx 12$ for the tropical Atlantic sector. For less extreme versions of smoothing we were allowed to use larger values of N as more independent sources within b) had entered V. In that sense $2\sigma \approx 2\sqrt{(V/(N-1))}$ with $N \approx 12$ provides a conservative estimate. We thus derive an estimate of 2.96 ± 0.85°C of the 2σ range for mean tropical Atlantic SST cooling.

We cannot address, however, systematic errors in paleo temperature reconstructions beyond the quality tests of transfer-function (TF) methods, as e.g. described in PFLAUMANN et al. (2003). Reconstructed temperature anomalies from geochemical methods (GC) agree with (TF) based LGM cooling estimates for most regions of low latitudes (BARD, 2001; NIEBLER et al., 2003; BARKER et al., 2005). Yet some systematic bias arises for regions of pronounced cooling (especially in the eastern tropical Atlantic). To account for this bias we confine maximum cooling in our used data set to 4°C (which corresponds to the upper limit of tropical Atlantic SST cooling derived by GC methods (ROSELL- MELE et al., 2004; BARKER et al., 2005). This shifts the mean about 0.2°C to less cooling and at the same time narrows the standard deviation of mean SST cooling. Thus this revised data estimate, which might be regarded as more representative for GC reconstructions, is included in the range of 3±0.9°C of our FT based estimate and is not separately discussed for constraining $\Delta T_{2x.}$

Given pronounced spatial inhomogeneities we emphasize that by describing mean tropical Atlantic SST anomalies, we discuss the mean annual cooling averaged from 20°N to 20°S over the whole Atlantic sector. Thus the effect of sediment cores, which show strong local effects (e.g. in upwelling regions) is minimized, and the mean SST anomaly should be more representative for large scale tropical conditions (dominated by large scale forcings, such as lowered CO_2 concentrations). Modelling and data-analysis studies show, that the mean cooling for the tropical Atlantic section is slightly larger than comparable estimates from the Pacific and Indian sector. When considering a global tropical SST data constraint, an average tropical cooling of about 2.5°C would have to be considered to constrain the same ΔT_{2x} range (as derived from tropical Atlantic).

References

ALLEN, M. (1999): Do-it-yourself climate prediction. Nature **401**(6754): 642-642.

ALLEN, M. R. and S. F. B. TETT (1999): Checking for model consistency in optimal fingerprinting. Climate Dynamics **15**(6): 419-434.

ANDERSON, T. L., R. J. CHARLSON, S. E. SCHWARTZ, R. KNUTTI, O. BOUCHER, H. RODHE and J. HEINTZENBERG (2003): Climate Forcing by Aerosol - a Hazy Picture. Science **300**(5622): 1103-1104.

ANDREAE, M. O., C. D. JONES and P. M. COX (2005): Strong present-day aerosol cooling implies a hot future. Nature **435**(7046): 1187-1190.

ANDRONOVA, N. and M. E. SCHLESINGER (2001): Objective estimation of the probability distribution for climate sensitivity. Journal of Geophysical Research **106**: 22605-22612.

ANNAN, J., J. HARGREAVES, R. OHGAITO, A. ABE-OUCHI and S. EMORI (2005): Efficiently Constraining Climate Sensitivity with Ensembles of Paleoclimate Simulations. SOLA **1**: 181-184.

ARRHENIUS, S. (1896): On the influence of carbonic acid in the air upon the temperature of the ground. London Edinburgh Dublin Philos. Mag. J. Sci. **41**: 237-276.

BARD, E. (2001): Comparison of alkenone estimates with other paleotemperature proxies. Geochemistry Geophysics Geosystems **2**.

BARKER, S., I. CACHO, H. BENWAY and K. TACHIKAWA (2005): Planktonic foraminiferal Mg/Ca as a proxy for past oceanic temperatures: a methodological overview and data compilation for the Last Glacial Maximum. Quaternary Science Reviews **24**(7-9): 821-834.

BAUER, E., M. CLAUSSEN, V. BROVKIN and A. HUENERBEIN (2003): Assessing climate forcings of the Earth system for the past millennium. Geophysical Research Letters **30**(6): 1276-1279.

BOER, G. J. and B. YU (2003): Climate sensitivity and climate state. Climate Dynamics **21**(2): 167-176.

BROCCOLI, A. J. (2000): Tropical cooling at the last glacial maximum: An atmosphere-mixed layer ocean model simulation. Journal of Climate **13**(5): 951-976.

BRYAN, K. and L. J. LEWIS (1979): Water Mass Model of the World Ocean. Journal of Geophysical Research-Oceans and Atmospheres **84**(C5): 2503-2517.

CAVALIERI, D. J., C. L. PARKINSON and K. Y. VINNIKOV (2003): 30-Year satellite record reveals contrasting Arctic and Antarctic decadal sea ice variability. Geophysical Research Letters **30**(18).

CESS, R. D., G. L. POTTER, J. P. BLANCHET, G. J. BOER, A. D. DELGENIO, M. DEQUE, V. DYMNIKOV, V. GALIN, W. L. GATES, S. J. GHAN, J. T. KIEHL, A. A. LACIS, H. LETREUT, Z. X. LI, X. Z. LIANG, B. J. MCAVANEY, V. P. MELESHKO, J. F. B. MITCHELL, J. J. MORCRETTE, D. A. RANDALL, L. RIKUS, E. ROECKNER, J. F. ROYER, U. SCHLESE, D. A. SHEININ, A. SLINGO, A. P. SOKOLOV, K. E. TAYLOR, W. M. WASHINGTON, R. T. WETHERALD, I. YAGAI and M. H. ZHANG (1990): Intercomparison and Interpretation of Climate Feedback Processes in 19 Atmospheric General-Circulation Models. Journal of Geophysical Research-Atmospheres **95**(D10): 16601-16615.

CESS, R. D., M. H. ZHANG, G. L. POTTER, H. W. BARKER, R. A. COLMAN, D. A. DAZLICH, A. D. DELGENIO, M. ESCH, J. R. FRASER, V. GALIN, W. L. GATES, J. J. HACK, W. J. INGRAM, J. T. KIEHL, A. A. LACIS, H. LETREUT, Z. X. LI, X. Z. LIANG, J. F. MAHFOUF, B. J. MCAVANEY, V. P. MELESHKO, J. J. MORCRETTE, D. A. RANDALL, E. ROECKNER, J. F. ROYER, A. P. SOKOLOV, P. V. SPORYSHEV, K. E. TAYLOR, W. C. WANG and R. T. WETHERALD (1993): Uncertainties in Carbon-Dioxide Radiative Forcing in Atmospheric General-Circulation Models. Science **262**(5137): 1252-1255.

CHARNEY, J. G. (1979): Carbon Dioxide and Climate: A Scientific Assessment. Washington, DC., National Academy Press**:** 22 pp.

CLAQUIN, T., M. SCHULZ, Y. BALKANSKI and O. BOUCHER (1998): Uncertainties in assessing radiative forcing by mineral dust. Tellus Series B-Chemical and Physical Meteorology **50**(5): 491-505.

CLAUSSEN, M., L. A. MYSAK, A. J. WEAVER, M. CRUCIFIX, T. FICHEFET, M. F. LOUTRE, S. L. WEBER, J. ALCAMO, V. A. ALEXEEV, A. BERGER, R. CALOV, A. GANOPOLSKI, H. GOOSSE, G. LOHMANN, F. LUNKEIT, MOKHOV, II, V. PETOUKHOV, P. STONE and Z. WANG (2002): Earth system models of intermediate complexity: closing the gap in the spectrum of climate system models. Climate Dynamics **18**(7): 579-586.

COLMAN, R. (2003a): A comparison of climate feedbacks in general circulation models. Climate Dynamics **20**(7-8): 865-873.

COLMAN, R. (2003b): Seasonal contributions to climate feedbacks. Climate Dynamics **20**(7-8): 825-841.

COLMAN, R., J. FRASER and L. ROTSTAYN (2001): Climate feedbacks in a general circulation model incorporating prognostic clouds. Climate Dynamics **18**(1-2): 103-122.

COLMAN, R. A. (2001): On the vertical extent of atmospheric feedbacks. Climate Dynamics **17**(5-6): 391-405.

COLMAN, R. A. and B. J. MCAVANEY (1997): A study of general circulation model climate feedbacks determined from perturbed sea surface temperature experiments. Journal of Geophysical Research-Atmospheres **102**(D16): 19383-19402.

COLMAN, R. A., S. B. POWER and B. J. MCAVANEY (1997): Non-linear climate feedback analysis in an atmospheric general circulation model. Climate Dynamics **13**(10): 717-731.

COVEY, C., K. M. ACHUTARAO, U. CUBASCH, P. JONES, S. J. LAMBERT, M. E. MANN, T. J. PHILLIPS and K. E. TAYLOR (2003): An overview of results from the Coupled Model Intercomparison Project. Global and Planetary Change **37**(1-2): 103-133.

COVEY, C., L. C. SLOAN and M. I. HOFFERT (1996): Paleoclimate data constraints on climate sensitivity: The paleocalibration method. Climatic Change **32**(2): 165-184.

CROWLEY, T. J. (1992): North Atlantic Deep Water cools the Southern Hemisphere. Paleoceanography **7**: 489.

CROWLEY, T. J. (2000): CLIMAP SSTs re-revisited. Climate Dynamics **16**(4): 241-255.

DAHL-JENSEN, D., K. MOSEGAARD, N. GUNDESTRUP, G. D. CLOW, S. J. JOHNSEN, A. W. HANSEN and N. BALLING (1998): Past temperatures directly from the Greenland Ice Sheet. Science **282**(5387): 268-271.

DESSAI, S. and M. HULME (2004): Does climate adaptation policy need probabilities? Climate Policy **4**(2): 107-128.

FARRERA, I., S. P. HARRISON, I. C. PRENTICE, G. RAMSTEIN, J. GUIOT, P. J. BARTLEIN, R. BONNEFILLE, M. BUSH, W. CRAMER, U. VON GRAFENSTEIN, K. HOLMGREN, H. HOOGHIEMSTRA, G. HOPE, D. JOLLY, S. E. LAURITZEN, Y. ONO, S. PINOT, M. STUTE and G. YU (1999): Tropical climates at the Last Glacial Maximum: a new synthesis of terrestrial palaeoclimate data. I. Vegetation, lake levels and geochemistry. Climate Dynamics **15**(11): 823-856.

FLECHSIG, M., U. BÖHM, T. NOCKE and C. RACHIMOW (2005): Techniques for Quality Assurance of Models in a Multi-Run Simulation Environment. Sensitivity Analysis of Model Output. Proceedings of the 4th International Conference on Sensitivity Analysis of Model Output (SAMO'04), Los Alamos National Laboratory, Los Alamos, U.S.A.

FOREST, C. E., P. H. STONE, A. P. SOKOLOV, M. R. ALLEN and M. D. WEBSTER (2002): Quantifying Uncertainties in Climate System Properties with the Use of Recent Climate Observations. Science **295**(5552): 113-117.

FRAME, D. J., B. B. B. BOOTH, J. A. KETTLEBOROUGH, D. A. STAINFORTH, J. M. GREGORY, M. COLLINS and M. R. ALLEN (2005): Constraining climate forecasts: The role of prior assumptions. Geophysical Research Letters **32**(9).

GANACHAUD, A. and C. WUNSCH (2003): Large-scale ocean heat and freshwater transports during the World Ocean Circulation Experiment. Journal of Climate **16**(4): 696-705.

GANOPOLSKI, A. (2003): Glacial integrative modelling. Philosophical Transactions of the Royal Society of London Series a-Mathematical Physical and Engineering Sciences **361**(1810): 1871-1883.

GANOPOLSKI, A., V. PETOUKHOV, S. RAHMSTORF, V. BROVKIN, M. CLAUSSEN, A. ELISEEV and C. KUBATZKI (2001): CLIMBER-2: a climate system model of intermediate complexity. Part II: model sensitivity. Climate Dynamics **17**: 735.

GANOPOLSKI, A. and S. RAHMSTORF (2001): Rapid changes of glacial climate simulated in a coupled climate model. Nature **409**: 153.

GANOPOLSKI, A., S. RAHMSTORF, V. PETOUKHOV and M. CLAUSSEN (1998): Simulation of modern and glacial climates with a coupled global model of intermediate complexity. Nature **391**: 351.

GREGORY, J. M., R. J. STOUFFER, S. C. B. RAPER, P. A. STOTT and N. A. RAYNER (2002): An observationally based estimate of the climate sensitivity. Journal of Climate **15**(22): 3117-3121.

GUACA, G. U. A. C. A. (1993)., NCDC, NOAA.

HANSEN, J., A. LACIS, D. H. RIND, G. RUSSELL, I. FUNG, R. RUEDY and J. LERNER (1984): Climate sensitivity: analysis of feedback mechanisms. Washington DC, American Geophysical Union.

HANSEN, J., A. LACIS, R. RUEDY, M. SATO and H. WILSON (1993): How Sensitive Is the Worlds Climate. Research & Exploration **9**(2): 142-158.

HANSEN, J., L. NAZARENKO, R. RUEDY, M. SATO, J. WILLIS, A. DEL GENIO, D. KOCH, A. LACIS, K. LO, S. MENON, T. NOVAKOV, J. PERLWITZ, G. RUSSELL, G. A. SCHMIDT and N. TAUSNEV (2005a): Earth's Energy Imbalance: Confirmation and Implications. Science **308**(5727): 1431-1435.

HANSEN, J., M. SATO and R. RUEDY (1997): Radiative forcing and climate response. Journal of Geophysical Research-Atmospheres **102**(D6): 6831-6864.

HANSEN, J., M. SATO, R. RUEDY, L. NAZARENKO, A. LACIS, G. A. SCHMIDT, G. RUSSELL, I. ALEINOV, M. BAUER, S. BAUER, N. BELL, B. CAIRNS, V. CANUTO, M. CHANDLER, Y. CHENG, A. DEL GENIO, G. FALUVEGI, E. FLEMING, A. FRIEND, T. HALL, C. JACKMAN, M. KELLEY, N. KIANG, D. KOCH, J. LEAN, J. LERNER, K. LO, S. MENON, R. MILLER, P. MINNIS, T. NOVAKOV, V. OINAS, J. PERLWITZ, D. RIND, A. ROMANOU, D. SHINDELL, P. STONE, S. SUN, N. TAUSNEV, D. THRESHER, B. WIELICKI, T. WONG, M. YAO and S. ZHANG (2005b): Efficacy of climate forcings. Journal of Geophysical Research-Atmospheres **110**(D18).

HARVEY, D. (2000): Global Warming, The Hard Science. Harlow, Prentice Hall.

HASSELMANN, K. (1976): Stochastic Climate Models .1. Theory. Tellus **28**(6): 473-485.

HASSELMANN, K. (1993): Optimal Fingerprints for the Detection of Time-Dependent Climate-Change. Journal of Climate **6**(10): 1957-1971.

HELD, I. M. and B. J. SODEN (2000): Water vapor feedback and global warming. Annual Review of Energy and the Environment **25**: 441-475.

HELTON, J. C. and R. L. IMAN (1982): Sensitivity Analysis of a Model for the Environmental Movement of Radionuclides. Health Physics **42**(5): 565-584.

HEWITT, C. D. and J. F. B. MITCHELL (1997): Radiative forcing and response of a GCM to ice age boundary conditions: cloud feedback and climate sensitivity. Climate Dynamics **13**(11): 821-834.

HOFFERT, M. I. and C. COVEY (1992): Deriving Global Climate Sensitivity from Paleoclimate Reconstructions. Nature **360**(6404): 573-576.

HOUGHTON, J. T. (2001): Climate Change 2001: The Scientific Basis. Cambridge, Cambridge Univ. Press.

IMAN, R. L. and W. J. CONOVER (1982): A Distribution-Free Approach to Inducing Rank Correlation among Input Variables. Communications in Statistics Part B-Simulation and Computation **11**(3): 311-334.

IPCC (2001): IPCC, 2001: Climate Change 2001: The Scientific Basis. Contribution of Working Group I to the Third Assessment Report of the Intergovernmental Panel on Climate Change. Cambridge, United Kingdom, Cambridge University Press.

IPCC WG-I (2004): Workshop on Climate Sensitivity, Paris, 26-29 July 2004.

JAEGER, L. (1976): Monatskarten des Niederschlags für die ganze Erde. Berichte des Deutschen Wetterdienstes **18**(139): 38 pp.

JONES, P. D., M. NEW, D. E. PARKER, S. MARTIN and I. G. RIGOR (1999): Surface air temperature and its changes over the past 150 years. Rev. Geophys. **37**: 173-199.

JOSHI, M., K. SHINE, M. PONATER, N. STUBER, R. SAUSEN and L. LI (2003): A comparison of climate response to different radiative forcings in three general circulation models: towards an improved metric of climate change. Climate Dynamics **20**(7-8): 843-854.

JOUZEL, J., F. VIMEUX, N. CAILLON, G. DELAYGUE, G. HOFFMANN, V. MASSON-DELMOTTE and F. PARRENIN (2003): Magnitude of isotope/temperature scaling for interpretation of central Antarctic ice cores. Journal of Geophysical Research-Atmospheres **108**(D12).

KERR, R. A. (2004): CLIMATE CHANGE: Three Degrees of Consensus. Science **305**(5686): 932-934.

KNUTTI, R., G. A. MEEHL, M. R. ALLEN and D. A. STAINFORTH (2006): Constraining climate sensitivity from the seasonal cycle in surface temperature. Journal of Climate, in press.

KNUTTI, R., T. F. STOCKER, F. JOOS and G.-K. PLATTNER (2002): Constraints on radiative forcing and future climate change from observations and climate model ensembles. Nature **416**(6882): 719-723.

KUCERA, M., A. ROSELL-MELE, R. SCHNEIDER, C. WAELBROECK and M. WEINELT (2005): Multiproxy approach for the reconstruction of the glacial ocean surface (MARGO). Quaternary Science Reviews **24**(7-9): 813-819.

LEA, D. W. (2004): The 100 000-yr cycle in tropical SST, greenhouse forcing, and climate sensitivity. Journal of Climate **17**(11): 2170-2179.

LEA, D. W., D. K. PAK, L. C. PETERSON and K. A. HUGHEN (2003): Synchroneity of tropical and high-latitude Atlantic temperatures over the last glacial termination. Science **301**(5638): 1361-1364.

LEGATES, D. R. (1995): Global and Terrestrial Precipitation - a Comparative-Assessment of Existing Climatologies. International Journal of Climatology **15**(3): 237-258.

LEMKE, P. (1977): Stochastic Climate Models .3. Application to Zonally Averaged Energy Models. Tellus **29**(5): 385-392.

LEVITUS, S. (2001): Anthropogenic warming of Earth's climate system. Science **292**: 267-270.

LEVITUS, S., J. ANTONOV and T. BOYER (2005): Warming of the world ocean, 1955-2003. Geophysical Research Letters **32**(2): L02604.

LORIUS, C., J. JOUZEL, D. RAYNAUD, J. HANSEN and H. LE TREUT (1990): The ice-core record: climate sensitivity and future greenhouse warming. Nature **347**: 139-145.

MASSON-DELMOTTE, V., M. KAGEYAMA, P. BRACONNOT, S. CHARBIT, G. KRINNER and C. RITZ (2006): Past and future polar amplification of climate change: climate model intercomparisons

and ice-core constraints. Climate Dynamics, in press.

MEEHL, G. A., W. M. WASHINGTON, J. M. ARBLASTER and A. X. HU (2004): Factors affecting climate sensitivity in global coupled models. Journal of Climate **17**(7): 1584-1596.

MINSCHWANER, K. and A. E. DESSLER (2004): Water vapor feedback in the tropical upper troposphere: Model results and observations. Journal of Climate **17**(6): 1272-1282.

MITCHELL, J. M. (1976): An overview of climatic variability and its causal mechansims. Quat Res **6**: 481-493.

MURPHY, J. M., D. M. H. SEXTON, D. N. BARNETT, G. S. JONES, M. J. WEBB, M. COLLINS and D. A. STAINFORTH (2004): Quantification of modelling uncertainties in a large ensemble of climate change simulations. Nature **430**(7001): 768-772.

NIEBLER, H. S., H. W. ARZ, B. DONNER, S. MULITZA, J. PATZOLD and G. WEFER (2003): Sea surface temperatures in the equatorial and South Atlantic Ocean during the last glacial maximum (23-19 ka). Paleoceanography **18**(3).

OORT, A. and R. EM (1971): Atmospheric circulation statistics. NOAA Prof Pap **5**: 323 pp.

PELTIER, W. R. (1994): Ice age paleotopography. Science **265**: 195-201.

PELTIER, W. R. (2004): Global glacial isostasy and the surface of the ice-age earth: The ice-5G (VM2) model and grace. Annual Review of Earth and Planetary Sciences **32**: 111-149.

PETIT, J. R., J. JOUZEL, D. RAYNAUD, N. I. BARKOV, J. M. BARNOLA, I. BASILE, M. BENDER, J. CHAPPELLAZ, M. DAVIS, G. DELAYGUE, M. DELMOTTE, V. M. KOTLYAKOV, M. LEGRAND, V. Y. LIPENKOV, C. LORIUS, L. PEPIN, C. RITZ, E. SALTZMAN and M. STIEVENARD (1999): Climate and atmospheric history of the past 420,000 years from the Vostok ice core, Antarctica. Nature **399**(6735): 429-436.

PETOUKHOV, V., A. GANOPOLSKI, V. BROVKIN, M. CLAUSSEN, A. ELISEEV, C. KUBATZKI and S. RAHMSTORF (2000): CLIMBER-2: a climate system model of intermediate complexity. Part I: model description and performance for present climate. Climate Dynamics **16**: 1.

PFLAUMANN, U., M. SARNTHEIN, M. CHAPMAN, L. D'ABREU, B. FUNNELL, M. HUELS, T. KIEFER, M. MASLIN, H. SCHULZ, J. SWALLOW, S. VAN KREVELD, M. VAUTRAVERS, E. VOGELSANG and M. WEINELT (2003): Glacial North Atlantic: Sea-surface conditions reconstructed by GLAMAP 2000. Paleoceanography **18**(3).

PINOT, S., G. RAMSTEIN, S. P. HARRISON, I. C. PRENTICE, J. GUIOT, M. STUTE and S. JOUSSAUME (1999): Tropical paleoclimates at the Last Glacial Maximum: comparison of Paleoclimate Modeling Intercomparison Project (PMIP) simulations and paleodata. Climate Dynamics **15**(11): 857-874.

RANDALL, D. A., R. D. CESS, J. P. BLANCHET, S. CHALITA, R. COLMAN, D. A. DAZLICH, A. D. DELGENIO, E. KEUP, A. LACIS, H. LETREUT, X. Z. LIANG, B. J. MCAVANEY, J. F. MAHFOUF, V. P. MELESHKO, J. J. MORCRETTE, P. M. NORRIS, G. L. POTTER, L. RIKUS, E. ROECKNER, J. F. ROYER, U. SCHLESE, D. A. SHEININ, A. P. SOKOLOV, K. E. TAYLOR, R. T. WETHERALD, I. YAGAI and M. H. ZHANG (1994): Analysis of Snow Feedbacks in 14 General-Circulation Models. Journal of Geophysical Research-Atmospheres **99**(D10): 20757-20771.

ROSELL- MELE, A., E. BARD, K. C. EMEIS, B. GRIEGER, C. HEWITT, P. J. MULLER and R. R. SCHNEIDER (2004): Sea surface temperature anomalies in the oceans at the LGM estimated from the alkenone-U-37(K ') index: comparison with GCMs. Geophysical Research Letters **31**(3).

SALTZMAN, B. (1978): A survey of statistical-dynamical models of the terrestrial climate. Adv Geophys **20**: 183-304.

SARNTHEIN, M., R. GERSONDE, S. NIEBLER, U. PFLAUMANN, R. SPIELHAGEN, J. THIEDE, G. WEFER and M. WEINELT (2003): Overview of Glacial Atlantic Ocean Mapping (GLAMAP 2000). Paleoceanography **18**(2).

SCHÄFER-NETH, C. and A. PAUL (2003): Gridded Global LGM SST and Salinity Reconstruction, IGBP PAGES/World Data Center for Paleoclimatology, Boulder,NOAA/NGDC Paleoclimatology Program, Boulder CO, USA.

SCHÄFER-NETH, C., A. PAUL and S. MULITZA Perspectives on mapping the MARGO reconstructions by variogram analysis/kriging and objective analysis. Quaternary Science Reviews 24:1095-1107.

SCHLESINGER, M. (1988): Quantitative analysis of feedbacks in climate model simulations of CO2 induced warming. Dordrecht, Netherlands, Kluwer Academic.

SCHNEIDER VON DEIMLING, T., A. V. GANOPOLSKI, H. HELD and S. RAHMSTORF: Last Glacial Maximum: Ensemble based estimate of global cooling. Submitted to Geophysical Research Letters.

SCHNEIDER VON DEIMLING, T., H. HELD, A. GANOPOLSKI and S. RAHMSTORF (accepted): Climate sensitivity estimated from ensemble simulations of glacial climate. Climate Dynamics.

SCHWARTZ, S. E. (2004): Uncertainty requirements in radiative forcing of climate change. Journal of the Air & Waste Management Association **54**(11): 1351-1359.

SENIOR, C. A. and J. F. B. MITCHELL (2000): The time-dependence of climate sensitivity. Geophysical Research Letters **27**(17): 2685-2688.

SHINE, K. P., J. COOK, E. J. HIGHWOOD and M. M. JOSHI (2003): An alternative to radiative forcing for estimating the relative importance of climate change mechanisms. Geophysical Research

Letters **30**(20).

SODEN, B. J., A. J. BROCCOLI and R. S. HEMLER (2004): On the use of cloud forcing to estimate cloud feedback. Journal of Climate **17**(19): 3661-3665.

SODEN, B. J. and I. HELD An Assessment of Climate Feedbacks in Coupled Ocean-Atmosphere Models. Submitted to the Journal of Climate - Letters.

SODEN, B. J., D. L. JACKSON, V. RAMASWAMY, M. D. SCHWARZKOPF and X. L. HUANG (2005): The radiative signature of upper tropospheric moistening. Science **310**(5749): 841-844.

SOKOLIK, I. N. and O. B. TOON (1999): Incorporation of mineralogical composition into models of the radiative properties of mineral aerosol from UV to IR wavelengths. Journal of Geophysical Research-Atmospheres **104**(D8): 9423-9444.

STAINFORTH, D. A., T. AINA, C. CHRISTENSEN, M. COLLINS, N. FAULL, D. J. FRAME, J. A. KETTLEBOROUGH, S. KNIGHT, A. MARTIN, J. M. MURPHY, C. PIANI, D. SEXTON, L. A. SMITH, R. A. SPICER, A. J. THORPE and M. R. ALLEN (2005): Uncertainty in predictions of the climate response to rising levels of greenhouse gases. Nature **433**(7024): 403-406.

STAUFFER, B., J. FLUCKIGER, E. WOLFF and P. BARNES (2004): The EPICA deep ice cores: first results and perspectives. Annals of Glaciology, Vol 39, 2005 **39**: 93-100.

STIER, P., J. FEICHTER, S. KINNE, S. KLOSTER, E. VIGNATI and J. WILSON (2004): The aerosol-climate model ECHAM5-HAM. Atmos. Chem. Phys. Discuss. **4**: 5551-5623.

STOCKER, T. F. (1998): The Seesaw Effect. Science **282**: 61.

STOCKER, T. F., D. G. WRIGHT and L. A. MYSAK (1992): A zonally averaged, coupled ocean-atmosphere model for paleoclimate studies. J. Clim. **5**: 773-797.

STOTT, P. A. and J. A. KETTLEBOROUGH (2002): Origins and estimates of uncertainty in predictions of twenty-first century temperature rise (vol 416, pg 723, 2002). Nature **417**(6885): 205-205.

STOUFFER, R. J. and S. MANABE (2003): Equilibrium response of thermohaline circulation to large changes in atmospheric CO_2 concentration. Climate Dynamics **20**: 759.

TALLEY, L. D., J. L. REID and P. E. ROBBINS (2003): Data-Based Meridional Overturning Streamfunctions for the Global Ocean. Journal of Climate **16**: 3213.

VIMEUX, F., K. M. CUFFEY and J. JOUZEL (2002): New insights into Southern Hemisphere temperature changes from Vostok ice cores using deuterium excess correction. Earth and Planetary Science Letters **203**(3-4): 829-843.

VINNICHENKO, N. K. (1970): The kinetic energy spectrum in the free atmosphere - 1 second to 5 years. Tellus **22**: 158-166.

WALLACE, J. and P. HOBBS (1977): Atmospheric science: An introductory survey. New York, Academic Press.

WARREN, S. (1988): TN317 Technical Note, NCAR.

WATANABE, O., J. JOUZEL, S. JOHNSEN, F. PARRENIN, H. SHOJI and N. YOSHIDA (2003): Homogeneous climate variability across East Antarctica over the past three glacial cycles. Nature **422**(6931): 509-512.

WATTERSON, I. G. (2000): Interpretation of simulated global warming using a simple model. Journal of Climate **13**(1): 202-215.

WATTERSON, I. G., M. R. DIX and R. A. COLMAN (1999): A comparison of present and doubled CO2 climates and feedbacks simulated by three general circulation models. Journal of Geophysical Research-Atmospheres **104**(D2): 1943-1956.

WETHERALD, R. T. and S. MANABE (1988): Cloud Feedback Processes in a General-Circulation Model. Journal of the Atmospheric Sciences **45**(8): 1397-1415.

YAO, M. S. and A. D. DEL GENIO (1999): Effects of cloud parameterization on the simulation of climate changes in the GISS GCM. Journal of Climate **12**(3): 761-779.

Danksagung

An dieser Stelle möchte ich all jenen danken, die zum Gelingen dieser Arbeit beigetragen haben:

- Stefan Rahmstorf für die Betreuung und Hilfestellung bei der konkreten Ausrichtung dieser Arbeit;
- John Schellnhuber, der es mir ermöglichte, am PIK zu promovieren;
- Ganz besonderen Dank an Hermann Held, welcher diese Arbeit zu jeder Zeit inhaltlich begleitet und unterstützt sowie in vielen anregenden Diskussionen diese Arbeit mit gestaltet hat;
- Ebenfalls besonderen Dank an Andrey Ganopolski, der mir in zahlreichen Diskussionen einen tieferen Einblick in die Welt der Klimamodellierung ermöglicht hat;
- Elmar Kriegler für die Bereitstellung von Daten sowie zahlreiche anregende Diskussionen;
- Brigitte Knopf, Kirsten Zickfeld und Klaus Eisenack für die nette „Arbeitszimmer-Atmosphäre“ sowie für hilfreiche Diskussionen und Unterstützung. In diesem Sinne meinen Dank ebenfalls an Till Kuhlbrodt, Malaak Kallache, Alexa Griesel, Henning Rust, Eva Bauer, Susanne Nawrath, Anders Levermann, Vladimir Petuokhov, Victor Brovkin, Reinhard Calov und Torsten Grothmann;
- Gitta Krukenberg für ihre jederzeit hilfsbereite Art und Unterstützung;
- Karsten Kramer, Michael Flechsig, Achim Glauer, welche die aufwendigen Simulationen dieser Arbeit ermöglicht haben;
- Werner von Bloh für Tipps und Tricks aus der UNIX-Welt;
- Martin Werner für die Bereitstellung von GCM-Daten;
- Ein herzliches Dankeschön auch an all die vielen noch ungenannten Kollegen;
- Meinem Bruder, der bei manchen Matlab-Schwierigkeiten eine Hilfe war.

- Mein ganz besonderer und herzlicher Dank gilt meinen Eltern!